

Jennet Akech Ojur

The Effect of Polymeric Flocculants on the Settling of Clinoptilolite Ion Exchange Material Used for Remediation of Nuclear Wastewater

School of Water, Energy and Environment
Water and Wastewater Processes (Engineering Route)

MSc
Academic Year: 2024 - 2025

Supervisor: Peter Jarvis and Bruce Jefferson
Associate Supervisor: Alex Lockwood
September 2025



This thesis is submitted in partial fulfilment of the requirements for the degree of Water and Wastewater Processes (Engineering Route)

Academic integrity declaration

I declare that:

- the thesis submitted has been written by me alone.
- the thesis submitted has not been previously submitted to this university or any other.
- that all content, including primary and/or secondary data, is true to the best of my knowledge.
- that all quotations and references have been duly acknowledged according to the requirements of academic research.

I understand that to knowingly submit work in violation of the above statement will be considered by examiners as academic misconduct.

Abstract

Effective management of spent ion exchange (IEX) media is a critical challenge for nuclear wastewater remediation, particularly at Sellafield's Site Ion Exchange Effluent Plant (SIXEP). The hydraulic transfer of clinoptilolite IEX material generates fine suspensions with poor settleability, high water content, and limited consolidation. This increases the storage demands and complicates downstream treatment. Polymeric flocculants offer a promising, low-cost solution; however, their performance is strongly influenced by molecular structure and operating conditions.

This study evaluated the flocculation behaviour of two cationic polymers: a high-molecular-weight linear polyacrylamide (Flopam FO 4650 MPM, A1) and a branched polyamine-epichlorohydrin resin (Praestol DW31, A2) across solids concentrations of 0.1, 1, and 10 % (v/v) under normal and shear conditions. Flocculation performance was assessed through turbidity reduction, zeta potential, settled bed volume, polymer adsorption, floc size, fractal dimension, and microscopy.

A1 consistently achieved superior clarification and formed more dense and compact flocs (D_f ~2.8) through polymer bridging. These flocs presented stronger resilience to shear and achieved a regrowth capacity of ~50 %. In contrast, A2 operated primarily by patch flocculation, producing larger but fragile flocs (Df ~1.9) with a narrow effective dosage window and poorer shear resistance. These mechanistic differences present the importance of polymer architecture in governing both floc strength and operational robustness.

Overall, Flopam FO 4650 MPM was the preferred flocculant for SIXEP sludges. The polymer demonstrated effective performance across a range of solids concentrations and operational conditions. Recommended dosages are 5 – 10 PPM for dilute suspensions, 10 – 15 PPM for medium solids, and 50 – 100 PPM for dense sludges. By linking polymer structure to settling efficiency and shear resilience, this work provides a framework for polymer selection in nuclear sludge

treatment and contributes to the optimisation of flocculation strategies for long-term waste management.

Acknowledgements

This journey has been one of the most challenging and rewarding experiences of my life, and it would not have been possible without the people and organisations who stood beside me.

To my supervisors, Professor Peter Jarvis and Professor Bruce Jefferson, I owe my deepest thanks for your wisdom and for consistently pushing me to think more rigorously. Your guidance strengthened my research skills and helped me grow as both a student and a scientist. To Dr Alex Lockwood, I am deeply grateful for your insight into the realities of nuclear systems, which grounded this work in its true purpose, and for your steady support throughout this journey.

I am profoundly grateful to Sellafield Ltd for sponsoring this research and providing the industrial perspective that ensured its relevance and impact. I also gratefully acknowledge the support of the International Atomic Energy Agency (IAEA) Marie Skłodowska-Curie Fellowship Programme, without which I would not have been able to pursue this MSc. The opportunity to contribute to research at the intersection of nuclear and wastewater treatment has been both inspiring and formative for my future career.

To my family, friends, and closest companions: thank you for being my anchor. Your patience, encouragement, and belief in me carried me through the long nights and heavy days.

And above all, I give glory to God Almighty, who granted me strength when I felt weak, clarity when I felt lost, and perseverance to reach this point. This work is as much a reflection of His grace as it is of my effort.

Table of Contents

Academic integrity declaration i
Abstract ii
Acknowledgements iv
List of Figures vii
List of Tables ix
List of Equations x
List of Abbreviations xi
1 Introduction 1
1.1 Background and Context 1
1.1.1 Nuclear Fuel Cyle 1
1.1.2 The Sellafield Site and SIXEP 1
1.1.3 The problem of sludge management 2
1.2 Science of Flocculation 3
1.2.1 Colloidal Destabilisation Mechanisms 3
1.2.2 Polymer Characteristics 4
1.2.3 Floc strength and dynamics 5
1.3 Knowledge Gap and Research Rationale 6
1.4 Research Aim and Objectives 6
1.4.1 Research aim 6
1.4.2 Research objectives 7
1.5 Thesis Structure 7
2 Materials and Methods 8
2.1 Materials 8
2.1.1 Raw Materials 8
2.1.2 Preparation Materials 10
2.2 Methods 11
2.2.1 Jar Testing 11
2.2.2 Water Analysis 12
2.2.3 Shear Condition Water Analysis 14
2.2.4 Floc Imagery 14
3 Results 16
3.1 Normal-Condition Results 16
3.1.1 Turbidity 16
3.1.2 Zeta Potential 18
3.1.3 Settled Bed Volume 22
3.1.4 Total Organic Carbon and Adsorption Behaviour 24
3.1.5 Floc Size and Fractal Dimension 27
3.1.6 Microscope Imagery 28
3.2 Shear-Condition Results 30
3.2.1 Turbidity 30

3.2.2 Settled Bed Volume 33
3.2.3 Total Organic Carbon and Adsorption Behaviour 36
3.2.4 Floc Size and Fractal Dimension 39
3.2.5 Microscope Imagery 40
4 Discussion 43
4.1 Polymer Selection for Variable Sludge Conditions: Implications for Sellafield 43
4.2 Study Limitations 45
4.3 Future research directions 45
5 Conclusion 46
5.1 Synthesis of Findings 46
5.2 Recommendations 47
5.3 Contribution to knowledge 47
References 48
Appendices 53
Appendix A 54
Appendix B 55
Appendix C 59
Appendix D : Flopam (A1) Results 60
Appendix E : Praestol (A2) Results 69

List of Figures

Figure 1-1: Simplified process flow diagram of the Site Ion Exchange Effluent Plant (SIXEP) (Image taken directly from (International Atomic Energy Agency, 2002)) 2

Figure 1-2: Schematic to describe charge neutralisation. 3

Figure 1-3: Schematic to describe patch flocculation. 4

Figure 1-4: Schematic to describe polymer bridging. 4

Figure 2-1: Chemical Structure of a cationic polyacrylamide (Image taken directly from Estrada et al. (2020)). 9

Figure 2-2: Chemical Structure of Dimethylamine, Polymer with Epichlorohydrin And N-Methylmethanamine (Prestel DW31) (Image was taken directly from Jackson (2022) 9

Figure 2-3: Conical settled bed volume created from slow mixing. 12

Figure 3-1: The effect of polymer dosage on turbidity at low solids content. 16

Figure 3-2: The effect of polymer dosage on turbidity at medium solids content. 17

Figure 3-3: The effect of polymer dosage on turbidity at high solids content. ... 18

Figure 3-4: The effect of polymer dosage on zeta potential at low solids content (0.1 %). 19

Figure 3-5: The effect of polymer dosage on zeta potential at medium solids content (1 %). 20

Figure 3-6: The effect of polymer dosage on zeta potential at high solids content (10 %). 21

Figure 3-7: The effect of polymer dosage on settled bed volume at low solids content (0.1 %). 22

Figure 3-8: The effect of polymer dosage on settled bed volume at medium solids content (1 %). 23

Figure 3-9: The effect of polymer dosage on settled bed volume at high solids content (10 %). 24

Figure 3-10: The effect of polymer dosage on residual TOC at low solids content (0.1 %). 25

Figure 3-11: The effect of polymer dosage on residual TOC at low solids content (1 %). 26

Figure 3-12: The effect of polymer dosage on residual TOC at high solids content (10 %). 27

Figure 3-13: Example of microscope images of flocs formed by polymer A1. .. 29

Figure 3-14: Example of microscope images of flocs formed by polymer A2. .. 30

Figure 3-15: The effect of mechanical shear on turbidity at low solids content (0.1 %). 31

Figure 3-16: The effect of mechanical shear on turbidity at medium solids content (1 %). 32

Figure 3-17: The effect of mechanical shear on turbidity at high solids content (10 %). 33

Figure 3-18: The effect of mechanical shear on settled bed volume at low solids content (0.1 %). 34

Figure 3-19: The effect of mechanical shear on settled bed volume at medium solids content (1 %). 35

Figure 3-20: The effect of mechanical shear on settled bed volume at high solids content (10 %). 36

Figure 3-21: The effect of mechanical shear on residual TOC at low solids content (0.1 %). 37

Figure 3-22: The effect of mechanical shear on residual TOC at medium solids content (1 %). 38

Figure 3-23: The effect of mechanical shear on residual TOC at high solids content (10 %). 39

Figure 3-24: Example of microscope images of post-shear flocs formed by polymer A1 41

Figure 3-25: Example of microscope images of post-shear flocs formed by polymer A2 42

List of Tables

Table 2-1: Physical properties of Clinoptilolite media (data obtained from the supplier, RS Minerals Ltd (2025)). 8

Table 2-2: Characteristics of the polymer used in this study (information as given by suppliers otherwise noted). 10

Table 2-3: Synthetic solutions used in this study. 10

Table 2-4: Polymer dosages applied in this study. 11

Table 3-1: Maximum floc size at the optimal dosage range for medium solids content at 10 % dilution. 28

Table 3-2: Fractal dimension at the optimal dosage range for medium solids content at 10 % dilution. 28

Table 3-3: Post-shear floc size responses for polymers A1 and A2 at medium solids content at 10 % dilution. 40

Table 3-4: Fractal dimension (D_f) of flocs post-shear at medium solids content at 10 % dilution. 40

Table 4-1:comparative performance of Flopam (A1) and Praestol (A2) polymers across key flocculation parameters. 43

List of Equations

$\boldsymbol{Df = -m = \log(I)\log(q)}$
Equation 2-1 14

List of Abbreviations

A1	Flopam FO 4650 MPM
A2	Praestol™ DW31 Coagulant
Cs	Caesium-137
D_f	Fractal Dimension
HLW	High-Level Waste
IEX	Ion Exchange
PAM	Polyacrylamide
PAE	Polyamine-epichlorohydrin
PPM	Parts Per Million
SDS	Safety Data Sheet
SIXEP	Site Ion Exchange Effluent Plant
SS	Suspended Solids
Sr	Strontium-90
TOC	Total Organic Carbon
v/v%	Volume per Volume Percentage

1 Introduction

1.1 Background and Context

1.1.1 Nuclear Fuel Cyle

The nuclear fuel cycle is divided into the front-end and back-end operations. The front-end involves processes from uranium mining to fuel fabrication for reactor use. The back-end deals with the management of spent nuclear fuel and radioactive waste after energy production (World Nuclear Association, 2025). Spent fuel, which is classified as high-level radioactive waste (HLW), is initially stored in cooling ponds. This storage generates aqueous effluents containing low to intermediate radioactive wastes (International Atomic Energy Agency, 2011). It is critical to ensure the radioactive materials are managed in a safe, secure and robust manner (International Commission on Radiological Protection, 1998). Ion exchange (IEX) is a widely accepted and efficient method for removing radionuclides from such waste streams (International Atomic Energy Agency, 2002) .

1.1.2 The Sellafield Site and SIXEP

The Sellafield site in West Cumbria, UK, is a complex nuclear facility which focuses on the decommissioning and waste management of its legacy facilities (Committee of Public Accounts, 2025). Commencing operation in May 1985, Site Ion Exchange Effluent Plant (SIXEP), treats radioactive aqueous waste through a multi-stage process (Figure 1-1*)* (International Atomic Energy Agency, 2002). The initial treatment removes solids via sand filtration and then adjusts the pH in a carbonation tower. The core treatment involves the selective adsorption of radionuclides, particularly caesium-137 (Cs) and strontium-90 (Sr), using a natural and inorganic zeolite ion exchange material named Clinoptilolite. The IEX material was selected for its high selectivity for these key radionuclides. Upon reaching its exchange capacity, the spent IEX material is not regenerated but rather hydraulically pumped into storage tanks (International Atomic Energy Agency, 2002). The transfer process subjects the IEX material to significant shear forces which fractures the material, causing fine particles in suspension.

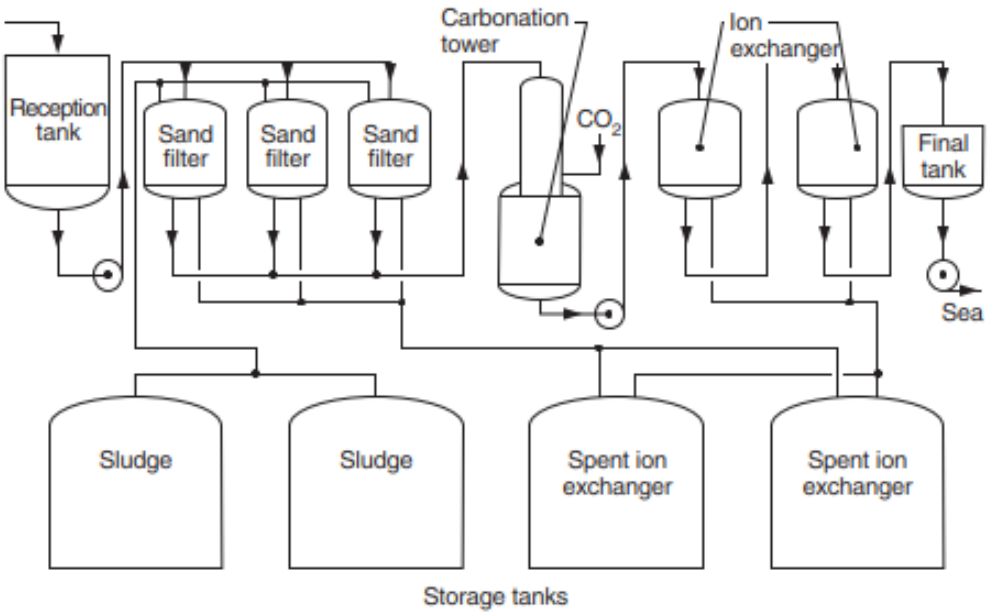


Figure 1-1: Simplified process flow diagram of the Site Ion Exchange Effluent Plant (SIXEP) (Image taken directly from (International Atomic Energy Agency, 2002))

1.1.3 The problem of sludge management

The presence of fine particles in suspension creates significant challenges for storage and downstream processes. The colloidal nature of these suspensions prevents efficient consolidation which results in stored sludge with high-water content and low solids fraction (Eder et al., 2025). Similar issues of poorly settling sludge with high water content are widely reported across the nuclear industry, as well as in municipal wastewater and mining operations (International Atomic Energy Agency, 2002; Zhang et al., 2022). This inefficiency directly increases operational costs by requiring a greater number of storage tanks and more frequent sludge transfers. Li & Chen (2024) reviewed a wide range of treatment and disposal strategies for spent ion exchange materials, including immobilisation, high-integrity containers, compaction, and oxidation. While these approaches aim to reduce volume and secure long-term storage, they remain costly and technically challenging. In contrast, Lockwood (2021) highlighted that polymeric flocculants are receiving increasing interest as cheap, easily deployable reagents for aggregating fine radwaste particulates, thereby improving sedimentation, flotation, and dewatering. Although immobilisation in cement is not currently undertaken, the sludge's high-water content and poor settleability could hinder future developments, as excess water compromises the structural integrity of the waste form (International Atomic Energy Agency, 2002). Therefore, to improve the

consolidation of the IEX material, the fine particles must be aggregated to form larger, more settleable flocs through the process of flocculation (Hocking et al., 1999).

1.2 Science of Flocculation

1.2.1 Colloidal Destabilisation Mechanisms

The stability of colloidal suspensions is governed by the balance of interparticle forces, including van der Waals attraction, electrostatic repulsion, steric interactions and hydration forces. Of these, electrostatic interactions are often the most significant in aqueous suspensions, as charged particle surfaces generate repulsive forces that inhibit aggregation and settling (Hocking et al., 1999). However, electrostatics are not always the dominant factor; in systems with high polymer concentrations or steric stabilisers, mechanisms such as polymer bridging and other non-electrostatic interactions can instead govern colloidal stability. The primary mechanisms for colloidal destabilisation are charge neutralisation, charge patch flocculation and polymer bridging (Ajaya Bhattarai, 2020; Hocking et al., 1999).

1.2.1.1 Charge neutralisation

This mechanism reduces the electrostatic repulsive forces through the adsorption of an oppositely charged polymer onto the particle's surface (Figure 1-2). This adsorption shifts the zeta potential to near neutral and thus reduces the energy barrier to aggregation (Eder et al., 2025; Hocking et al., 1999).

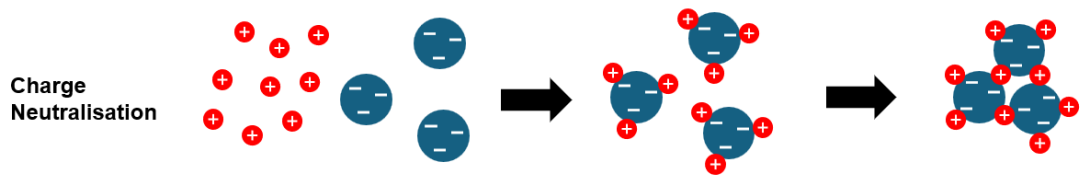


Figure 1-2: Schematic to describe charge neutralisation.

1.2.1.2 Charge patch flocculation

This mechanism occurs when high-charge-density polymers adsorb onto the particle's surface, creating localised areas of charge (Figure 1-3). These patches electrostatically attract oppositely charged regions, leading to aggregation (Eder et al., 2025). Notably, this mechanism does not require the overall zeta potential of the particles to be fully neutralised (Eder et al., 2025; Hocking et al., 1999).

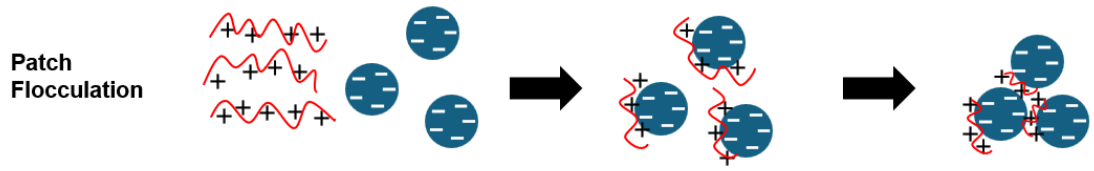


Figure 1-3: Schematic to describe patch flocculation.

1.2.1.3 Polymer bridging

This mechanism involves high molecular weight polymers with long chain structures. These polymers adsorb onto the surface of one or more particles and extend their free chain segments into the surrounding suspension, where they can attach to other particles (Figure 1-4). In this way, a single polymer molecule can physically connect multiple particles to form a network of flocs. Unlike charge neutralisation, polymer bridging does not necessarily require electrostatic interactions as adsorption can occur through hydrogen bonding, van der Waals forces, or hydrophobic interactions. Effective bridging requires sufficient polymer chain length and adequate particle surface area to allow multiple attachment points (Gregory & Barany, 2011; Hocking et al., 1999; Hoogeveen, 1996).

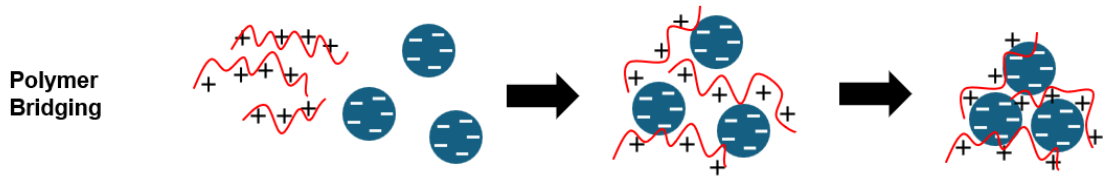


Figure 1-4: Schematic to describe polymer bridging.

1.2.2 Polymer Characteristics

1.2.2.1 Charge density

This refers to the proportion of charged functional groups per polymer molecule. It influences colloid destabilisation by determining the number of potential attachment sites available on particle surfaces. A higher charge density increases the number of electrostatic interactions, thereby increasing the overall strength of adsorption (Gregory & Barany, 2011; Hocking et al., 1999). Consequently, polymers with higher charge density generally require lower dosages to achieve effective charge neutralisation or patch flocculation. However, excessively high charge density can reduce polymer chain flexibility due to intra-chain repulsion, which limits bridging.

Moreover, extensive surface coverage may overcompensate the particle charge, making it net positively charged and restabilising the suspension (Hoogeveen, 1996).

1.2.2.2 Molecular weight

This refers to the length of polymer chains and is typically associated with polymer bridging capacity. Polymers with high molecular weights can extend their chains over greater distances between particles. This results in larger and stronger flocs. Notably, very high molecular weights may hinder diffusion and adsorption kinetics (Gregory & Barany, 2011; Hocking et al., 1999).

1.2.2.3 Molecular structure

This defines the structural arrangement of the polymer's chains, and it influences the dominant flocculation mechanism utilised. The main arrangements are linear, branched, cross-linked and network structures. Linear polymers promote extended polymer bridging and form large, dense flocs. Branched and cross-linked polymers enhance charge-patch flocculation due to their high charge density. Network polymers enmesh particles in a matrix through charge neutralisation and sweep flocculation (Ajaya Bhattarai, 2020; Gregory & Barany, 2011; Hocking et al., 1999).

1.2.3 Floc strength and dynamics

1.2.3.1 Aggregation kinetics

Aggregation kinetics refers to the rate at which particles collide and attach to form flocs. The process is influenced by particle concentration, mixing energy and the efficiency of attachment following collision (Gregory & Barany, 2011; Hocking et al., 1999)

1.2.3.2 Floc Breakage

The application of shear forces, primarily through mixing and pumping, induce floc breakage. This may occur either by fragmentation, where flocs split into smaller particles, or by erosion, where surface particles are gradually stripped away (Fan et al., 2020). The degree of breakage indicates the resultant settling efficiency and effluent clarity. The susceptibility of floc breakage is influenced by the intrinsic strength of the floc and the magnitude of the applied shear (Hocking et al., 1999; Nan et al., 2016).

1.2.3.3 Floc Regrowth

The ability of fragmented flocs to re-aggregate is an indicator of the systems resilience. Regrowth potential is not guaranteed and is dependent on the polymer's binding mechanism. Effective regrowth occurs when the polymer remains adsorbed to the particle's surface post-shear. Notably, the polymer can experience degradation from the shear forces which can reduce its aggregating capacity (Bartiko & De Julio, 2014; Nan et al., 2016).

1.3 Knowledge Gap and Research Rationale

Flocculation is a known process, and the mechanisms or polymeric flocculants have been well research in general contexts (Gregory & Barany, 2011; Hocking et al., 1999; Hoogeveen, 1996). Studies on other mineral suspensions provide insight into the role of polymer structure, particularly the distinction between linear and branched architectures. For example, Ziółkowska et al. (2011) compared dextran-graft-polyacrylamide copolymers with linear polyacrylamides for kaolin dispersions and found that branched copolymers at higher doses produced larger, denser flocs and more efficient clarification than their linear counterparts. However, the comparative analysis of linear and branched polymer structures for treating inorganic ion exchange material, specifically clinoptilolite remains sparse. Consequently, this study provides a foundational understanding of how polymer structure dictates flocculation performance, floc properties, and shear resistance for this specific application.

1.4 Research Aim and Objectives

1.4.1 Research aim

This study investigates the flocculation efficiency and shear resilience of linear and branched cationic polymers on synthetic suspensions representative of Sellafield's SIXEP ion exchange (IEX) sludge. The aim is to identify a robust polymeric flocculant to enhance the settling of clinoptilolite IEX material for nuclear wastewater remediation.

1.4.2 Research objectives

1. Assess the flocculation performance of a linear (Flopam FO 4650 MPM) and a branched (Praestol DW31) polymer across a range of solids contents and dosages.
2. Determine the dominant colloidal destabilisation mechanism for each polymer at low, medium, and high solids content.
3. Characterise the physical properties of the formed flocs.
4. Evaluate the shear resilience of the flocs by analysing their breakage and regrowth potential post-application of mechanical shear.
5. Correlate polymer adsorption behaviour with flocculation performance under both normal and high shear conditions.
6. Qualitatively analyse floc morphology and structure.

1.5 Thesis Structure

This thesis is structured into five sections and has been illustrated in the figure below. Following this introduction, *Section 2: Materials and Methods* details the experimental procedure. *Section 3: Results* presents that key findings from the experimental work. *Section 4: Discussion* provides an overall interpretation of the results against the stated objectives. *Section 5: Conclusion* summarises the key findings and provides recommendations. The thesis is supported by a list of *References* and *Appendices* which contain raw data and supplementary information.

2 Materials and Methods

2.1 Materials

2.1.1 Raw Materials

2.1.1.1 Ion Exchange Material

Clinoptilolite, a natural inorganic zeolite ion-exchange media, was supplied by RS Minerals UK (Guisborough, UK). The media included sub-100 and sub-200-micron material. The empirical formula of the zeolite is $(Ca, Fe, K, Mg, Na)_{3-6}Si_{30}Al_6O_{72}.24H_2O$. The physical properties of the material are summarised in Table 2-1.

Table 2-1: Physical properties of Clinoptilolite media (data obtained from the supplier, RS Minerals Ltd (2025)**).**

Property	Value	Unit
Colour	Off-white or ivory	N/A
Bulk Density	650 – 750	g/l
Cation Exchange Capacity	1.5 – 1.9	meq/g
pH	7 - 9	N/A

2.1.1.2 Ionic Strength of Clinoptilolite Suspension

Initially, the salinity was meant to vary between 0.01M. 0.1M and 1M. However, the SIXEP storage waters are sourced from fuel pond effluents and are expected to have a salinity less than seawater levels which is 0.6 M (Johnson & Pytkowicz, 1981). Literature from the International Atomic Energy Agency (2002) indicates that the waste would likely have a total dissolved salts content between 1 – 2 g/L. Experimental work by Wallace et al. (2012) investigated radionuclide sorption in groundwater representative of the Sellafield site and these experiments used ionic strengths ranging from <0.01 M up to 0.03 M. The final salinity chosen was 0.03 M (1.8 g/L), as it is high enough to reflect the potential salinity on site, without being too high to result in polymer inefficiencies.

2.1.1.3 Polymers

Two commercially available polymers were tested in this work: Flopam FO 4650 MPM (SNF UK) is a linear cationic polyacrylamide (PAM) with a high molecular weight and was supplied as a granular powder (SNF, 2017) (Figure 2-1; Table 2-2). Praestol™ DW31 Coagulant is a branched and lightly crosslinked cationic polyamine-epichlorohydrin (PAE) resin with an estimated molecular weight of 10,000 – 300,000 g/mol (Herbert H. Espy, 1995) (Figure 2-2; Table 2-2). The PAE was supplied as an aqueous solution containing 50 – 60 % active polymer (Solensis, 2021).

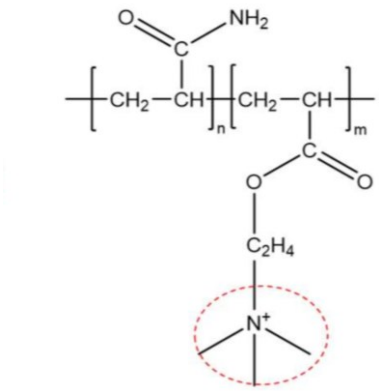


Figure 2-1: Chemical Structure of a cationic polyacrylamide (Image taken directly from Estrada et al. (2020)**).**

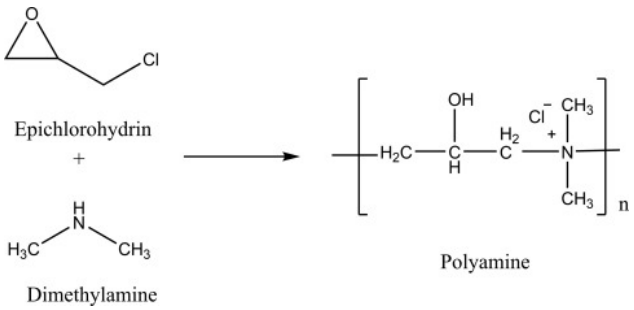


Figure 2-2: Chemical Structure of Dimethylamine, Polymer with Epichlorohydrin And N-Methylmethanamine (Prestel DW31) (Image was taken directly from Jackson (2022)

Table 2-2: Characteristics of the polymer used in this study (information as given by suppliers otherwise noted).

Polymer	Charge	Degree of Charge	Molecular Weight	Apparent viscosity [mPa.s]	Chemical Structure
Flopam FO 4650 MPM	Cationic	High	High	350 (at 5g/L, 25'C)	Linear
Praestol™ DW31 Coagulant	Cationic	Very High	Low to Medium	N/A	Branched, lightly crosslinked

2.1.2 Preparation Materials

2.1.2.1 Synthetic Suspension

The synthetic media suspension (1 L) was prepared by mixing the zeolite at varying volume fractions (0.1. 1 and 10 %), in deionised water containing 0.03 M NaCl for 15 minutes (Table 2-3). Before the zeolite was used, it was sieved to ensure the particle size distribution was sub-200 microns. The variation in solids content enabled evaluation of how the density of sludge affects flocculation performance and settling behaviour and was representative of solids content that may be experienced from the legacy accumulation of ion-exchange media in the SIEXP storage tanks (Lockwood, 2021).

Table 2-3: Synthetic solutions used in this study.

Solution No.	Solids Content		Ionic Strength		Deionized Water	
	v/v%	g/L	Mole (M)	g/L	mL	g
1	0.1	1			898.2	898.2
2	1	10	0.03	1.8	988.2	988.2
3	10	100			997.2	997.2

2.1.2.2 Polymer Stock Solutions

The Flopam FO 4650 MPM stock solution was prepared by mixing 5 g of the flocculant powder with 995 mL of deionised water for 1 hour using a magnetic stirrer. Praestol DW31 was diluted to 5 g/L by weighing 9.09 g of the polymer and mixing it with 990 mL of water for 1 hour using a magnetic stirrer. Both solutions were stored in a cool and dry place. When Flopam was used in the experiments it was directly dosed from the stock solution while the Praestol was stirred for 5 minutes prior to use to re-suspend the polymer, which tends to settle at the bottom of the container (Table 2-4).

Table 2-4: Polymer dosages applied in this study.

No.	Flocculant name	Stock concentration	Dosage	
			PPM	Volume of stock solution required, mL
1	Praestol™ DW31	5 g/L	5, 10, 15, 25, 50, 100	1, 2, 3, 5, 10,20
2	Flopam FO 4650 MPM		5, 10, 15, 25, 50, 10	1, 2, 3, 5, 10,20

2.2 Methods

2.2.1 Jar Testing

The jar testing protocol typically follows stages of rapid mixing, slow stir, and settlement (Nyström et al., 2020). An adapted process was adopted here because the flocs began to settle during the slow stir phase that resulted in a conical shaped settled bed caused by the vortex during the slow stir (Figure 2-3). The updated jar test procedure was as follows: a rapid mix at 200 rpm for 2 minutes and a settling period for 10 minutes. Six beakers were used per jar test experiment allowing multiple variables to be tested and replicated. For each polymer, a series of doses (0, 5, 10, 15, 25, 50, and 100 ppm) was applied to all three investigated IEX solids concentrations (0.1, 1, and 10 v/v%) (Appendix B).

Each experimental condition was replicated three times, with the data reported as an average and standard deviation of these values.

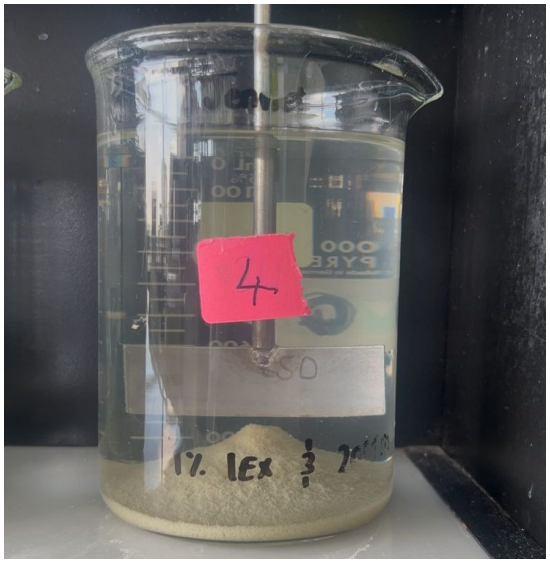


Figure 2-3: Conical settled bed volume created from slow mixing.

2.2.2 Water Analysis

Once the jar tests were completed several parameters were tested to evaluate the performance of the polymers in settling the suspension solution.

2.2.2.1 Zeta Potential

Zeta potential (electrical potential) was measured using a Zetasizer Nano (Malvern Panalytic, Malvern UK). 1 mL of the supernatant from the completed settled jar test was sampled using a 1 mL syringe and placed into a disposable folded capillary cell (DTS1070).

2.2.2.2 Turbidity

Turbidity was measured using a Turbidimeter (2100N Laboratory Turbidimeter (EPA, USA), indicated the settleability of the fine particles that were initially in suspension. 20 ml of the supernatant was sampled using a 10 mL pipette and placed into turbidity cuvette.

2.2.2.3 Suspended Solids Concentration

The suspended solids concentration was analysed by collecting a 2 mL sample of the supernatant and placing it on 45-micron filter paper in a metal tray dish of known weight. It was then placed into an oven for 24 hours at 105 °C. The sample was reweighed and converted to g/L.

2.2.2.4 Settled Bed Volume

The settled bed volume was determined directly from calibrated measurements. For low solids concentrations, samples were transferred to a cylindrical measuring flask graduated in 1 mL increments, giving a measurement accuracy of ± 0.5 mL. For medium and high solids concentrations, the volume was read directly from the jar graduations, which were marked in 100 mL increments, corresponding to a measurement accuracy of ± 50 mL.

2.2.2.5 Total Organic Carbon

The total organic carbon (TOC) content was measured using a TOC analyser (Shimadzu TOC-V Series Total Organic Carbon Analyzer, Japan). The settled supernatant was filtered using a 0.45-micron filter paper as this allowed the solids and liquids to separate. The liquid was then analysed using the TOC analyser, which oxidised the sample and then measured the amount of CO_2 produced. This data indicated the amount of polymer that interacted with the fine particles in suspension and the amount that was left in solution.

The TOC content of the polymers was first quantified to establish a baseline to evaluate the residual polymer in the supernatant and the amount absorbed. Due to measurement errors with the dilution stock of A2, all the displayed values were calculated based on the active polymer concentration specified in the supplier's safety data sheet (SDS) (Appendix B).

2.2.2.6 Floc Size

The floc growth following polymer addition was analysed using a Malvern Mastersizer 3000 (Malvern Panalytical, UK) with a manual accessory unit. To ensure the measurements were reliable, a sample at 1% solids content was diluted by a factor of 10. This consisted of 2g of IEX material, 0.36 g of NaCl and

1.997 L of deionised water. The dilution was required to maintain an obscuration range of less than 25%, as undiluted samples exceeded the instruments detection limits (>50 % obscuration). The optimal dosing conditions were tested to measure floc growth.

2.2.2.7 Fractal Dimension

The data from the Mastersizer tests were used to calculate the fractal dimension. The fractal dimension was determined by analysing the logarithmic relationship between the scattering intensity (I) and the wave vector (q) (Anitas, 2020). For flocs formed from each polymer dose, a slope in the linear region of the graph was used to calculate D_f.

$$\boldsymbol{D_f = -m = \frac{\log(I)}{\log(q)}} \qquad \textbf{Equation 2-1}$$

2.2.3 Shear Condition Water Analysis

Following the normal floc growth experiments, additional tests were carried out where the formed flocs were exposed to high shear rate conditions tests to evaluate the floc strength and resilience under mechanical stress. The three optimal polymer dosages for each solids content were tested. The shear-condition jar-testing followed the same method as the normal-condition procedure. However, after the 10-minute settling phase, the suspension was subjected to a high shear of 300 rpm for 2 minutes. This approach allowed flocs to stabilise before shear was applied, providing a measure of their resistance once fully formed and reflecting the conditions they may experience during transfer from storage tanks. Following this the solution was allowed to settle for 10 minutes before further tests were conducted. The following parameters were analysed to evaluate the floc resilience and potential regrowth: turbidity, settled bed volume, total organic carbon, floc size and fractal dimension.

2.2.4 Floc Imagery

The flocs formed under normal and shear- conditions were captured using a Brightfield microscope and a Lumenera Infinity 3-3UR Monochrome CCD

Camera (Teledyne Lumenera, Canada). The scaled images were analysed using image analysis software following calibration using a Sedgewick Rafter cell.

3 Results

3.1 Normal-Condition Results

3.1.1 Turbidity

At low solids content (0.1 %), Flopam FO 4650 MPM (A1) achieved lower turbidity over a broader dosage range than Praestol DW31 (A2) (Figure 3-1). A1 reduced the initial turbidity of 48.9 ± 17.2 NTU to 1.7 ± 0.4 NTU and 2.2 ± 0.5 NTU at 5 PPM and 10 PPM, respectively. There was a gradual increase in turbidity with a further increase of dosage, and the turbidity at 100 PPM was 12.5 ± 4.5 NTU. This trend aligns with mild overdosing effects, as the maximum turbidity reported is approximately 25 % of the initial turbidity (Hua & Hamburg, 2020). In contrast, A2 reduced the initial turbidity to 9.8 ± 2.6 NTU at a dose of 5 PPM, which is 5.8 times higher than the turbidity reported with A1 at the same polymer dosage. Subsequent dosages led to a rapid deterioration in clarity with a maximum reported turbidity of 37 ± 8.4 NTU at 100 PPM. This indicates that the polymer is highly sensitive to overdosing and would be most effective at doses lower than those evaluated in this study (López-Maldonado et al., 2014).

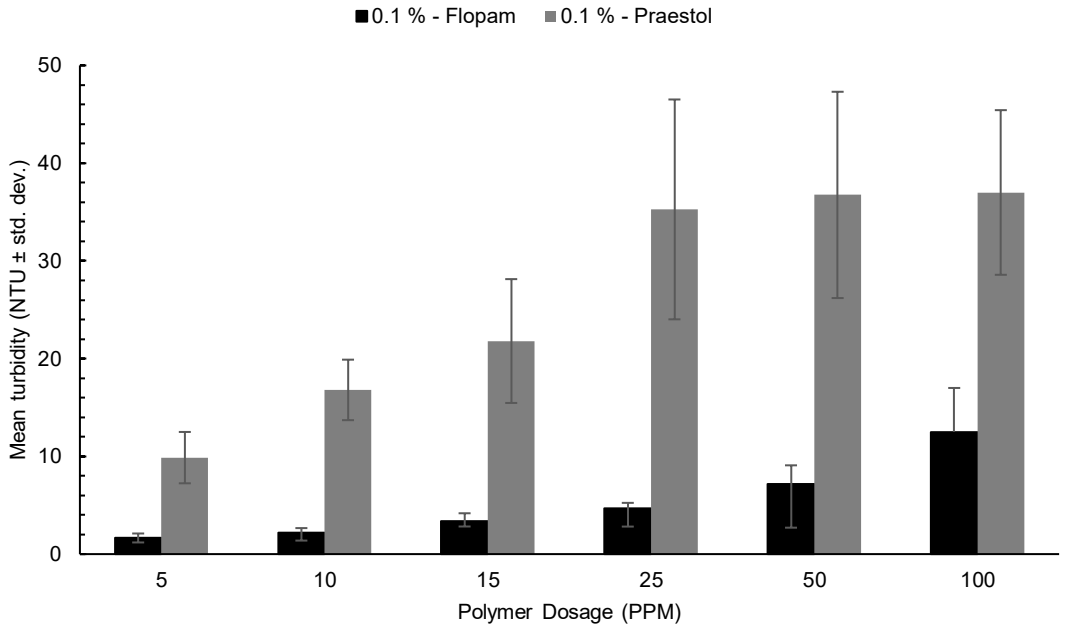


Figure 3-1: The effect of polymer dosage on turbidity at low solids content.

At medium solids content (1%), A1 again presented lower turbidity values over a broader dosage range than A2 (Figure 3-2). A1 reduced the initial turbidity of 147.7 ± 60.9 to 1.4 ± 0.6, 1.4 ± 0.6, 1.0 ± 0.3 NTU and 1.7 ± 1.0 at 5, 10, 15 and 25 PPM respectively. This range indicated that the optimal dosage for A1 at medium solids content was 15 PPM. After which minor overdosing effects became evident with the turbidity rising to 8.6 ± 4.1 NTU at 100 PPM (Hua & Hamburg, 2020). Consistently, A2 presented a narrow optimal window with the lowest turbidity recorded as 1.07 ± 0.17 NTU at 5 PPM. After which the turbidity steeply increased to 43.9 ± 12.7 NTU at 100 PPM. This again suggests that A2 would be most effective at doses lower than those evaluated in this study.

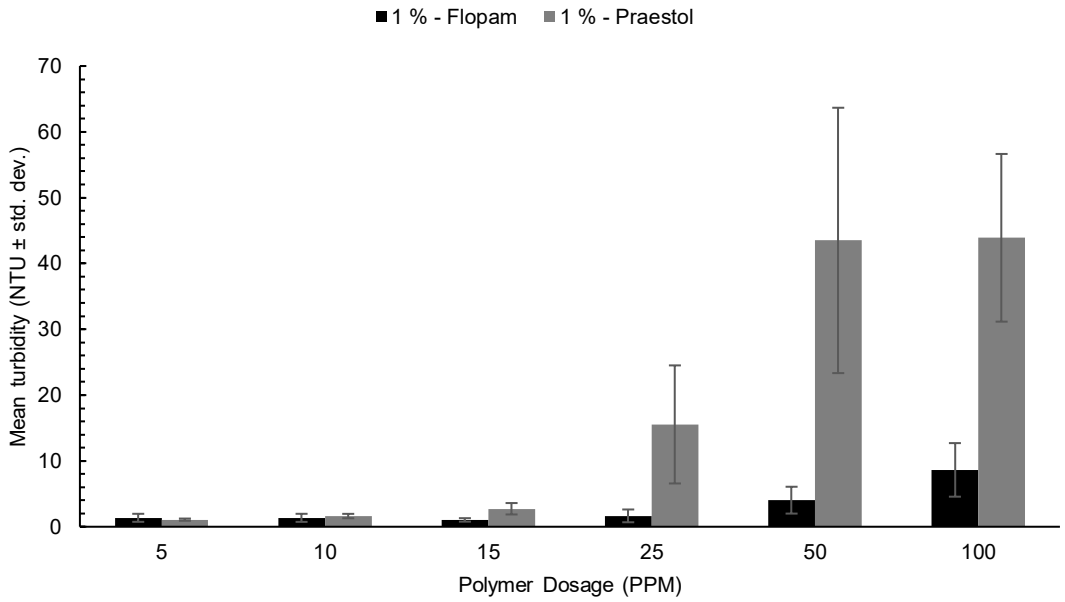


Figure 3-2: The effect of polymer dosage on turbidity at medium solids content.

At high solids contents (10%), A1 and A2 presented continuous improvement in turbidity reduction with increasing dosage (Figure 3-3). A1 and A2 achieved a final turbidity at 100 PPM of 0.5 ± 0.3 NTU and 0.7 ± 0.38 NTU, respectively. Both polymers did not present signs of restabilisation and thus an optimal dosage could be possible at higher values.

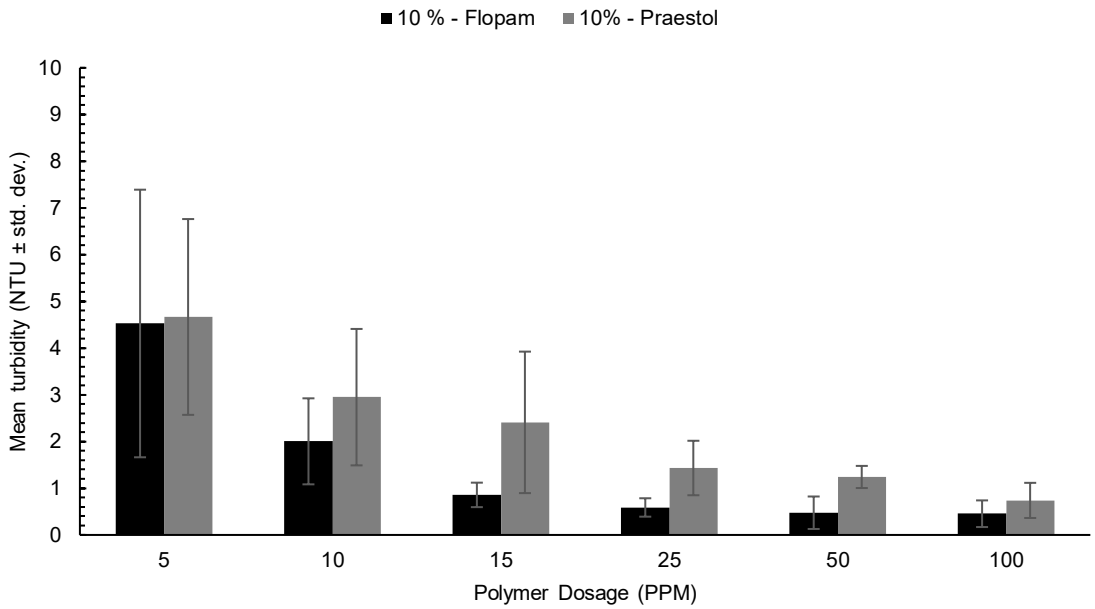


Figure 3-3: The effect of polymer dosage on turbidity at high solids content.

Overall, at low and medium solids content, A1 was able to maintain effective turbidity reduction over a broad range of dosages. For high solids content, A1 and A2 performed similarly by reducing turbidity with an increasing dosage. Notably, A1 was able to achieve the lowest turbidity reductions for all three ranges.

3.1.2 Zeta Potential

All the solid contents before polymer dosing presented highly negative zeta potentials. The initial values for the low, medium and high solids content were - 33.2 ± 5.9 mV, - 28.0 ± 7.2 mV and - 21.3 ± 2.3 mV, respectively. This indicated that the suspension solutions were highly stable and thus exerted strong electrostatic repulsion forces (Gregory & Barany, 2011).

At low solids content, both polymers produced immediate charge reversal (Figure 3-4). At 5 ppm, zeta potentials shifted to +36.9 ± 4.8 mV for A1 and +41.7 ± 7.8 mV for A2, with corresponding turbidity reductions of 95 % and 80 %, respectively. The persistence of effective flocculation at these strongly positive values indicates that charge neutralisation was not the dominant mechanism. Instead, A1 (linear high-MW PAM) achieved high clarity through its ability to form

extended inter-particle bridges despite the overcompensated surface charge (Hocking et al., 1999). In contrast, A2 (branched, very-high-charge PAE) induced greater charge overcompensation; however, its lower turbidity reduction across the tested dosage range suggests that bridging was less effective, likely due to steric limitations imposed by its structure (Bolto & Gregory, 2007). This became evident at dosages exceeding the optimal 5 PPM, where turbidity increased sharply, with only a 25% reduction at 100 PPM. This behaviour aligns with (Lockwood, 2021), who described how high-charge density, low molecular weight polymers like A2 predominantly form localised charge patches on particle surfaces in dilute suspensions, rather than extending into chains required for bridging. As the dosage increased, excess polymer adsorbed to the surface, saturating these localized patches and reducing aggregation efficiency. Therefore, these findings strongly suggest that patch-type aggregation is the dominant mechanism driving A2's behaviour.

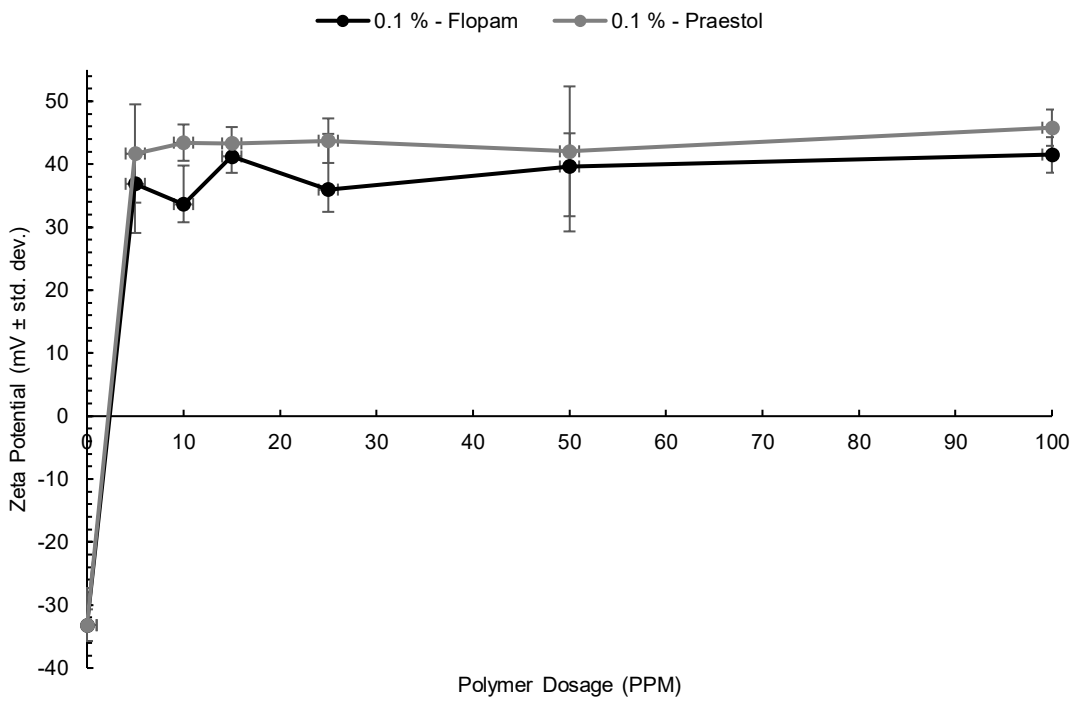


Figure 3-4: The effect of polymer dosage on zeta potential at low solids content (0.1 %).

At medium solids content, both polymers shifted suspensions to positive zeta potentials from 5 PPM (Figure 3-5). Flocculation performance remained high, as both polymers achieved maximum turbidity reductions of ~99 %. The occurrence of effective aggregation substantially away from near-neutral zeta values again indicates that charge neutralisation was not controlling. Instead, the results suggest a transitional regime where both bridging and patch adsorption contributed. A1 required a higher optimal dose (15 PPM), consistent with its lower charge density but sufficient chain length to form strong inter-particle bridges (Hoogeveen, 1996). A2 achieved optimal performance at 5 PPM, reflected rapid adsorption and patch-driven destabilisation. This mechanism is consistent with the electrostatic patch model described by Hocking et al. (1999), who showed that low molecular weight, high charge density polymers adsorb onto particle surfaces and undergo conformational changes that create localised charge patches. Notably, A1 maintained a broader effective dosage window, consistent with the greater stability of bridging flocs compared with the more fragile patch aggregates formed by A2 (Gregory & Barany, 2011).

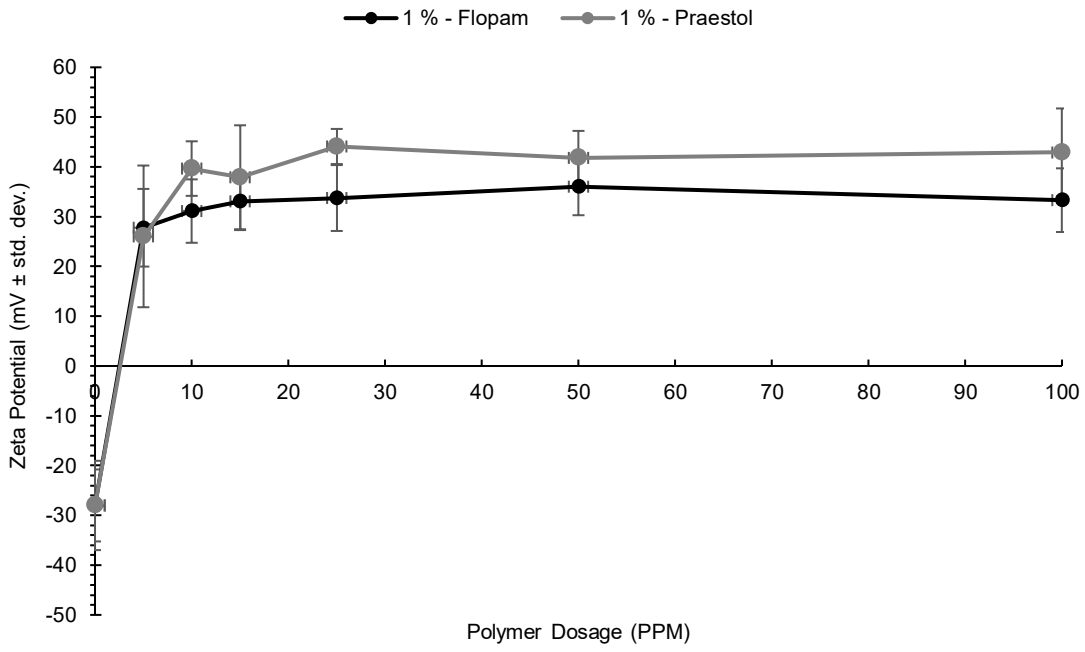


Figure 3-5: The effect of polymer dosage on zeta potential at medium solids content (1 %).

At high solids content, the polymers diverged in both zeta potential response (Figure 3-6). A1 presented a steady positive shift with increase dose, achieving a maximum zeta potential of +27.9 ± 15.5 mV at 100 PPM. This is the same dosage point where the system achieved its lowest turbidity of 0.5 ± 0.3 NTU at the highest dose. This progressive response reflects the capacity of A1's long linear chains to sustain bridging interactions under particle-rich conditions (Hoogeveen, 1996). In contrast, A2 presented a more irregular zeta potential profile, with the values fluctuating around neutrality across the dosage range. It reached a slightly positive value of + 2.6 ± 9.0 mV at 100 PPM. Despite this unstable electrostatic behaviour, the lowest turbidity (0.7 ± 0.38 NTU) was also observed at 100 PPM. The lack of alignment between near-neutral zeta potentials and flocculation efficiency indicates that charge neutralisation was not the operative mechanism. Instead, the pattern is more consistent with patch flocculation, arising from the uneven adsorption of its highly charged, branched polyamide structure. The narrower functional window and weaker bridging capacity compared with A1 highlight the steric constraints imposed by this architecture (Gregory & Barany, 2011; Hocking et al., 1999).

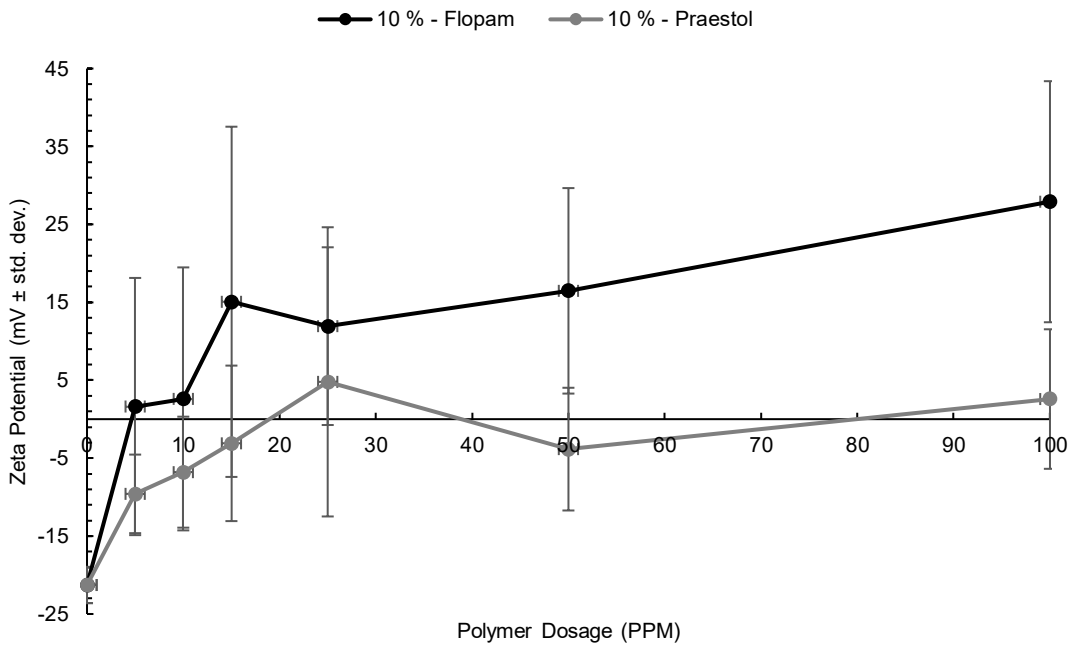


Figure 3-6: The effect of polymer dosage on zeta potential at high solids content (10 %).

3.1.3 Settled Bed Volume

The initial SBV values for low, medium and high solids contents were 4.6 ± 3.5, 47.5 ± 7.5 and 222.9 ± 17.7, respectively.

At low solids content, SBV for both polymers were relatively stable acres the tested dosage range (Figure 3-7*)*. A1 ranged from 9.7 ± 2.1 mL to 15.4 ± 1.7 mL, while A2 ranged from 8.2 ± 3.9 mL to 12.8 ± .7 mL. Given the magnitude of the standard deviations, these differences are not statistically significant, indicating that SBV was largely unaffected by polymer dose for both polymers under these conditions.

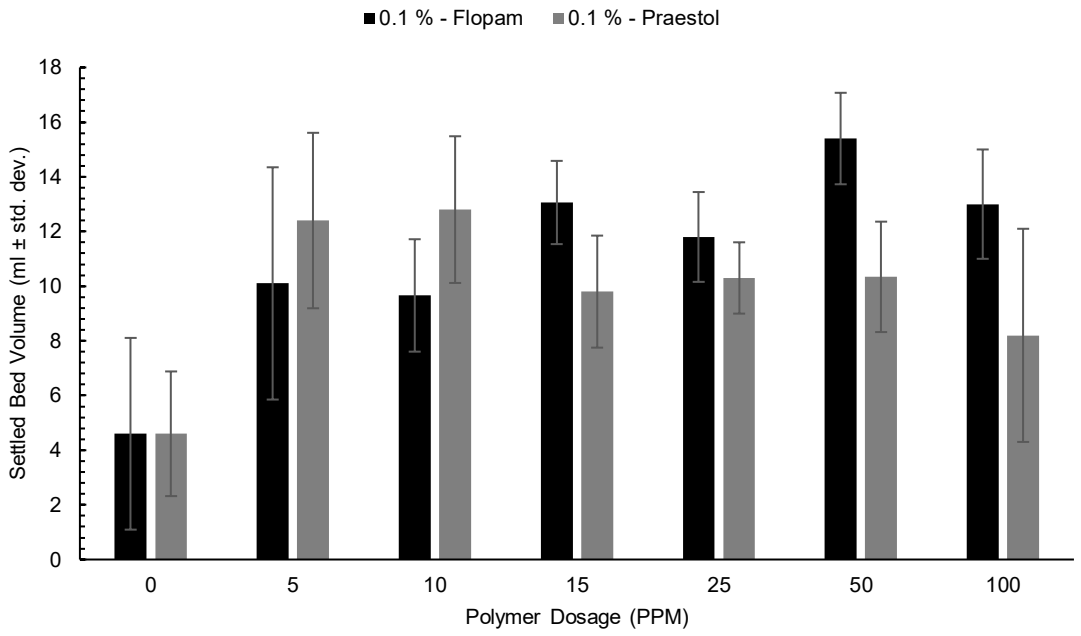


Figure 3-7: The effect of polymer dosage on settled bed volume at low solids content (0.1 %).

At medium solids content, both polymers exhibited their highest SBV values at the same dosages that achieved optimal turbidity reduction (Figure 3-8). For A1, SBV increased progressively with dose, reaching 119.8 ± 21.7 mL at 15 PPM. This is consistent with the development of an extended, open floc network formed through bridging interactions (Hogg, 2013). In contrast A1 peaked at 100.6 ± 23.7 mL at 5 PPM but then declined steadily to approximately 80 mL at higher dosages. This decline in SBV was observed with a deterioration of turbidity

reduction. The parallel decline in SBV and clarity beyond ~15 PPM indicates overdose-induced restabilisation, consistent with a narrow patch-driven window for A2, whereas A1's linear architecture sustains a more open floc network over a wider operational range (Palomino et al., 2010; Ziółkowska et al., 2011).

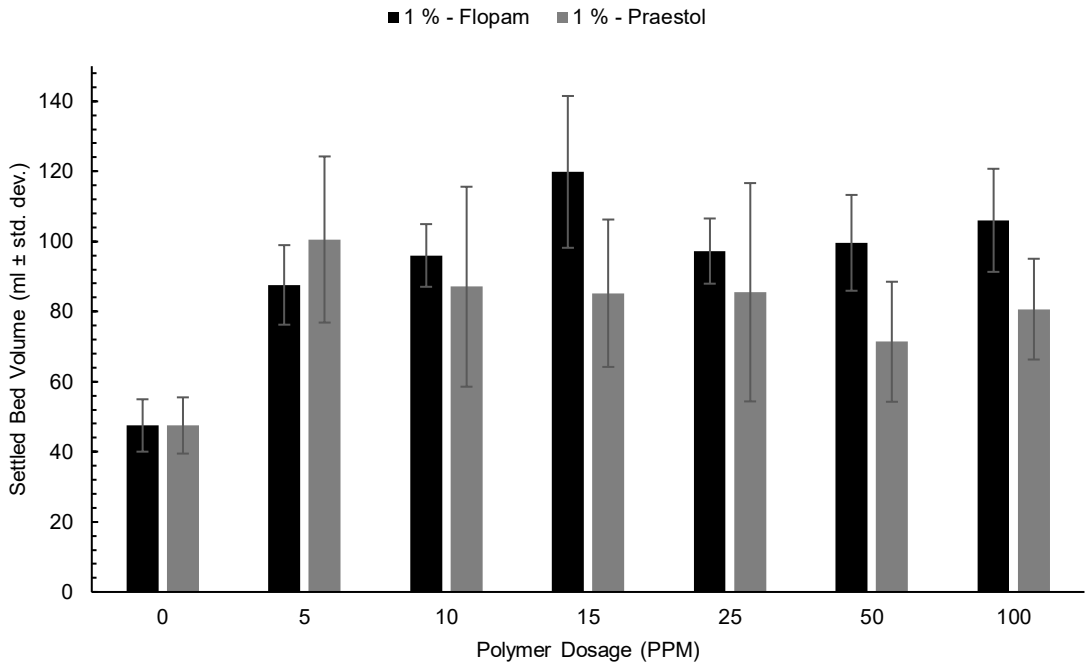


Figure 3-8: The effect of polymer dosage on settled bed volume at medium solids content (1 %).

At higher solids content, both polymers presented continuous SBV increases with the increase in polymer dosage (Figure 3-9). At 100 PPM, A1 achieved a max SBV of 416.6 ± 39.4 mL and A2 achieved a max SBV of 386.8 ± 62.6 ml. These trends reflect that neither system has experienced its overdosing thresholds, and thus, steric constraints were delayed as the available particle surfaces were not saturated (Fan et al., 2020). The 7 % greater max SBV achieved by A1 again confirms that the linear structure of A1 proved more effective at forming an extensive floc network.

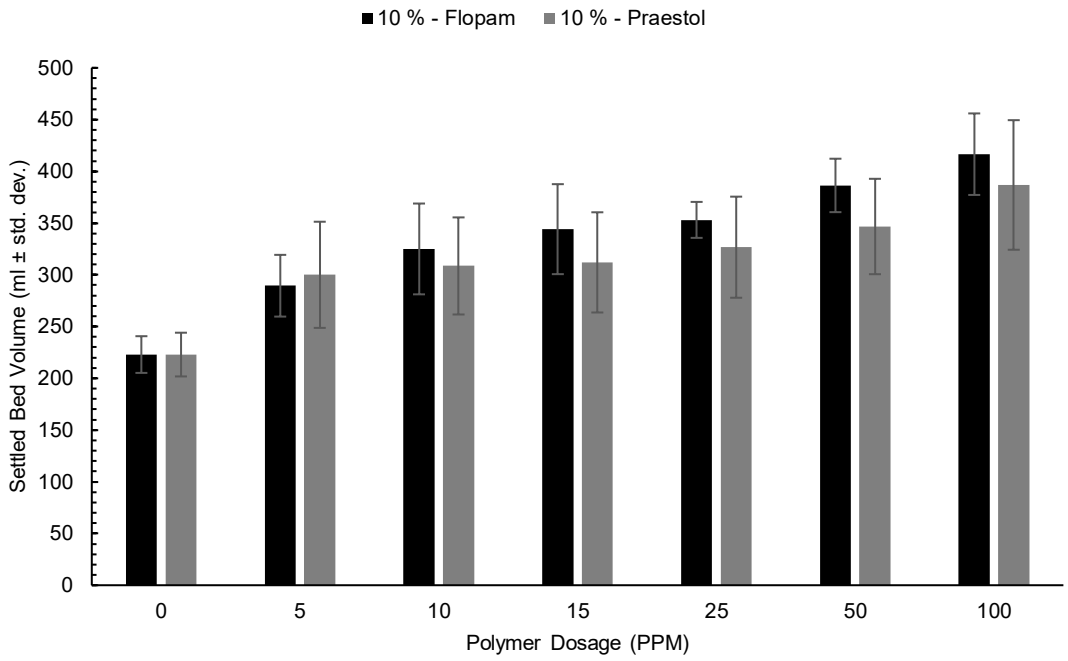


Figure 3-9: The effect of polymer dosage on settled bed volume at high solids content (10 %).

3.1.4 Total Organic Carbon and Adsorption Behaviour

Before the polymer addition, the initial measured TOC content of the IEX material for the low, medium and high solids content was 0.5 ± 0.4 mg/L, 0.6 ± 0.4 mg/L and 0.7 ± 0.1 mg/L, respectively. These values represent the baseline organic fraction present in the suspension solution.

At low solids content, analysis of residual TOC reveals that 5 PPM was a supra-optimal dose for both polymers, with less than 40 % of both polymers adsorbed (Figure 3-10). A1 demonstrated an optimal turbidity reduction of 1.7 ± 0.4 NTU at 5 PPM but presented a residual TOC of 1.7 ± 0.7 mg/L (68 % of the dosed polymer). A2 presented a slightly better adsorption efficiency of 37 %, with an observed residual TOC of 0.94 ± 0.4 mg/L at 5 PPM.

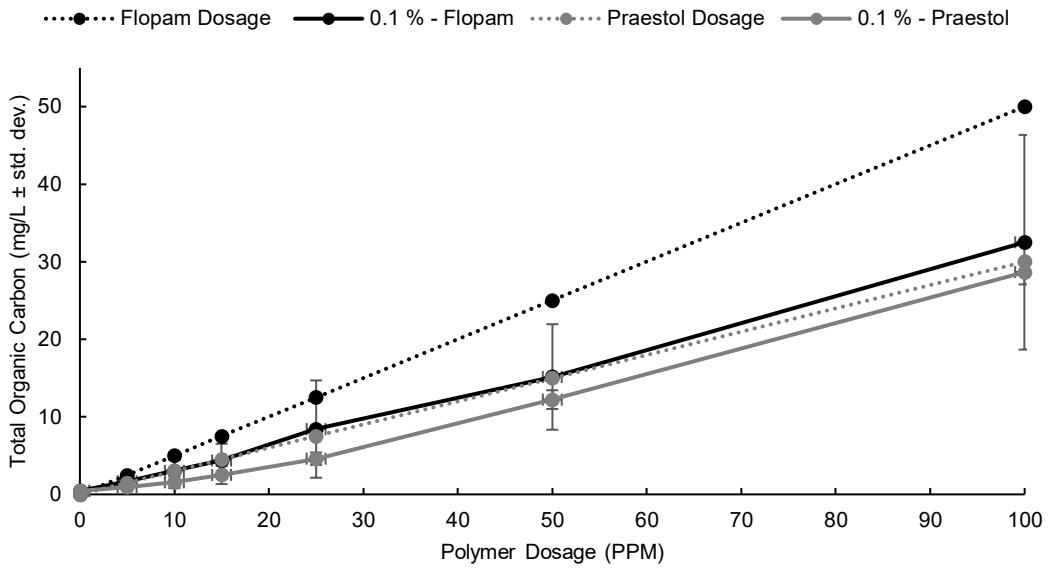


Figure 3-10: The effect of polymer dosage on residual TOC at low solids content (0.1 %).

At medium solids content, both polymers showed improved adsorption. A1 had an optimal turbidity dosage range up to 15 PPM with turbidity less than 2 NTU (Figure 3-11). This aligned with the gradual TOC increase from 1.1 ± 0.6 mg/L at 5 PPM to 6.5 ± 0.7 mg/L at 15 PPM. Notably, this increased to 30.5 ± 3.6 mg/L at 100PPM. This suggests that adsorption efficiency declines at dosages above 25 PPM, likely due to site saturation or polymer overdosing effects. A2 maintained a more consistent residual TOC below 3.0 mg/L until 25 PPM and then increased to 13.4 ± 12.7 mg/L at 100 PPM. This demonstrated the sensitivity of the polymer.

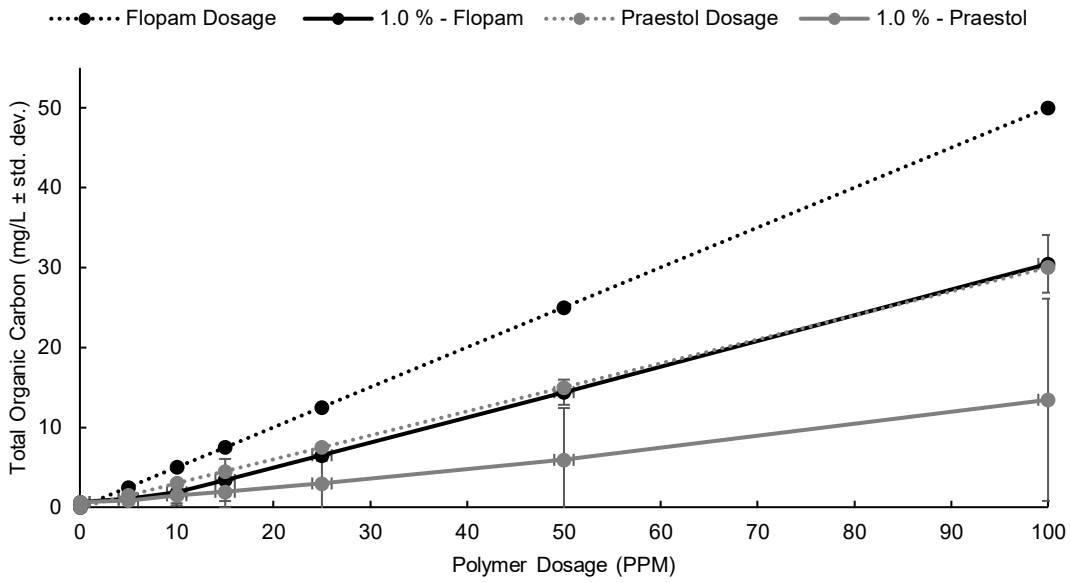


Figure 3-11: The effect of polymer dosage on residual TOC at low solids content (1 %).

At high solids content, both A1 and A2 presented near-complete polymer adsorption and sub-1 NTU (Figure 3-12). A1 maintained residual TOC values below 2.5 mg/L up to 50 PPM, which represents an adsorption efficiency greater than 90 %. A2 performed better adsorption ability, by having a measured residual TOC of less than 0.47 mg/L for all dosages. This confirms that the particle surfaces were sufficient to capture all dosed polymer, and the turbidity reduction was due to mixing kinetics rather than available polymer (Gregory & Barany, 2011).

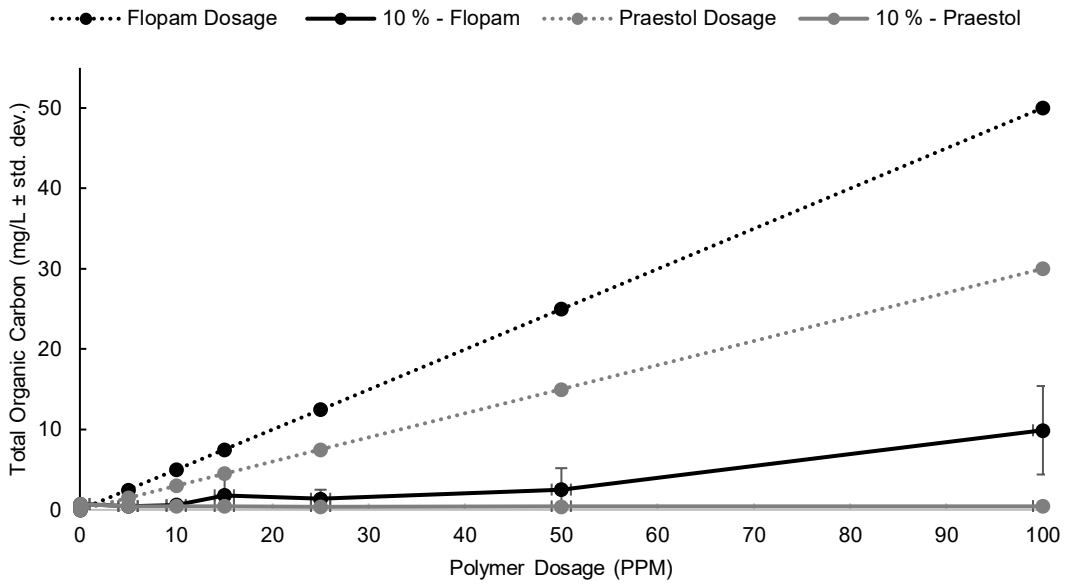


Figure 3-12: The effect of polymer dosage on residual TOC at high solids content (10 %).

3.1.5 Floc Size and Fractal Dimension

The maximum floc size was recorded for the medium solids content at a 10 % dilution (Table 3-1). This allowed for a maintained obscuration within the instrument's limits. The analysis focused on the optimal dosage range of 5–15 PPM. This range was selected because turbidity, settled bed volume, and residual TOC all showed their most favourable values within it.

At 5 PPM, both A1 and A2 produced similar floc sizes of 266 ± 4.1 and 267 ± 2.3 µm, respectively. This aligns with the near identical turbidity results of 1.4 ± 0.6 NTU and 1.07 ± 0.17 NTU at A1 and A2, respectively. As well as aligning with the zeta potential that indicated charge reversal for both polymers, confirming effective destabilisation. At higher dosages of 15 PPM, A2 formed significantly larger flocs (479 ± 8.0 µm) than A1 (382 ± 7.4 µm). This aligned with the higher SBV and lower residual TOC achieved by A2.

The fractal dimension (D_f) measurements provided additional information on the structural properties of the formed flocs (Table 3-2). A1 produced flocs that have high D_f values of 2.6, 2.8 and 3.0 at 5, 10 and 15 PPM, respectively. This high range indicates that the flocs are more dense and compact (Moruzzi et al., 2017).

This aligns with the A1's linear structure, which uses the mechanism of extended bridging to form a tighter floc network. In contrast, A2 maintained lower D_f values of 1.9 at 5, 10 and 15 PPM. This indicates that the floc structure was more open and loosely bound floc structure (Moruzzi et al., 2017). For overdose conditions, this floc structural morphology was prone to breakage, resulting in restabilsation of particles and elevated turbidity.

Table 3-1: Maximum floc size at the optimal dosage range for medium solids content at 10 % dilution.

Polymer Dosage	A1	A2
PPM	***µm***	***µm***
5	266 ± 4.1	267 ± 2.3
10	338 ± 12.3	398 ± 6.2
15	382 ± 7.4	479 ± 8.0

Table 3-2: Fractal dimension at the optimal dosage range for medium solids content at 10 % dilution.

Polymer Dosage	A1	A2
PPM		
5	2.6	1.9
10	2.8	1.9
15	3.0	1.9

3.1.6 Microscope Imagery

To further validate the particle size and fractal dimension results, microscope images were obtained. The microscope images shown in Figure 3-13 and Figure 3-14 show the distinct structural differences between the flocs formed by A1 and A2.

A1 flocs were consistent with the linear structure of the polymer, as it forms floc that can be characterised as connected in a “chain-like” formation (Eder et al., 2025). This results in floc morphology that is compact. While the recorded maximum floc size was 382 ± 7.4 µm, the microscope images clearly show the presence of many larger flocs exceeding 500 µm. This discrepancy is likely due to the larger flocs being denser and thus settling faster, which resulted in them not being captured in the slow mixing solution, so were not measured by the Mastersizer.

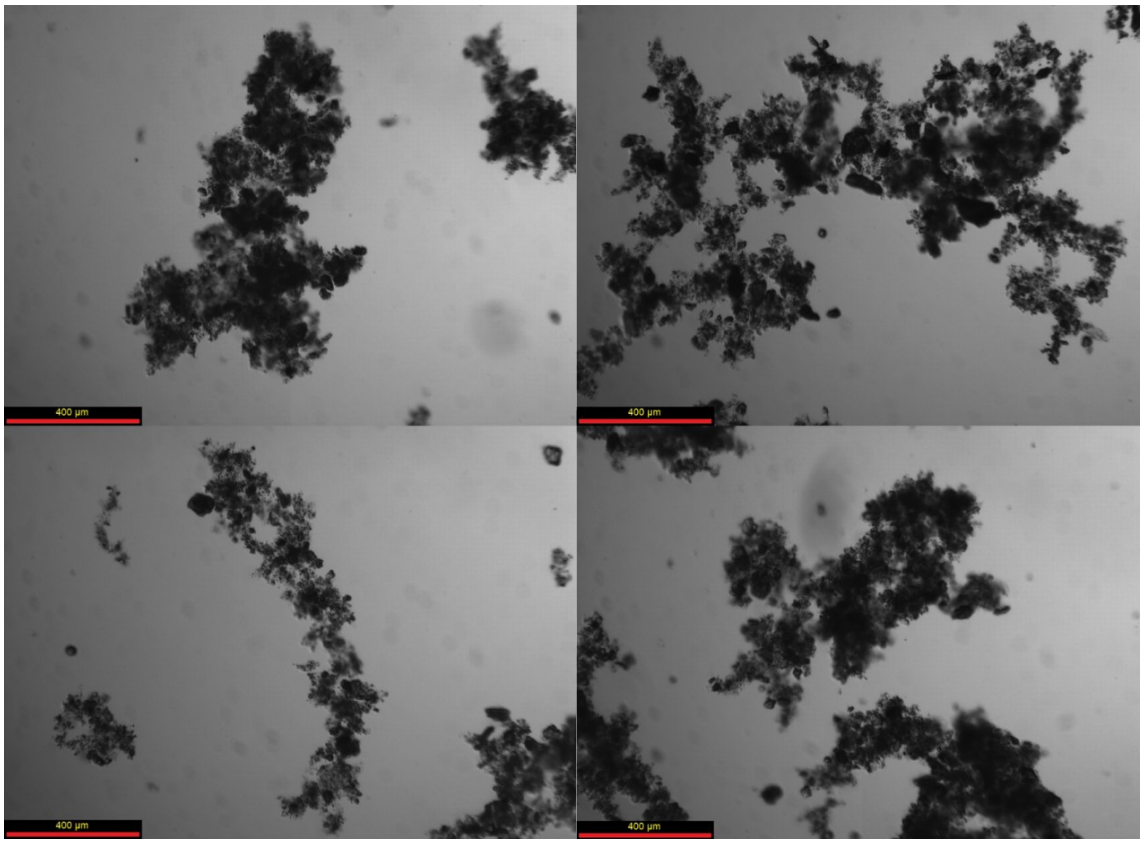


Figure 3-13: Example of microscope images of flocs formed by polymer A1.

The flocs formed by the branched polymer A2 presented Df data that indicated the flocs should be “fluffy” and open in structure (Moruzzi et al., 2017). However, the microscope images captured in Figure 3-14 show more dense and compact morphology compared to those formed by A1. The maximum size captured for A2 was 479 ± 8.0 µm and aligns with the sizes seen in the microscope images.

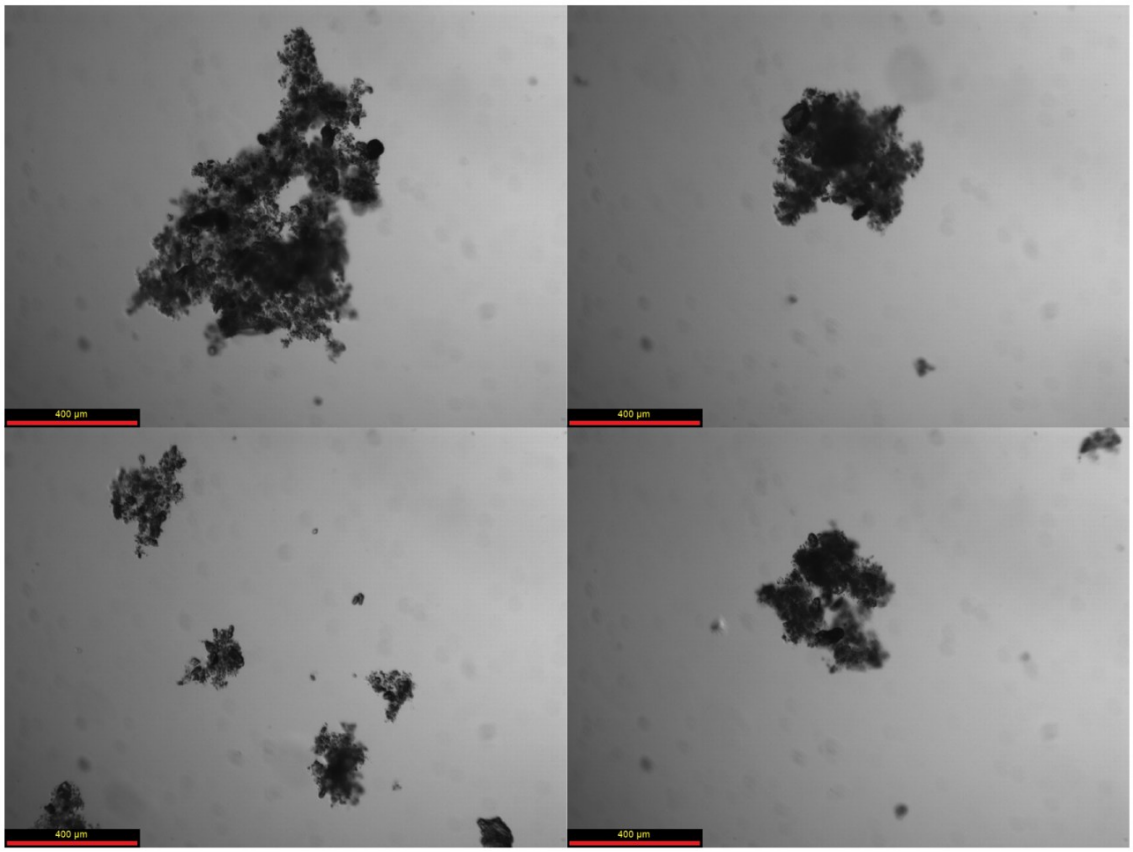


Figure 3-14: Example of microscope images of flocs formed by polymer A2.

3.2 Shear-Condition Results

3.2.1 Turbidity

At low solids content, A1 demonstrated effective shear resistance, maintaining consistently lower post-shear turbidity across the entire dosage range (Figure 3-15). This confirms that that flocs formed by A1 were robust as they withstood the mechanical shear and prevented the release of fines into suspension (Fan et al., 2020). In contrast, A2 was more dose dependent. At 5 PPM, shear improved turbidity by enhancing aggregation kinetics (Gregory & Barany, 2011). However, at high dosages, performance deteriorated.

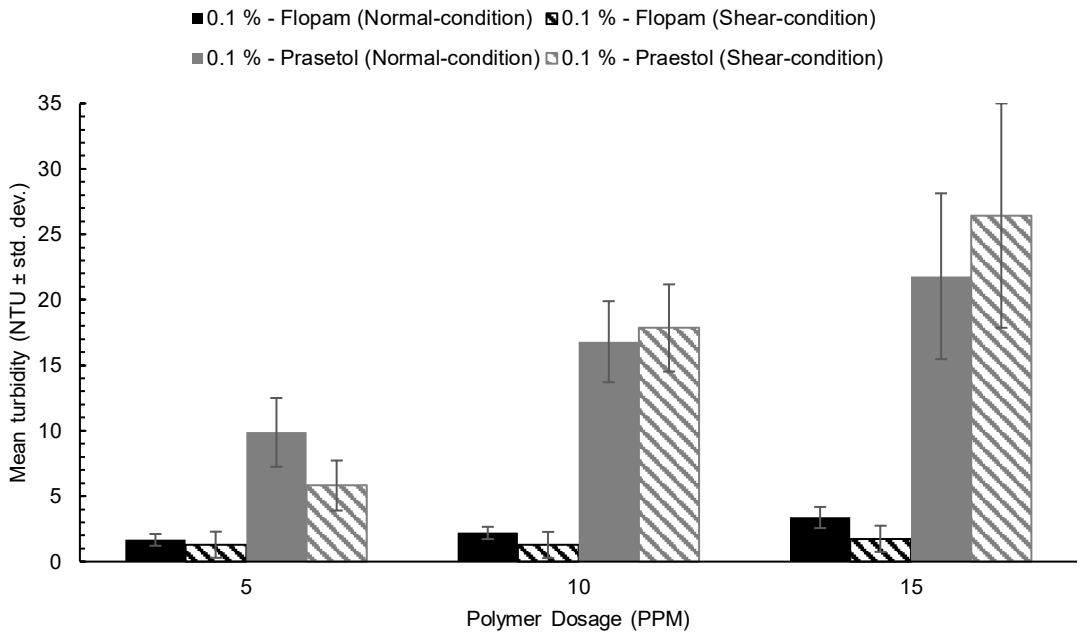


Figure 3-15: The effect of mechanical shear on turbidity at low solids content (0.1 %).

At medium solids content, an improving trend was observed for both polymers (Figure 3-16). Both polymers experienced an improved turbidity post-shear for the 10 and 15 PPM dosages. This trend indicates that the ability of flocs to resist or recover from shear is dosage-dependent, with optimal recovery occurring within a specific dosage range rather than at the minimum dose required for destabilisation.

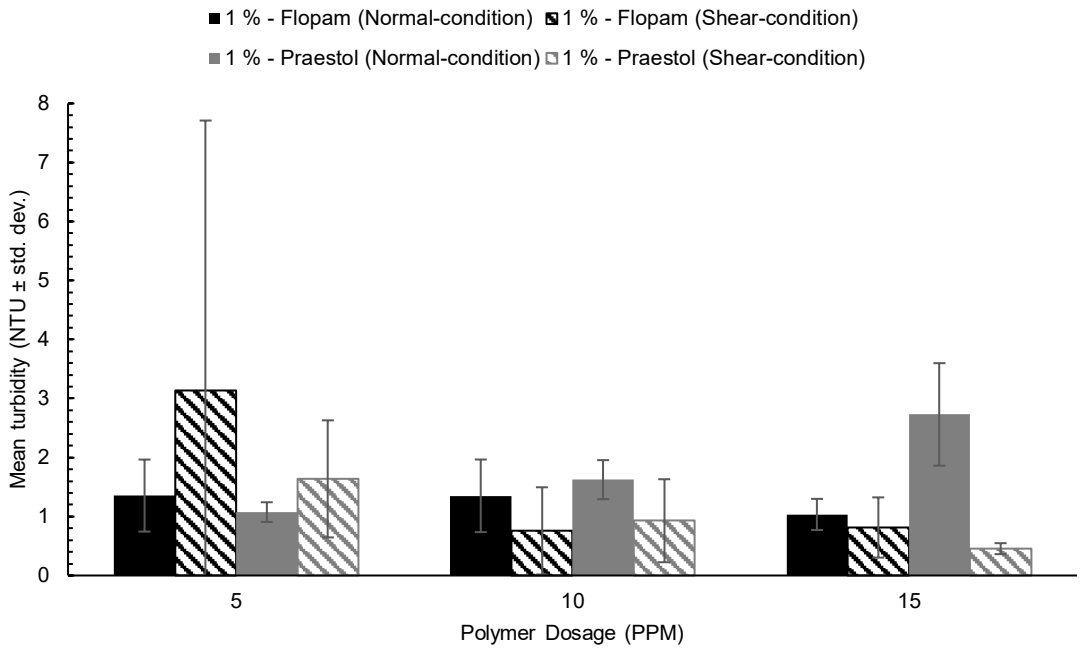


Figure 3-16: The effect of mechanical shear on turbidity at medium solids content (1 %).

At high solids content, neither polymer achieved lower post-shear turbidity values (Figure 3-17). Since neither polymer presented an overdosing trend, it was assumed that their optimal dosages would be greater than the dosages investigated in this study. This was further justified by the limited polymer observed in the supernatant. The results demonstrate that flocs formed at high solids content possessed ineffective shear-resistant properties. The consistent degradation in performance after shear application, combined with the absence of an overdosing trend, points to limited floc strength caused by insufficient polymer availability per particle (Hocking et al., 1999).

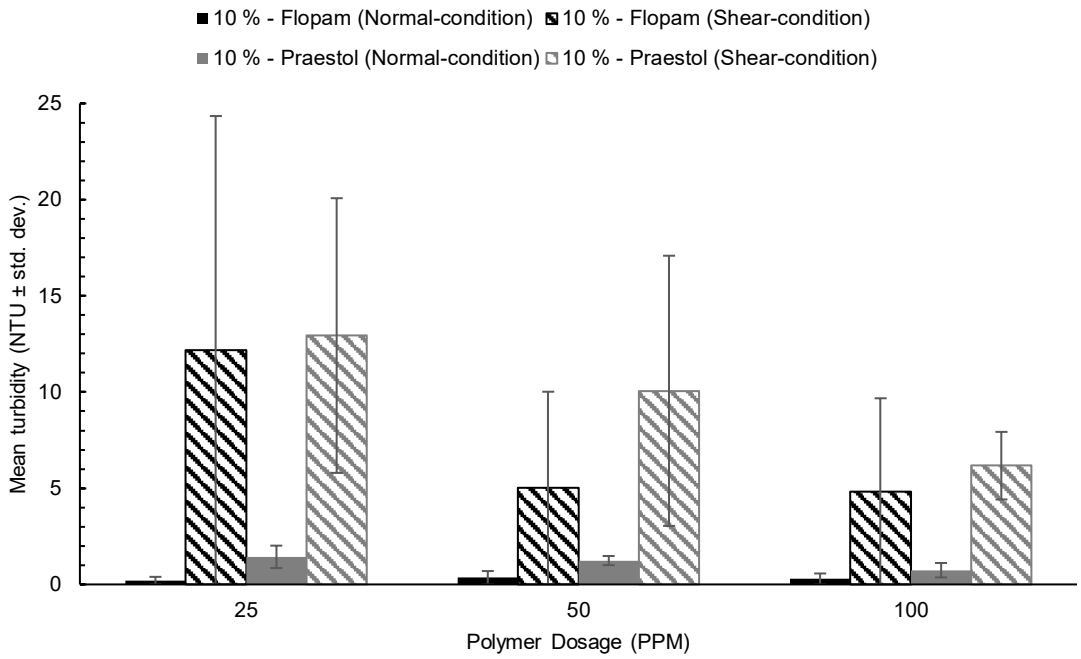


Figure 3-17: The effect of mechanical shear on turbidity at high solids content (10 %).

3.2.2 Settled Bed Volume

At low solids content, applied shear increased the SBV for both polymers, with A1 producing greater SBVs than A2 (Figure 3-18). This indicates that shear fractured the large flocs into smaller fragments that settled into a less compact, more open structure (Hocking et al., 1999). The higher SBV for A1 suggests its flocs fractured into larger, more voluminous fragments, while A2's flocs fragmented into finer particles that could pack slightly more densely (Fan et al., 2020).

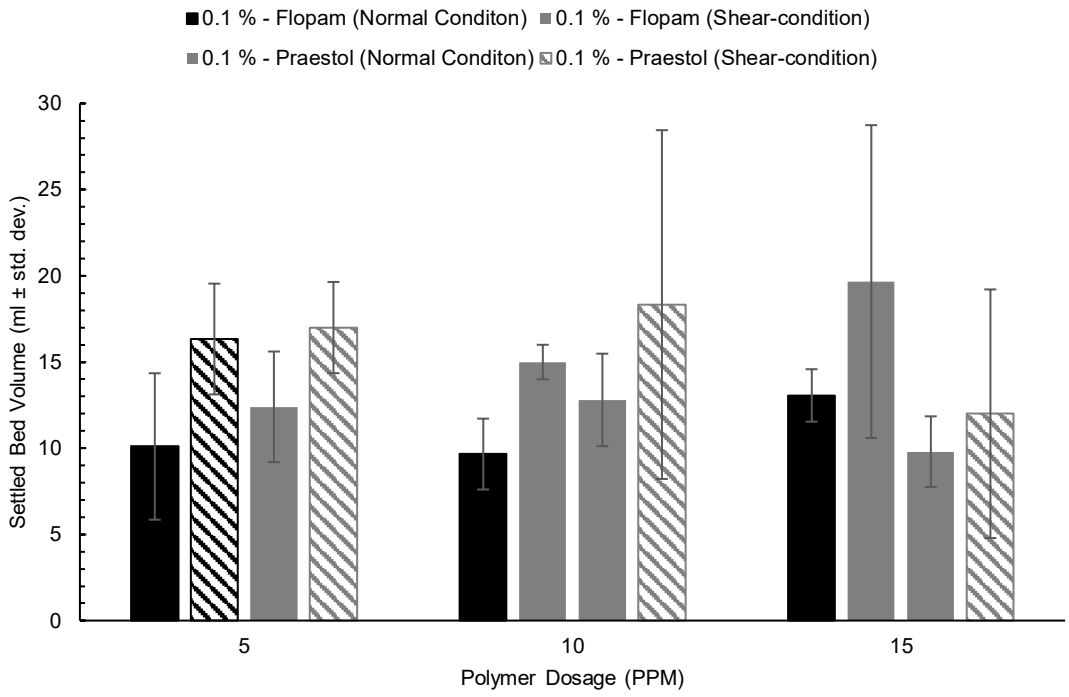


Figure 3-18: The effect of mechanical shear on settled bed volume at low solids content (0.1 %).

At medium solids content, the SBV response was polymer-dependent and aligned with the turbidity data (Figure 3-19). A1's sheared flocs settled into a more compact bed than under normal conditions. In contrast, A2's SBV values remained like normal conditions.

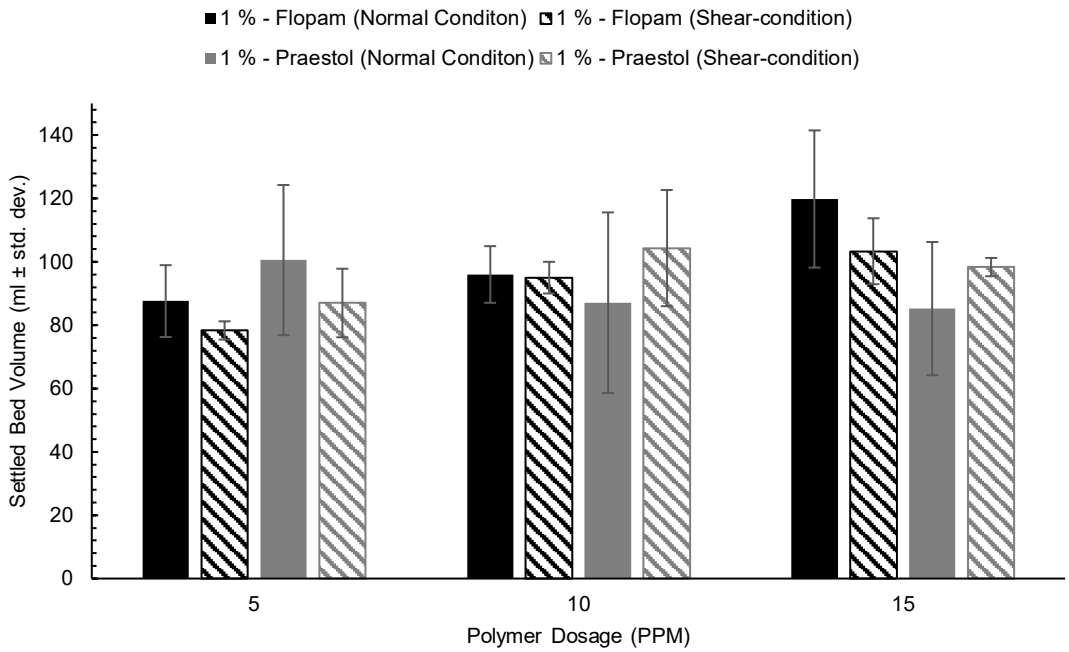


Figure 3-19: The effect of mechanical shear on settled bed volume at medium solids content (1 %).

At high solids content, the post-shear SBV for both polymers were significantly lower that the volumes achieved under normal conditions (Figure 3-20). While shear resulted in higher turbidity and SS concentration, it produced more compact bed volumes.

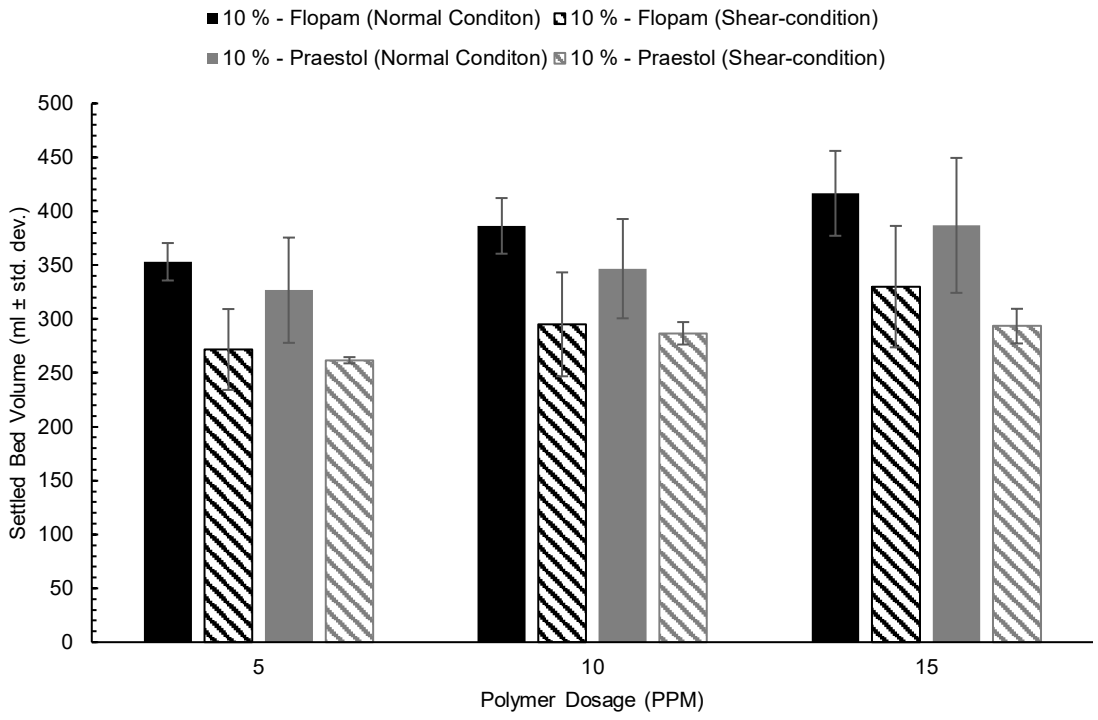


Figure 3-20: The effect of mechanical shear on settled bed volume at high solids content (10 %).

3.2.3 Total Organic Carbon and Adsorption Behaviour

At low solids content, residual TOC analysis revealed that shear significantly enhanced the adsorption of both polymers (Figure 3-21). A1 achieved residual TOC values of 0.9 ± 0.0, 2.8 ± 0.2 and 4.9 ± 0.2 mg/L at 5, 10 and 15 PPM, respectively. At 5 PPM, the post-shear residual TOC was 45 % lower than normal conditions. The improvement diminished with increasing dosage, as a 12 % increase was observed at 15 PPM. This suggests that although shear improved the adsorption at low doses, its linear structure may be susceptible to mechanical degradation at non-optimal concentrations. In contrast, A2 achieved a more significant improvement (> 50 %) in post-shear residual TOC compared to normal conditions. A2 achieved residual TOC of 0.5 ± 0.0, 0.5 ± 0.2 and 1.0 ± 0.1 mg/L at 5, 10 and 15 PPM, respectively. This demonstrates that shear forces enhanced the adsorption ability of A2's branched structure and thus improving its clarification performance.

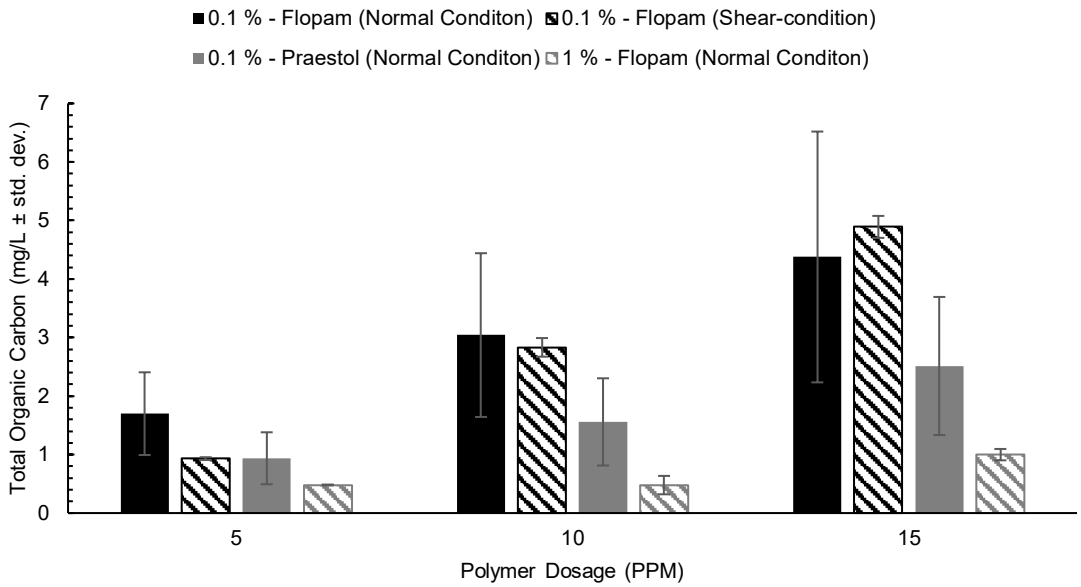


Figure 3-21: The effect of mechanical shear on residual TOC at low solids content (0.1 %).

At medium solids content, the residual TOC data confirmed shear-enhanced adsorption. Both polymers achieved near-background levels (< 0.9 mg/L) across all dosages (Figure 3-22). A1 achieved residual TOC of 0.2 ± 0.1, 0.3 ± 0.0 and 0.9 ± 0.3 mg/L at 5, 10 and 15 PPM, respectively. Similarly, A2 achieved residual TOC of 0.1 ± 0.2, 0.7 ± 1.1 and 0.2 ± 0.0 mg/L at the same dosages. These minimal values confirm that shear did not hinder adsorption but rather enhanced re-flocculation and settling efficiency (Mortimer & Fairweather, 2024).

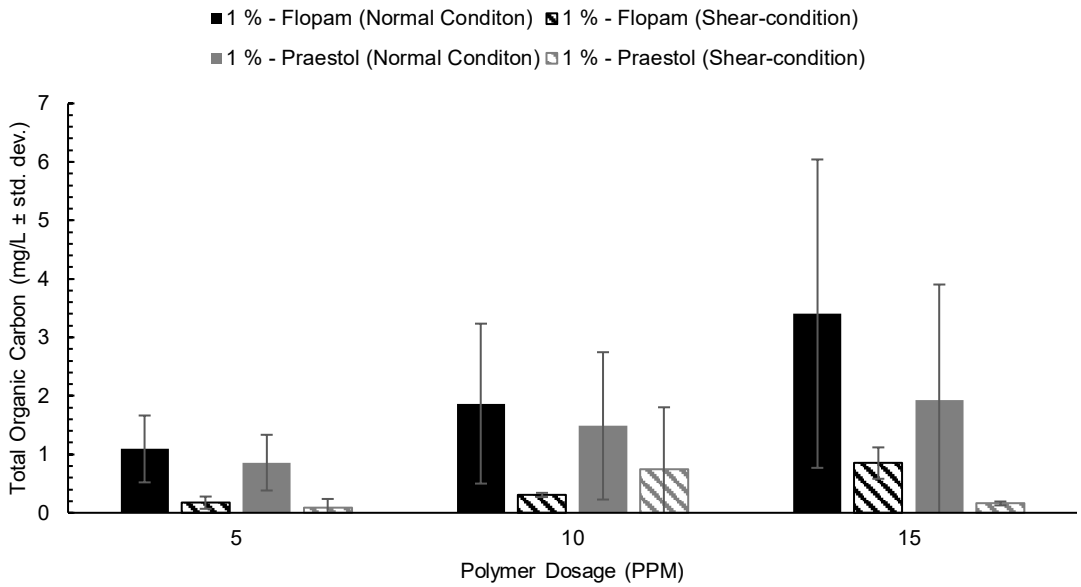


Figure 3-22: The effect of mechanical shear on residual TOC at medium solids content (1 %).

At high solids content, the residual TOC data validated the contrasting settling performance observed for A1 and A2. A1 maintained a consistently low post-shear residual TOC values of 0.7 ± 0.1, 0.9 ± 0.0 and 0.7 ± 0.0 mg/L at 5, 10 and 15 PPM, respectively (Figure 3-23). This aligns with the normal condition data, confirming that large particle surface area effectively adsorbed A1. In contrast, A2 achieved an increase in residual polymer post-shear, with values of 0.8 ± 0.1, 0.6 ± 0.0 and 0.7 ± 0.1 mg/L at 5, 10 and 15 PPM, respectively. This suggest that the shear forces desorbed a fraction of A2 from the particles. The excess polymer in the supernatant contributed to the stabilisation of fine particles (Hocking et al., 1999). This hindered effective re-flocculation, and thus poor clarification was observed (Figure 3-17).

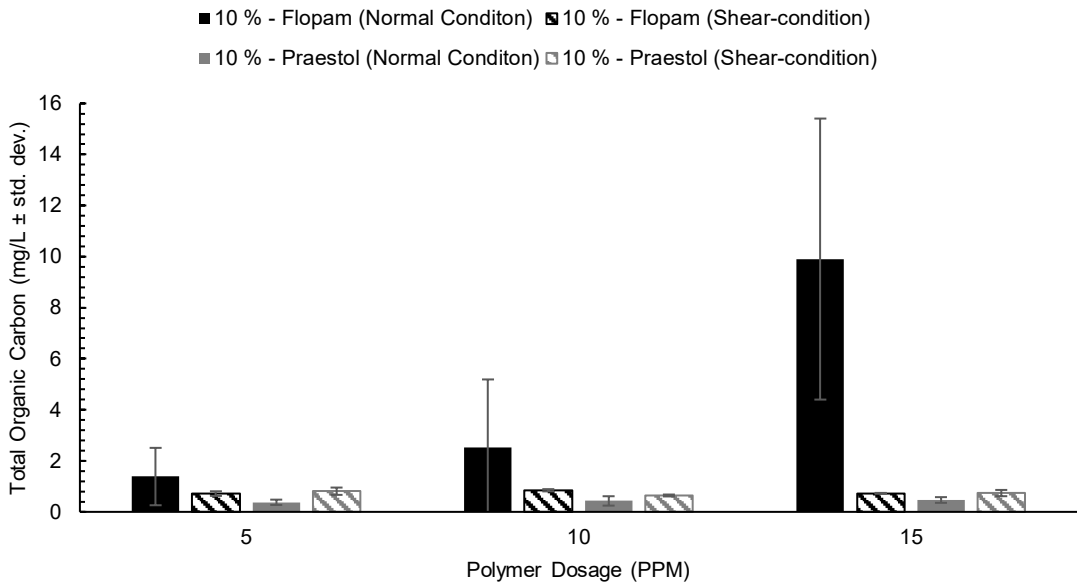


Figure 3-23: The effect of mechanical shear on residual TOC at high solids content (10 %).

3.2.4 Floc Size and Fractal Dimension

The flocs were subjected to shear forces and their minimum size and subsequent regrowth size were recorded alongside their fractal dimension values. The data proves that effective clarification performance post shear is not defined by the initial floc size but by the structural density and regrowth capacity.

Floc formed by A1 experienced significant fragmentation despite their highly compact floc structure (Table 3-3). Their floc sizes reduced by at least 59 %. This was evident with its lowest floc sizes ranging from 96, 141 and 151 µm at 5, 10 and 15 PPM respectively. Notably the broken flocs maintained high dimensional fractions of 2.7 and 2.8, at 5 and 10 PPM, respectively. The flocs formed by A2 which were inherently open and weak, were reduced in size by at least 48 %. This was evident with floc sizes reducing to 140, 180 and 250 µm at 5, 10 and 15 PPM, respectively. The sheared flocs maintained low fractal dimension values of 1.8, 1.8 and 1.9, at similar dosages. This confirms that the normal flocs fragmented into similar weak structures (Moruzzi et al., 2017).

The regrowth presented by A1 flocs demonstrated slight regrowth with sizes of 148, 168 and 184 µm at 5, 10 and 15 PPM, respectively (Table 3-4). These flocs

were highly compact with D_f values increasing to 2.7, 1.8 and 2.5 at similar doses (Moruzzi et al., 2017). In contrast, A2 showed more effective regrowth, with floc sizes of 171, 206 and 264 µm at 5, 10 and 15 PPM, respectively. However, the fractal dimension of the regrown flocs remained low at 1.8, 1.9 and 1.9 at similar doses (Moruzzi et al., 2017).

Table 3-3: Post-shear floc size responses for polymers A1 and A2 at medium solids content at 10 % dilution.

Polymer Dosage	A1		A2	
	Lowest Size	Regrowth Size	Lowest Size	Regrowth Size
PPM	*µm*		*µm*	
5	96	148	140	171
10	141	168	180	206
15	151	184	250	264

Table 3-4: Fractal dimension (D_f) of flocs post-shear at medium solids content at 10 % dilution.

Polymer Dosage	A1		A2	
	Lowest D_f	Regrowth D_f	Lowest D_f	Regrowth D_f
PPM				
5	2.7	2.7	1.8	1.8
10	1.4	1.8	1.8	1.9
15	2.8	2.5	1.9	1.9

3.2.5 Microscope Imagery

The post-shear microscope images of A1 confirm the quantitative data obtained from the laser diffraction analysis (Figure 3-24). The microscope images showed

a higher presence of smaller flocs (<170 μm), consistent with the observed Mastersizer data. Despite the fragmentation, the individual flocs appear to retain their dense, “chain-like” structure with dark, irregular clusters being present. This aligns with the high D_f values measured that indicated the large flocs broke at weak points but overall, the structure stayed the same. Notably, there are micro-flocs dispersed consistently across the visual fields. This represents the eroded fines that were not recaptured and led to the increase in turbidity and suspended solids.

The microscope images of sheared A2 flocs reveal a wide variety of floc structures that correspond with poor recovery (Figure 3-25). The background was filled with a haze of unaggregated colloidal fines, that provide visual evidence of the ineffective re-flocculation which led to higher turbidity. Notably, the images contained with large, “stringy and fluffy” flocs that appear more open and looser than those formed under normal conditions. The structures are due to the fragmented flocs re-adhering in a poor manner.

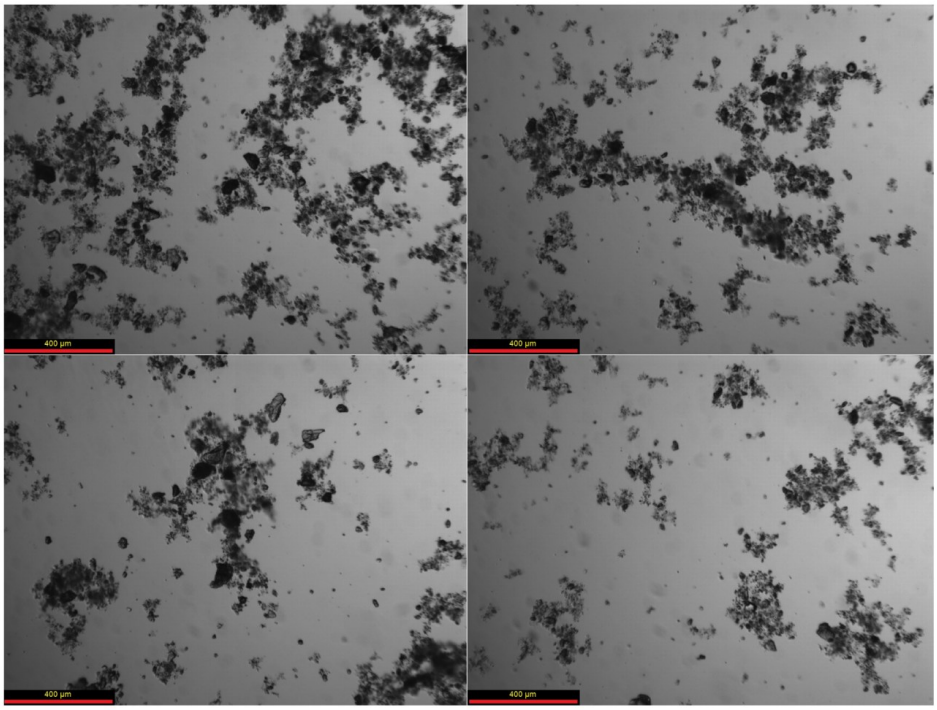


Figure 3-24: Example of microscope images of post-shear flocs formed by polymer A1

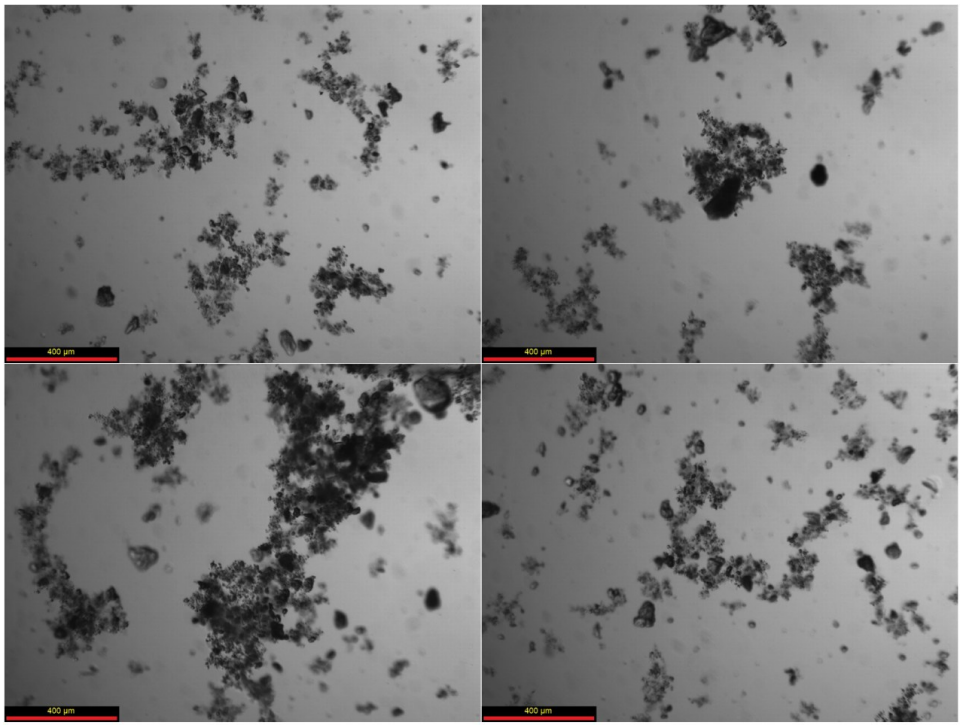


Figure 3-25: Example of microscope images of post-shear flocs formed by polymer A2

4 Discussion

4.1 Polymer Selection for Variable Sludge Conditions: Implications for Sellafield

The flocculation behaviour of clinoptilolite suspensions is highly sensitive to solids concentration, with each phase (dilute, medium, and dense) presenting a different dose response curve in terms of polymer efficacy (Chen et al., 2002). At Sellafield, the variability in solids concentration reflects a diverse range of waste stream compositions, from freshly diluted to more consolidated legacy sludges. This inconsistency presents challenges in polymer dosing, risking both under- and over-dosing. To maintain effective flocculation without the need for precise real-time adjustments, polymers must be robust enough to perform across fluctuating solids concentrations.

Sellafield faces the dual challenge of managing sludge both safely and efficiently, striking a delicate balance between rapid processing and the need for robust, adaptable solutions. The varying solids concentrations across storage tanks require a polymer that performs reliably across a broad spectrum of conditions.

A1 (linear polyacrylamide) and A2 (branched polyamine) were compared to evaluate their performance across varying solids concentrations (Table 4-1). This offered insights into their effectiveness in handling Sellafield's fluctuating waste stream conditions.

Table 4-1:comparative performance of Flopam (A1) and Praestol (A2) polymers across key flocculation parameters.

Parameter	Flopam (A1)	Praestol (A2)
Turbidity Reduction	Effective across a wide range of dosages, achieving the lowest turbidity values	Narrow optimal dosage range with higher turbidity at higher dosages due to particle restabilisation.

Parameter	Flopam (A1)	Praestol (A2)
Zeta Potential	Shifts to positive values	Shifts to more significantly positive values
Flocculation Mechanism	Polymer bridging	Patch flocculation
Settled Bed Volume	High SBVs	Lower SBVs
Max Floc Size	382 ± 7.4 μm	479 ± 8.0 μm
Fractal Dimension	High (~ 2.8), reflecting dense, stable flocs.	Low (~ 1.9), reflecting fragile, loose flocs.
Shear Resilience	Floc regrowth to ~ 50 % of their original size	Floc regrowth to ~ 58 % of their original size

A1 consistently demonstrated superior performance across a wide range of solids concentrations. It achieved optimal turbidity reduction and formed dense, compact flocs due to its polymer bridging mechanism. This ability to form stable, compact flocs that settle effectively aligns with previous studies in wastewater treatment, where linear polymers have been shown to be highly efficient in aggregating particles across varying solid conditions, particularly in high-solids suspensions (Mahadevan & Valiyaveettil, 2025). A1's high shear resilience ensures that flocs maintain their integrity under mechanical stress, an essential feature for solid-liquid separation in industrial applications (Fan et al., 2020). Moreover, the high fractal dimension of the flocs generated by A1 underscores the strength and robustness of the flocs, which are critical for stable settling under the fluctuating sludge conditions at Sellafield (Zhang et al., 2017).

Conversely, A2 predominantly operates via patch flocculation, resulting in the formation of larger but weaker flocs. Branched polymers tend to produce larger aggregates, yet their structural integrity is often compromised due to the nature of their architecture, leading to looser flocs prone to shear breakage (Lim et al.,

2022). This fragility aligns with other studies of branched flocculants, which are less shear-resistant and less effective in recovering from floc breakage, especially under harsh mechanical conditions (Fan et al., 2020; Mortimer & Fairweather, 2024). While A2 showed some efficiency in consolidation at lower dosages, its limited regrowth potential and narrow dosage range make it less adaptable in environments where sludge composition fluctuates.

Based on the performance comparison of (A1) and (A2) across varying solids concentrations, FLOPAM FO 4650 MPM (A1) is recommended as the polymer of choice for Sellafield's SIXEP plant. Based on the experimental results, the target operational dosage ranges were determined as follows:

- Low solids (0.1 %): 5 – 10 PPM
- Medium solids (1 %): 10 – 15 PPM
- High solids (10 %): 50 – 100 PPM

4.2 Study Limitations

This study was conducted under controlled laboratory conditions, which simplify real-life complexities. The use of synthetics suspension, while necessary for controlled experimentation, may not fully represent the chemical heterogeneity of the actual SIXEP sludges. The jar tests, while standard, do not replicate the hydraulic shear profiles and flow dynamics that would be experienced from large-scale equipment.

4.3 Future research directions

To translate these foundational findings into industrial practice, future work should focus on two research. The first is pilot-scale validation using continuous-flow systems and authentic SIXEP sludge samples. This will assess the performance under realistic chemical and hydraulic conditions. The second is tracing the partitioning od key radionuclides is necessary to ensure the treatment process effectively isolates and concentrates the contaminants within the sludge phase.

5 Conclusion

5.1 Synthesis of Findings

This study demonstrated that the flocculation performance and shear resilience of cationic polymers for nuclear sludge treatment depends on both solids content and molecular architecture. The key findings have as summarised as follows:

Flopam FO 4650 MPM:

- Optimal turbidity reduction across a wide range of solids concentrations.
- Dense, compact flocs formed due to polymer bridging, leading to efficient settling and minimised SBV.
- Higher shear resilience, with flocs maintaining 50 % regrowth after shear, indicating strong floc stability under mechanical stress.
- High fractal dimension (~2.8), reflecting the compact and stable structure of flocs, critical for effective solid-liquid separation in Sellafield's fluctuating sludge conditions.
- Target dosages:
    - Low solids concentration: 5 – 10 PPM
    - Medium solids concentration: 10 – 25 PPM
    - High solids concentration: 25 – 50 PPM

Praestol DW31:

- Narrow optimal dosage range, with higher turbidity at higher dosages due to particle restabilisation.
- Larger but weaker flocs formed by patch flocculation, leading to less effective settling and higher SBV at dosages outside the narrow optimal window.
- Poorer shear resilience, with flocs showing limited regrowth (58 %) after shear, indicating fragility under mechanical stress.
- Low fractal dimension (~1.9), reflecting loose and fragile flocs, prone to breakage and less effective in turbulent conditions.
- Limited adaptability in environments with fluctuating solids concentrations, making it less suitable for Sellafield's diverse sludge characteristics.

- Target dosages:
    - Low solids concentration: 5 – 10 PPM (with caution to avoid overdosing)
    - Medium solids concentration: 10 – 15 PPM (must avoid exceeding this range)
    - High solids concentration: 50 – 100 PPM

5.2 Recommendations

Based on the comprehensive experimental findings of this study, Flopam FO 4650 MPM (A1) is the recommended as the preferred polymeric flocculant. It demonstrated superior clarification efficiency, sludge compaction and shear resilience across a range of solids concentrations. Based on the experimental results, the target operational dosage ranges were determined as follows:

- Low solids (0.1 %): 5 – 10 PPM
- Medium solids (1 %): 10 – 15 PPM
- High solids (10 %): 50 – 100 PPM

Flopam FO 4650 MPM (A1) is a robust and operationally practical choice for the complex sludge suspensions inherent to the SIXEP plant at Sellafield.

5.3 Contribution to knowledge

This study provides an original contribution to the field of colloidal science and nuclear wastewater by establishing a mechanistic framework for flocculation in ion-exchange (IEX) sludges, presenting the relationship between polymer molecular structure with flocculation performance and quantifying shear resilience and regrowth potential. These findings provide foundational data for future work.

References

Ajaya Bhattarai. (2020). A Review on Polyelectrolytes (PES) and Polyelectrolyte Complexes (PECs). *International Journal of Engineering Research And*, *V9*(08). https://doi.org/10.17577/IJERTV9IS080112

Anitas, E. M. (2020). Small-angle scattering from fractals: Differentiating between various types of structures. *Symmetry*, *12*(1). https://doi.org/10.3390/SYM12010065

Bartiko, D., & De Julio, M. (2014). *ESTUDO DA QUEBRA E RECRESCIMENTO DE FLOCOS EMPREGANDO UM EQUIPAMENTO DE MONITORAMENTO CONTÍNUO DA FLOCULAÇÃO STUDY OF FLOCS BREAKING AND REGROWTH EMPLOYING A CONTINUOS MONITORING OF FLOCCULATION EQUIPMENT*. *23*(2), 101–108.

Bolto, B., & Gregory, J. (2007). Organic polyelectrolytes in water treatment. In *Water Research* (Vol. 41, Issue 11, pp. 2301–2324). Elsevier Ltd. https://doi.org/10.1016/j.watres.2007.03.012

Chen, T., Maltesh, C., & Somasundaran, P. (2002). Effect of Solids Concentration on Polymer Adsorption and Conformation. In *Water Soluble Polymers* (pp. 23–30). Springer US. https://doi.org/10.1007/0-306-46915-4_2

Committee of Public Accounts. (2025). *Decommissioning Sellafield*. www.parliament.uk/copyright.

Eder, E. J. S., Karami, A., Heimovaara, T. J., Wolthers, M., & Jansen, B. (2025). Investigating the parameters influencing floc formation. *Journal of Water Process Engineering*, *70*, 107126. https://doi.org/10.1016/J.JWPE.2025.107126

Estrada, D., Echeverry, L., Ramirez, A., & Gutierrez, L. (2020). Molybdenite flotation in the presence of a polyacrylamide of low anionicity subjected to different conditions of mechanical shearing. *Minerals*, *10*(10), 1–12. https://doi.org/10.3390/min10100895

Fan, Y., Ma, X., Song, S., Dong, X., Chen, R., & Dong, Y. (2020). Effect of shear-induced breakage and reflocculation on the floc structure, settling, and dewatering of coal tailings. *Physicochemical Problems of Mineral Processing*, *56*(2), 363–373. https://doi.org/10.37190/ppmp/118148

Gregory, J., & Barany, S. (2011). Adsorption and flocculation by polymers and polymer mixtures. In *Advances in Colloid and Interface Science* (Vol. 169, Issue 1, pp. 1–12). Elsevier B.V. https://doi.org/10.1016/j.cis.2011.06.004

Herbert H. Espy. (1995). *The mechanism of wet-strength development in paper: a review*.

Hocking, M. B., Klimchuk, K. A., & Lowen, S. (1999). Polymeric flocculants and flocculation. *Journal of Macromolecular Science - Reviews in Macromolecular Chemistry and Physics*, *39 C*(2), 177–203. https://doi.org/10.1081/mc-100101419

Hogg, R. (2013). *Bridging Flocculation by Polymers*.

Hoogeveen, N. G. (1996). *Adsorption of polyelectrolytes and charged block copolymers on oxides consequences for colloidal stability*.

Hua, G., & Hamburg, J. (2020). *Using Flocculation to Reduce Turbidity of Construction Site Runoff*.

International Atomic Energy Agency. (2002). *Technical Reports Series No.408 Application of Ion Exchange Processes for the Treatment of Radioactive Waste and Management of Spent Ion Exchangers.*

International Atomic Energy Agency. (2011). *IAEA Safety Standards Disposal of Radioactive Waste for protecting people and the environment*. http://www-ns.iaea.org/standards/

International Commission on Radiological Protection. (1998). *Radiation Protection Recommendations as Applied to the Disposal of Long-lived Solid Radioactive Waste*. https://journals.sagepub.com/doi/pdf/10.1177/ANIB_28_4

Jackson, L. A. (2022). Polyelectrolyte polymers—Types, forms, and function. *Water-Formed Deposits: Fundamentals and Mitigation Strategies*, 747–764. https://doi.org/10.1016/B978-0-12-822896-8.00013-3

Johnson, K. S., & Pytkowicz, R. M. (1981). The activity of NaCl in seawater of 10–40‰ salinity and 5–25°C at 1 atmosphere. In *Marine Chemistry* (Vol. 10).

Li, B., & Chen, M. (2024). A comprehensive review on treatment technologies of spent ion exchange resins in nuclear power plants. *Environmental Chemical Engineering*, *12*(5).

Lim, V. H., Yamashita, Y., Ogawa, K., & Adachi, Y. (2022). Comparison of cationic flocculants with different branching structure for the flocculation of negatively charged particles coexisting with humic substances . *Journal of Environmental Chemical Engineering*, *10*(5).

Lockwood, A. P. G. (2021). *The Impact of Polymeric Flocculants on the Sedimentation, Flotation and Dewatering of Radwaste Suspensions*.

López-Maldonado, E. A., Oropeza-Guzmán, M. T., & Ochoa-Terán, A. (2014). Improving the efficiency of a coagulation-flocculation wastewater treatment of the semiconductor industry through zeta potential measurements. *Journal of Chemistry*, *2014*. https://doi.org/10.1155/2014/969720

Mahadevan, G., & Valiyaveettil, S. (2025). Structure – Function Correlation of Branched and Linear Polyaramides for Removal of Pollutants from Water. *RSC Applied Polymers*. https://doi.org/10.1039/d5lp00114e

Mortimer, L. F., & Fairweather, M. (2024). *Role of Shear Rate on Adsorption Conformation in Polymer-Induced Flocculation Simulations*. American Institute of Physics. https://eprints.whiterose.ac.uk/

Moruzzi, R. B., de Oliveira, A. L., da Conceição, F. T., Gregory, J., & Campos, L. C. (2017). Fractal dimension of large aggregates under different flocculation conditions. *Science of the Total Environment*, *609*, 807–814. https://doi.org/10.1016/j.scitotenv.2017.07.194

Nan, J., Yao, M., Chen, T., Li, S., Wang, Z., & Feng, G. (2016). Breakage and regrowth of flocs formed by sweep coagulation using additional coagulant of poly aluminium chloride and non-ionic polyacrylamide. *Environmental Science and Pollution Research*, *23*(16), 16336–16348. https://doi.org/10.1007/s11356-016-6805-z

Nyström, F., Nordqvist, K., Herrmann, I., Hedström, A., & Viklander, M. (2020). Laboratory scale evaluation of coagulants for treatment of stormwater. *Journal of Water Process Engineering*, *36*. https://doi.org/10.1016/j.jwpe.2020.101271

Palomino, D., Hunkeler, D., & Stoll, S. (2010). *Comparison of two cationic polymeric flocculant architectures on the destabilization of negatively charged latex suspensions*. *52*(44).

RS Minerals Ltd. (2025). *Tech - ZeoClin (0-200 microns)*.

SNF. (2017). *Powders Beads Poudres Billes*. https://www.snf.co.za/wp-content/uploads/2017/08/Flopam.pdf

Solensis. (2021). *PraestolTM DW31 Coagulant TM Safety Data Sheet*.

Wallace, S. H., Shaw, S., Morris, K., Small, J. S., Fuller, A. J., & Burke, I. T. (2012). *Effect of groundwater pH and ionic strength on strontium sorption in aquifer sediments: Implications for 90 Sr mobility at contaminated nuclear sites*.

World Nuclear Association. (2025, March 21). *Nuclear Fuel Cycle Overview*. https://world-nuclear.org/information-library/nuclear-fuel-cycle/introduction/nuclear-fuel-cycle-overview

Zhang, L., Min, F., Wang, L., & Shu, Q. (2022). Polymeric flocculants based on the interfacial characteristics of fine clay minerals: A review. *Physicochemical Problems of Mineral Processing*, *58*(4), 1–17. https://doi.org/10.37190/ppmp/149652

Ziółkowska, D., Kutsevol, N., Bezuglyi, M., & Shyichuk, A. (2011). Comparative study of branched and linear polymers for the regulation of clay dispersion stability. *Molecular Crystals and Liquid Crystals*, *536*, 173/[405]-181/[413]. https://doi.org/10.1080/15421406.2011.538604

Appendices

Appendix A

A.1 AI Tools Acknowledgement

I used AI-based tools (such as ChatGPT and Grammarly) to support improvements in sentence structure and grammar. All research content, analysis, and conclusions are my own.

Appendix B

B.1 Jar testing matrix composition

Jar Testing Matrix Composition

No.	IEX Solids Content (v/v%)	Ionic Strength (M)	FLOPAM FLO 4560 MPM (PPM)	Praestol DW31 (PPM)
1	10	0.03	0	-
2	10	0.03	5	-
3	10	0.03	10	-
4	10	0.03	15	-
5	10	0.03	25	-
6	10	0.03	50	-
7	10	0.03	100	-
8	1	0.03	0	-
9	1	0.03	5	-
10	1	0.03	10	-
11	1	0.03	15	-
12	1	0.03	25	-
13	1	0.03	50	-
14	1	0.03	100	-
15	0.1	0.03	0	-
16	0.1	0.03	5	-

No.	IEX Solids Content (v/v%)	Ionic Strength (M)	FLOPAM FLO 4560 MPM (PPM)	Praestol DW31 (PPM)
17	0.1	0.03	10	-
18	0.1	0.03	15	-
19	0.1	0.03	25	-
20	0.1	0.03	50	-
21	0.1	0.03	100	-
22	10	0.03	-	0
23	10	0.03	-	5
24	10	0.03	-	10
25	10	0.03	-	15
26	10	0.03	-	25
27	10	0.03	-	50
28	10	0.03	-	100
29	1	0.03	-	0
30	1	0.03	-	5
31	1	0.03	-	10
32	1	0.03	-	15
33	1	0.03	-	25
34	1	0.03	-	50
35	1	0.03	-	100

No.	IEX Solids Content (v/v%)	Ionic Strength (M)	FLOPAM FLO 4560 MPM (PPM)	Praestol DW31 (PPM)
36	0.1	0.03	-	0
37	0.1	0.03	-	5
38	0.1	0.03	-	10
39	0.1	0.03	-	15
40	0.1	0.03	-	25
41	0.1	0.03	-	50
42	0.1	0.03	-	100

B.2 TOC Content Calculations

Total Organic Carbon (TOC) concentration

$$TOC\left(\frac{mgC}{L}\right) = C_f \, x \, D$$

D = polymer dosage (mg/L), C_f = carbon mass fraction of the polymer

Flopam FO 4650 MPM (A1)

C_f = 0.5 (assumed for polyacrylamide-based flocculants)

Dosage (PPM)	TOC (mgC/L)
5	2.5
10	5.0
15	7.5
25	12.5
50	25
100	50

Praestol DW31 (A2)

C_f = 0.3

Dosage (PPM)	TOC (mgC/L)
5	1.5
10	3.0
15	4.5
25	7.5
50	15
100	30

Appendix C

C.1 Summary of Experimental Lab Work

Summary

This sheet has all the mean results from each test against the polymer and dosage as well as report tables and figures

FLOPAM - Normal	TURBIDITY			Zeta Potential			Suspended Solids			Settled Bed Volume			Total Organic Carbon			Max Floc Size	Lowest Shear Floc Size	Regrowth Shear Floc Size	Fractal Dimension - Normal	Fractal Dimension - Shear (Lowest Size)	Fractal Dimension - Shear (Regrowth Size)
Polymer Dosage	NTU			mV			g/L			ml			mg/L			um	um	um			
PPM	0.10	1.00	10.00	0.10	1.00	10.00	0.10	1.00	10.00	0.10	1.00	10.00	0.10	1.00	10.00	1.00	1.00	1.00	1.00	1.00	1.00
0	49.78	147.74	128.37	-33.20	-28.01	-21.28	1.72	2.24	2.35	4.60	47.50	222.92	0.46	0.64	0.74						
5	1.66	1.35	4.53	36.90	27.77	1.62	1.69	1.57	1.68	10.10	87.60	289.44	1.70	1.09	0.45	232	96	148	2.60	2.69	2.74
10	2.19	1.35	2.00	33.68	31.12	2.60	1.74	1.77	1.73	9.66	96.00	325.00	3.04	1.87	0.61	394	141	168	2.80	1.37	1.77
15	3.37	1.03	0.86	41.25	33.08	15.06	1.85	1.53	1.64	13.06	119.84	344.11	4.38	3.41	1.81	384	151	184	3.03	2.75	2.50
25	4.70	1.65	0.59	35.99	33.74	11.94	2.37	1.98	2.16	11.80	97.25	353.06	8.42	6.51	1.38						
50	7.20	4.04	0.48	39.66	36.02	16.47	2.45	2.15	2.18	15.40	99.60	386.36	15.14	14.39	2.52						
100	12.51	8.64	0.45	41.55	33.31	27.91	2.58	2.11	2.08	13.00	106.03	416.56	32.51	30.47	9.90						

Praestol - Normal	TURBIDITY			Zeta Potential			Suspended Solids			Settled Bed Volume			Total Organic Carbon			Max Floc Size	Lowest Shear Floc Size	Regrowth Shear Floc Size	Fractal Dimension - Normal	Fractal Dimension - Shear (Lowest Size)	Fractal Dimension - Shear (Regrowth Size)
Polymer Dosage	NTU			mV			g/L			ml			mg/L			um	um	um			
PPM	0.10	1.00	10.00	0.10	1.00	10.00	0.10	1.00	10.00	0.10	1.00	10.00	0.10	1.00	10.00	1.00	1.00	1.00	1.00	1.00	1.00
0	49.78	147.74	128.37	-33.20	-28.01	-21.28	1.72	2.24	2.35	4.60	47.50	222.92	0.46	0.64	0.74						
5	9.87	1.07	4.67	41.72	26.04	-9.59	1.65	1.74	2.32	12.40	100.55	300.00	0.94	0.86	0.45	267	140	171	1.86	1.75	1.82
10	16.80	1.62	2.95	43.44	39.66	-6.80	1.70	1.21	2.34	12.80	87.08	308.56	1.56	1.49	0.45	398	180	206	1.90	1.79	1.85
15	21.80	2.73	2.41	43.32	37.91	-3.10	1.66	1.42	2.42	9.80	85.22	312.00	2.51	1.93	0.47	479	250	264	1.91	1.85	1.87
25	35.27	15.54	1.43	43.76	44.10	4.79	2.09	1.60	2.34	10.30	85.51	326.67	4.60	2.98	0.38						
50	36.75	43.50	1.24	42.07	41.80	-3.84	2.07	2.12	2.35	10.34	71.38	346.67	12.22	5.93	0.43						
100	37.00	43.90	0.74	45.82	42.89	2.58	2.13	1.80	2.40	8.20	80.68	386.83	28.66	13.44	0.47						

0.93 7% 0.16

FLOPAM - Shear	TURBIDITY				Suspended Solids			Settled Bed Volume			Total Organic Carbon		
Polymer Dosage	NTU				g/L			ml			mg/L		
PPM	0.10	1.00	10.00		0.10	1.00	10.00	0.10	1.00	10.00	0.10	1.00	10.00
0	49.78	147.74	128.37		1.72	2.24	2.35	4.60	47.50	222.92	0.46	0.64	0.74
5	1.29	3.13			1.37	1.78		16.33	78.33		0.93	0.17	
10	1.27	0.76			1.43	1.55		15.00	95.00		2.83	0.31	
15	1.75	0.81			1.55	1.55		19.67	103.33		4.89	0.85	
25			18.79				1.83			271.67			0.72
50			11.14				1.85			295.00			0.85
100			7.31				1.75			330.00			0.73

Praestol DW31 - Shear	TURBIDITY				Suspended Solids			Settled Bed Volume			Total Organic Carbon		
Polymer Dosage	NTU				g/L			ml			mg/L		
PPM	0.10	1.00	10.00		0.10	1.00	10.00	0.10	1.00	10.00	0.10	1.00	10.00
0	49.78	147.74	128.37		1.72	2.24	2.35	4.60	47.50	222.92	0.46	0.64	0.74
5	5.81	1.64			1.57	1.67		17.00	87.00		0.48	0.09	
10	17.85	0.93			1.68	1.55		18.33	104.33		0.48	0.74	
15	26.43	0.45			1.30	1.68		12.00	98.33		1.00	0.16	
25			12.94				2.00			261.67			0.81
50			10.06				1.82			286.67			0.64
100			6.17				1.73			293.33			0.74

Appendix D : Flopam (A1) Results

D.1 Turbidity

Turbidity

The following results were captured using a turbiditimeter.

Suspension Solution and FLOPAM FO 4650 MPM

No.	IEX Solids (v/v%)	Ionic Strength (M)	Polymer Dosage (PPM)	Raw Data (NTU)																		Mean (NTU)	Standard Deviation (NTU)
1	10	0.03	0	143	198	139	196	110	93.8	136	65	74.5										128.37	47.8
2	10	0.03	5	4.83	10	5.2	3.21	5.02	1.03	2.4												4.5	2.9
3	10	0.03	10	2.05	2.97	3.53	1.3	1.59	1.02	1.57												2.0	0.9
4	10	0.03	15	0.991	0.693	0.788	1.39	0.818	0.664	0.657												0.9	0.3
5	10	0.03	25	0.786	0.763	0.612	0.649	0.452	0.269													0.6	0.2
6	10	0.03	50	0.906	1.12	0.191	0.225	0.367	0.398	0.4	0.198											0.5	0.3
7	10	0.03	100	0.734	0.375	0.189	0.197	0.777														0.5	0.3
8	1	0.03	0	177	70.6	96.6	201		240	110	139											147.7	60.9
9	1	0.03	5	0.855	0.72	0.572	2.15	2.11	1.47	1.26	1.7											1.4	0.6
10	1	0.03	10	1.97	1.95	2.2	0.526	0.935	1.25	0.813	1.16											1.4	0.6
11	1	0.03	15	0.789	1.15	1.18	0.724	1.33														1.0	0.3
12	1	0.03	25	0.783	1.67	3	1.15															1.7	1.0
13	1	0.03	50	2.16	5.25	6.27	2.46															4.0	2.0
14	1	0.03	100	3.01	10.6	12.4	8.53															8.6	4.1
15	0.1	0.03	0	65	74.5	42.3	60.8	45.3	43.7	27.4	22.4	68.3	68.5	37.9	41.2							49.8	17.2
16	0.1	0.03	5	1.79	1.26	1.36	1.22	2.28	2.06													1.7	0.4
17	0.1	0.03	10	2.79	2.6	1.84	1.77	1.96														2.2	0.5
18	0.1	0.03	15	4.73	3.08	2.88	3.45	2.71														3.4	0.8
19	0.1	0.03	25	3.89	4.89	4.96	5.06															4.7	0.5
20	0.1	0.03	50	6.23	9.37	6																7.2	1.9
21	0.1	0.03	100	12.3	17.1	8.12																12.5	4.5

No.	IEX Solids (v/v%)	Ionic Strength (M)	Polymer Dosage (PPM)	Raw Data (NTU) - shear																		Mean (NTU)	Standard Deviation (NTU)
1	10	0.03	0	143	198	139	196	110	93.8	136	65	74.5	.									128.37	47.8
5	10	0.03	25	27.7	30.8	9.23	7.41															18.79	12.2
6	10	0.03	50	14.7	13.3	5.41																11.14	5.0
7	10	0.03	100	10.1	10.1	1.72																7.31	4.8
8	1	0.03	0	177	70.6	96.6	201	0	240	110	139											129.28	76.9
9	1	0.03	5	0.661	0.676	2.48	11.2	0.638														3.13	4.6
10	1	0.03	10	0.461	0.479	0.53	0.355	2.26	0.452													0.76	0.7
11	1	0.03	15	0.497	0.464	0.288	1.48	1.41	0.741													0.81	0.5
15	0.1	0.03	0	65	74.5	42.3	60.8	45.3	43.7	27.4	22.4	68.3	68.5									51.82	18.2
16	0.1	0.03	5	0.807	2.22	0.847	1.15	1.42														1.29	0.6
17	0.1	0.03	10	0.947	1.53	1.03	1.58															1.27	0.3
18	0.1	0.03	15	1.35	2.56	1.79	1.28															1.75	0.6

D.2 Zeta Potential

Zeta-Potential

The following results were captured using a zetasizer.

Suspension Solution and FLOPAM FO 4650 MPM

| No. | IEX Solids (v/v%) | Ionic Strength (M) | Polymer Dosage (PPM) | Raw Data | | |

D.3 Suspended Solids

Suspended Solids

The following results were captured using filter paper, vacuum suction pump and 105'C oven

Conversion	
2ml	1
1L	500

Suspension Solution and FLOPAM FO 4650 MPM

No.	IEX Solids (v/v%)	Ionic Strength (M)	Polymer Dosage (PPM)	Raw Data (g/L)										Mean (g/L)	Standard Deviation (g/L)
1	10	0.03	0	2.45	2.95	1.9	2	2.45						2.35	0.42
2	10	0.03	5	1.45	0.8	0.7	1.85	3.15	1.95	1.85				1.68	0.82
3	10	0.03	10	1.35	0.9	0.4	2	3.1	2.15	2.2				1.73	0.91
4	10	0.03	15	1.2	0.55	0.6	1.85	3.1	2.15	2				1.64	0.92
5	10	0.03	25	1.35	1.9	3.1	2.25	2.2						2.16	0.64
6	10	0.03	50	1.35	1.9	3.05	2.3	2.3						2.18	0.62
7	10	0.03	100	1.25	1.75	2.8	2.3	2.3						2.08	0.59
8	1	0.03	0	3.3	3.1	1.2	2	1.65	2.2					2.24	0.82
9	1	0.03	5	1.70	1.40	1.85	0.9	1.85	1.75					1.57	0.37
10	1	0.03	10	1.85	2.05	2	1	2	1.7					1.77	0.40
11	1	0.03	15	1.80	1.90	2.1	0.75	1.85	0.8					1.53	0.60
12	1	0.03	25	1.25	0.75	1.9	3	3.2	1.8					1.98	0.96
13	1	0.03	50	2.45	0.8	1.45	3.15	3.25	1.8					2.15	0.97
14	1	0.03	100	1.4	0.9	1.75	3.4	3.3	1.9					2.11	1.02
15	0.1	0.03	0	1.65	1.95	1.6	1.9	1.95	1.5	1.5	1.9			1.72	0.21
16	0.1	0.03	5	1.45	1.75	1.4	2.2	1.45	1.9					1.69	0.32
17	0.1	0.03	10	1.75	1.55	1.7	1.7	2						1.74	0.16
18	0.1	0.03	15	1.85	1.85	1.85	1.75	1.95						1.85	0.07
19	0.1	0.03	25	1.85	3.2	2.05								2.37	0.73
20	0.1	0.03	50	2.05	3.25	2.05								2.45	0.69
21	0.1	0.03	100	1.85	3.7	2.2								2.58	0.98

1 2 3 4 5 6 7

No.	IEX Solids (v/v%)	Ionic Strength (M)	Polymer Dosage (PPM)	Raw Data (g/L)										Mean (g/L)	Standard Deviation (g/L)
2	10	0.03	5	1.75	1.9									1.83	0.11
3	10	0.03	10	1.8	1.9									1.85	0.07
4	10	0.03	15	1.8	1.7									1.75	0.07
9	1	0.03	5	1.70	1.85									1.78	0.11
10	1	0.03	10	1.70	1.40									1.55	0.21
11	1	0.03	15	1.80	1.30									1.55	0.35
16	0.1	0.03	5	1.45	1.3									1.37	0.11
17	0.1	0.03	10	1.35	1.5									1.43	0.11
18	0.1	0.03	15	1.7	1.4									1.55	0.21

D.4 Settled Bed Volume

Settled Bed Volume

The following results were captured using a cylindrical flask, images and a ruler.

Suspension Solution and FLOPAM FO 4650 MPM

No.	IEX Solids (v/v%)	Ionic Strength (M)	Polymer Dosage (PPM)	Raw Data (ml)																Mean (ml)	Standard Deviation (ml)
1	10	0.03	0	200	240	220	210	250	235	220	240	210	225	245	205	198				222.9	17.7
2	10	0.03	5	320	340	300	260	280	295	300	260	250								289.4	29.8
3	10	0.03	10	380	360	400	295	315	305	305	290	275								325.0	43.9
4	10	0.03	15	420	392	380	310	325	325	345	300	300								344.1	43.5
5	10	0.03	25	332.5	330	360	372	380	350	350	350									353.1	17.4
6	10	0.03	50	352.5	350	368.4	400	420	400	400	400									386.4	25.8
7	10	0.03	100	362.5	475	380	440	460	395	420	400									416.6	39.4
8	1	0.03	0	50	45	55	40	35	50	60	45	50	55							47.5	7.5
9	1	0.03	5	80	78	80	100	100												87.6	11.3
10	1	0.03	10	110	100	90	90	90												96.0	8.9
11	1	0.03	15	136	148.2	95	110	110												119.8	21.7
12	1	0.03	25	108	106	104	100	90	80	95	95									97.3	9.3
13	1	0.03	50	116	110	102	110	78.8	80	100	100									99.6	13.7
14	1	0.03	100	124	118	116	115	95.2	80	100	100									106.0	14.7
15	0.1	0.03	0	2	1	5	10	5												4.6	3.5
16	0.1	0.03	5	9	9	4.5	12	16												10.1	4.2
17	0.1	0.03	10	8	8	9.3	13	10												9.7	2.1
18	0.1	0.03	15	12	12	15.3	14	12												13.1	1.5
19	0.1	0.03	25	13	11	10	14	11												11.8	1.6
20	0.1	0.03	50	16	18	14	14	15												15.4	1.7
12	0.1	0.03	100	14	10	12	14	15												13.0	2.0

1 2 3 4 5 6

No.	IEX Solids (v/v%)	Ionic Strength (M)	Polymer Dosage (PPM)	Raw Data (ml)																Mean (ml)	Standard Deviation (ml)
2	10	0.03	25	250	250	315														271.7	37.53
3	10	0.03	50	260	275	350														295.0	48.22
4	10	0.03	100	295	300	395														330.0	56.35
9	1	0.03	5	80	80	75														78.3	2.89
10	1	0.03	10	100	90	95														95.0	5.00
11	1	0.03	15	100	95	115														103.3	10.41
16	0.1	0.03	5	20	15	14														16.3	3.21
17	0.1	0.03	10	14	15	16														15.0	1.00
18	0.1	0.03	15	13	30	16														19.7	9.07

D.5 Total Organic Carbon Concentration

Total Organic Carbon

The following results were captured using a TOC-analyser

Total Organic Carbon and FLOPAM FO 4650 MPM

No.	IEX Solids (v/v%)	Polymer Dosage (PPM)	Raw Data (mg/L)													Mean (mg/L)	Standard Deviation (mg/L)
1	10	0	0.6626	0.81												0.7	0.1
2	10	5	0.1429	0.00157	0.6469	0.2771	0.6132	1.001								0.4	0.4
3	10	10	0.7186	0.5587	0.4203	0.5372	0.5045	0.931								0.6	0.2
4	10	15	1.625	6.838	0.6826	0.3024	0.6471	0.7945								1.8	2.5
5	10	25	2.747	2.875	0.7628	0.303	0.8949	0.7188								1.4	1.1
6	10	50	5.697	6.177	0.2794	0.9523	1.198	0.8105								2.5	2.7
7	10	100	14.7	16.76	9.716	7.53	1.205	9.508								9.9	5.5
8	1	0	1.074	0.9636	0.7475	0.1849	0.2517									0.6	0.4
9	1	5	1.857	0.8328	1.536	0.6775	0.5578					0.4418				1.1	0.6
10	1	10	1.134	1.064	4.29	1.3	1.547					1.135				1.9	1.4
11	1	15	2.057	1.964	8.104	2.366	2.536					1.858				3.4	2.6
12	1	25	6.013	5.751	5.506	6.834	6.814	6.833	6.912	6.211	7.69	3.894				6.5	0.7
13	1	50	13.22	12.86	13.13	13.58	13.84	14.38	14.98	15.83	17.73	13.44				14.4	1.6
14	1	100	26.53	28	33.54	33.61	27.08				34.03	36.85				30.5	3.6
15	0.1	0	0.9148	0.7044	0.1684	0.03694										0.5	0.4
16	0.1	5	2.258	2.268	1.527	2.554	0.5165	1.433	1.334							1.7	0.7
17	0.1	10	3.701	4.028	4.265	0.4305	3.038	2.787								3.0	1.4
18	0.1	15	5.448	5.569	6.099	0.3683	5.212	3.563								4.4	2.1
19	0.1	25	7.441	6.901	6.841	0.6801	19.862	8.805								8.4	6.3
20	0.1	50	16.67	16.07	17.44	1.573	19.2	19.89								15.1	6.8
21	0.1	100	33.54	48.36	33.21	35.325	6.674	37.95								32.5	13.8
22	0	5	2.496	*2.25*	*2.373*	**2.5**										**2.5**	0.0
23	0	10	4.503	*4.5*	*4.5015*	**5**										**5**	0.0
24	0	15	6.503	*6.75*	*6.6265*	**7.5**										**7.5**	0.0
25	0	25	10.04	*11.25*	*10.645*	**12.5**										**12.5**	0.0
26	0	50	19.77	*22.5*	*21.135*	**25**										**25**	0.0
27	0	100	36.96	*45*	*40.98*	**50**										**50**	0.0
			Actual Measured			**Theoreical Calculation**											

No.	IEX Solids (v/v%)	Polymer Dosage (PPM)	Raw Data (mg/L)													Mean (mg/L)	Standard Deviation (mg/L)
2	10	25	0.6522	0.7808												0.72	0.09
3	10	50	0.8162	0.8783												0.85	0.04
4	10	100	0.7154	0.7384												0.73	0.02
9	1	5	0.2471	0.09911												0.17	0.10
10	1	10	0.2798	0.3307												0.31	0.04
11	1	15	1.04	0.6604												0.85	0.27
16	0.1	5	0.914	0.9477												0.93	0.02
17	0.1	10	2.719	2.944												2.83	0.16
18	0.1	15	5.023	4.758												4.89	0.19

D.6 Mastersizer Data

D.6.1 5 PPM

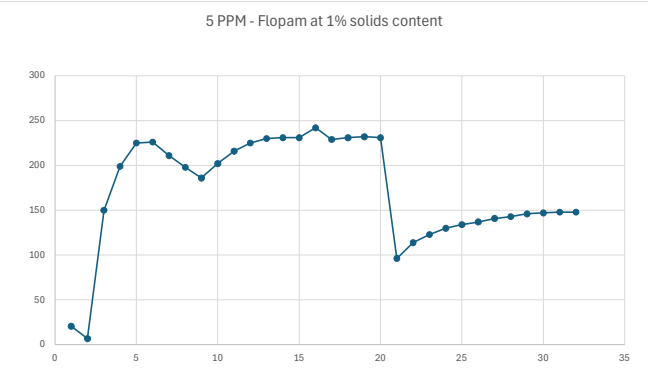
Mastersizer Data - Flopam - 5 PPM

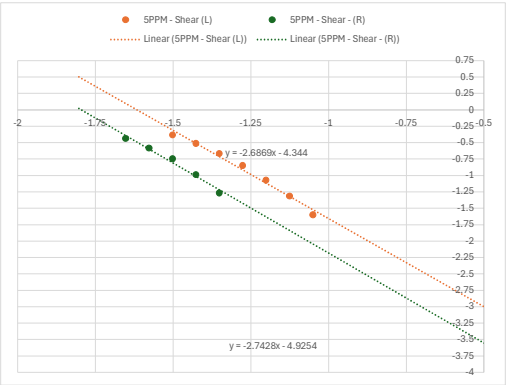
Record Number	Dx (10)	Dx (50)	Dx (90)	Weighted Residual	Mode	Result Below (2) µm	Result In Range (2,10) µm	Result In Range (10,100) um	Result Above (100) µm	Residual	Laser Obscuration	Scatter Intensity				
1	10.8	20.6	48.9	28.9	15.5	0	6.42	93.58	0.0008	122.7	0	0.00E+00	1.00E+00	0.00E+00	0.00E+00	0.00E+00
2	5.59	6.81	8.21	2.1	6.85	0	99.99	0.006	1E-14	2.11	0	0.00E+00	0.00E+00	0.00E+00	0.00E+00	0.00E+00
3	92	150	263	0.69	142	0	0	14.87	85.13	0.7	0	9.67E-01	1.00E+00	9.48E-01	9.15E-01	9.23E-01
4	117	199	352	0.57	191	0	0	3.83	96.17	0.58	0	9.76E-01	1.00E+00	9.21E-01	9.04E-01	8.93E-01
5	130	225	410	0.47	215	0	0	1.75	98.25	0.63	0	9.92E-01	1.00E+00	9.74E-01	9.36E-01	8.84E-01
6	130	226	403	0.52	219	0	0	1.75	98.25	0.52	0	1.00E+00	9.49E-01	8.90E-01	8.76E-01	8.70E-01
7	124	211	386	0.61	201	0	0	2.43	97.57	0.62	0	9.64E-01	1.00E+00	9.49E-01	8.86E-01	8.89E-01
8	116	198	356	0.53	189	0	0	3.97	96.03	0.54	0	1.00E+00	9.74E-01	9.80E-01	9.28E-01	9.27E-01
9	111	186	331	0.49	179	0	0	5.7	94.3	0.49	0	1.00E+00	9.35E-01	9.10E-01	8.97E-01	8.75E-01
10	122	202	354	0.6	194	0	0	2.59	97.41	0.62	0	9.90E-01	1.00E+00	9.46E-01	9.12E-01	8.95E-01
11	130	216	380	0.52	207	0	0	1.47	98.53	0.52	0	9.91E-01	1.00E+00	9.77E-01	9.38E-01	8.97E-01
12	136	225	384	0.59	220	0	0	0.8	99.2	0.59	0	1.00E+00	9.79E-01	8.88E-01	8.77E-01	8.65E-01
13	140	230	387	0.63	224	0	0	0.57	99.43	0.64	0	1.00E+00	9.99E-01	9.39E-01	9.18E-01	8.81E-01
14	142	231	392	0.61	224	0	0	0.48	99.52	0.61	0	1.00E+00	9.68E-01	9.88E-01	9.47E-01	8.69E-01
15	142	231	389	0.62	224	0	0	0.47	99.53	0.63	0	1.00E+00	9.81E-01	9.14E-01	8.91E-01	8.73E-01
16	146	242	496	0.63	227	0	0	0.32	99.68	0.64	0	1.00E+00	9.16E-01	8.27E-01	8.23E-01	7.92E-01
17	143	229	380	0.65	224	0	0	0.37	99.63	0.66	0	1.00E+00	9.69E-01	9.02E-01	8.69E-01	8.59E-01
18	144	231	391	0.68	224	0	0	0.37	99.63	0.69	0	1.00E+00	9.95E-01	9.42E-01	8.71E-01	8.74E-01
19	144	232	388	0.59	226	0	0	0.36	99.64	0.6	0	9.90E-01	1.00E+00	9.80E-01	9.29E-01	8.92E-01
20	145	231	384	0.72	225	0	0	0.31	99.69	0.73	0	1.00E+00	9.50E-01	8.94E-01	8.69E-01	8.62E-01
21	57.6	96.4	164	0.33	95.3	0	0	53.34	46.66	0.34	0	9.30E-01	1.00E+00	9.92E-01	9.49E-01	9.58E-01
22	70.6	114	189	0.47	111	0	0	37.1	62.9	0.48	0	9.85E-01	1.00E+00	1.00E+00	9.92E-01	9.90E-01
23	77.8	123	200	0.44	120	0	0	29.1	70.9	0.44	0	1.00E+00	9.81E-01	9.79E-01	9.95E-01	9.81E-01
24	82.6	130	210	0.54	127	0	0	23.8	76.2	0.55	0	1.00E+00	9.85E-01	9.46E-01	9.47E-01	9.47E-01
25	85.9	134	215	0.62	131	0	0	21.01	78.99	0.63	0	9.91E-01	1.00E+00	9.26E-01	9.08E-01	9.35E-01
26	87.8	137	224	0.51	134	0	0	19.1	80.9	0.68	0	9.55E-01	1.00E+00	9.13E-01	9.18E-01	9.20E-01
27	89.8	141	231	0.57	137	0	0	16.99	83.01	0.58	0	9.74E-01	1.00E+00	9.02E-01	9.05E-01	8.97E-01
28	92	143	230	0.5	140	0	0	15.22	84.78	0.51	0	9.77E-01	1.00E+00	9.77E-01	9.27E-01	9.36E-01
29	93.8	146	231	0.6	143	0	0	13.92	86.08	0.61	0	9.31E-01	1.00E+00	9.01E-01	8.56E-01	8.99E-01
30	94.9	147	235	0.6	143	0	0	13.22	86.78	0.61	0	9.91E-01	9.99E-01	1.00E+00	9.40E-01	9.51E-01
31	95.6	148	238	0.66	144	0	0	12.77	87.23	0.66	0	9.20E-01	1.00E+00	8.81E-01	8.76E-01	8.88E-01
32	95.5	148	236	0.75	144	0	0	12.81	87.19	0.76	0	9.62E-01	1.00E+00	9.56E-01	9.32E-01	9.26E-01

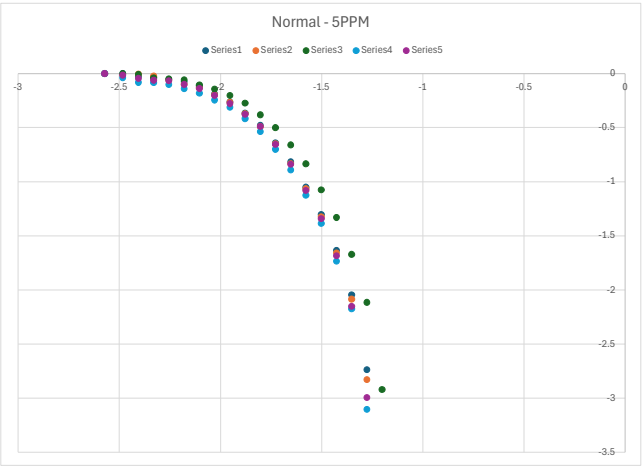
SD	4.086126
SDR	0.957427

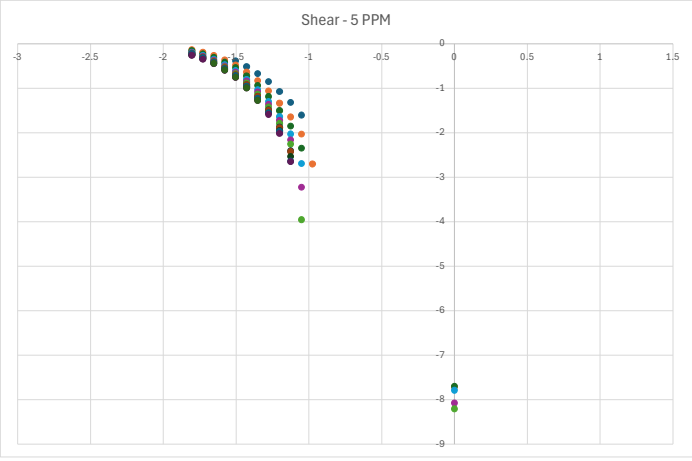
10PPM

DF	
Normal	2.6
Shear (lowest)	2.7
Shear (regrowth)	2.7







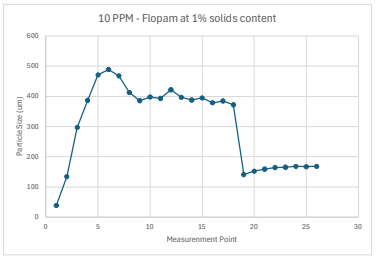


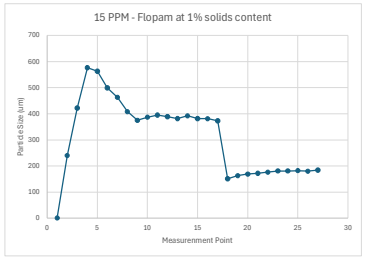
D.6.2 10 PPM and 15 PPM

Mastersizer Data - Flopam - 10 PPM and 15 PPM

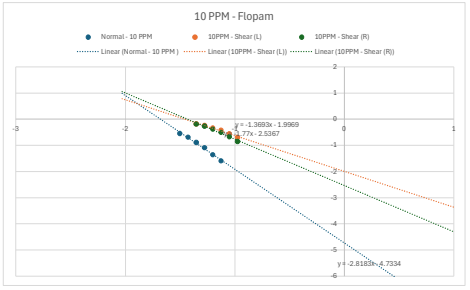
Record Nu	Sample Na	Dx (10)	Dx (50)	Dx (90)	Weighted I	Mode	Result Belc	Result In R	Result In R	Result Abo	Residual	Laser Obsc	Obscuratic	Analysis Date Time	Specific Su	Uniformity	0.01	0.0114	0.0129	0.0147	0.0167	0.0189	0.0215	0.0244	0.0278	0.0315	0.0358	0.0407	0.0463	0.0526	0.0597	0.0679	0.0771	0.0876	0.0995	0.113	0.128	0.146	0.166
101	IAO	24.3	38.8	58.4	5.42	41	0	0	100	0	7.76	0	0	09/08/2025 20:09	166.2	0.271	0	0	0	0	0	0	0	0	0	0	0	0	0	0	0	0	0	0	0	0	0	0	0	0
102	IAO	68.3	134	347	1.08	106	0	0	31.66	68.34	1.17	0	0	09/08/2025 20:09	48.67	1.416	0	0	0	0	0	0	0	0	0	0	0	0	0	0	0	0	0	0	0	0	0	0	0	0
103	IAO	161	297	529	0.66	311	0	0	0.28	99.72	0.66	0	0	09/08/2025 20:10	22.53	0.38	0	0	0	0	0	0	0	0	0	0	0	0	0	0	0	0	0	0	0	0	0	0	0	0
104	IAO	207	387	679	0.65	409	0	0	0.0003	100	0.65	0	0	09/08/2025 20:10	17.42	0.374	0	0	0	0	0	0	0	0	0	0	0	0	0	0	0	0	0	0	0	0	0	0	0	0
105	IAO	251	471	819	0.95	499	0	0	0	100	0.95	0	0	09/08/2025 20:10	14.36	0.368	0	0	0	0	0	0	0	0	0	0	0	0	0	0	0	0	0	0	0	0	0	0	0	0
106	IAO	262	489	889	0.69	502	0	0	0	100	0.69	0	0	09/08/2025 20:11	13.74	0.393	0	0	0	0	0	0	0	0	0	0	0	0	0	0	0	0	0	0	0	0	0	0	0	0
107	IAO	250	468	909	0.79	468	0	0	0	100	0.8	0	0	09/08/2025 20:11	14.19	0.488	0	0	0	0	0	0	0	0	0	0	0	0	0	0	0	0	0	0	0	0	0	0	0	0
108	IAO	230	413	698	0.69	435	0	0	0	100	0.69	0	0	09/08/2025 20:11	16.12	0.346	0	0	0	0	0	0	0	0	0	0	0	0	0	0	0	0	0	0	0	0	0	0	0	0
109	IAO	214	386	669	0.75	401	0	0	0.0003	100	0.75	0	0	09/08/2025 20:11	17.24	0.364	0	0	0	0	0	0	0	0	0	0	0	0	0	0	0	0	0	0	0	0	0	0	0	0
110	IAO	227	398	676	0.71	408	0	0	0	100	0.71	0	0	09/08/2025 20:12	16.52	0.347	0	0	0	0	0	0	0	0	0	0	0	0	0	0	0	0	0	0	0	0	0	0	0	0
111	IAO	229	393	665	0.77	397	0	0	0	100	0.78	0	0	09/08/2025 20:12	16.56	0.341	0	0	0	0	0	0	0	0	0	0	0	0	0	0	0	0	0	0	0	0	0	0	0	0
112	IAO	235	422	939	0.78	386	0	0	0	100	0.89	0	0	09/08/2025 20:12	15.24	0.541	0	0	0	0	0	0	0	0	0	0	0	0	0	0	0	0	0	0	0	0	0	0	0	0
113	IAO	235	397	661	0.58	401	0	0	0	100	0.58	0	0	09/08/2025 20:12	16.36	0.332	0	0	0	0	0	0	0	0	0	0	0	0	0	0	0	0	0	0	0	0	0	0	0	0
114	IAO	227	388	657	0.79	391	0	0	0	100	0.8	0	0	09/08/2025 20:13	16.77	0.341	0	0	0	0	0	0	0	0	0	0	0	0	0	0	0	0	0	0	0	0	0	0	0	0
115	IAO	230	395	733	0.61	382	0	0	0	100	0.76	0	0	09/08/2025 20:13	16.17	0.506	0	0	0	0	0	0	0	0	0	0	0	0	0	0	0	0	0	0	0	0	0	0	0	0
116	IAO	228	379	621	0.71	385	0	0	0	100	0.71	0	0	09/08/2025 20:13	17.04	0.314	0	0	0	0	0	0	0	0	0	0	0	0	0	0	0	0	0	0	0	0	0	0	0	0
117	IAO	226	385	656	0.66	383	0	0	0	100	0.66	0	0	09/08/2025 20:13	16.84	0.346	0	0	0	0	0	0	0	0	0	0	0	0	0	0	0	0	0	0	0	0	0	0	0	0
118	IAO	222	372	613	0.85	378	0	0	0	100	0.85	0	0	09/08/2025 20:14	17.43	0.319	0	0	0	0	0	0	0	0	0	0	0	0	0	0	0	0	0	0	0	0	0	0	0	0
119	IAO	82.6	141	255	0.42	136	0	0	21.31	78.69	0.43	0	0	09/08/2025 20:16	45.6	0.377	0	0	0	0	0	0	0	0	0	0	0	0	0	0	0	0	0	0	0	0	0	0	0	0
120	IAO	90.6	152	268	0.59	146	0	0	15.53	84.47	0.6	0	0	09/08/2025 20:16	42.19	0.357	0	0	0	0	0	0	0	0	0	0	0	0	0	0	0	0	0	0	0	0	0	0	0	0
121	IAO	95.9	159	280	0.48	153	0	0	12.21	87.79	0.49	0	0	09/08/2025 20:17	40.11	0.357	0	0	0	0	0	0	0	0	0	0	0	0	0	0	0	0	0	0	0	0	0	0	0	0
122	IAO	99.8	164	283	0.53	158	0	0	10.1	89.9	0.53	0	0	09/08/2025 20:17	38.96	0.345	0	0	0	0	0	0	0	0	0	0	0	0	0	0	0	0	0	0	0	0	0	0	0	0
123	IAO	101	165	276	0.61	161	0	0	9.26	90.74	0.62	0	0	09/08/2025 20:17	38.69	0.328	0	0	0	0	0	0	0	0	0	0	0	0	0	0	0	0	0	0	0	0	0	0	0	0
124	IAO	103	168	289	0.56	163	0	0	8.49	91.51	0.57	0	0	09/08/2025 20:17	37.85	0.34	0	0	0	0	0	0	0	0	0	0	0	0	0	0	0	0	0	0	0	0	0	0	0	0
125	IAO	103	167	281	0.55	163	0	0	8.27	91.73	0.56	0	0	09/08/2025 20:18	38.02	0.328	0	0	0	0	0	0	0	0	0	0	0	0	0	0	0	0	0	0	0	0	0	0	0	0
126	IAO	104	168	274	0.6	166	0	0	7.75	92.25	0.61	0	0	09/08/2025 20:18	37.9	0.311	0	0	0	0	0	0	0	0	0	0	0	0	0	0	0	0	0	0	0	0	0	0	0	0
127	IAO	0.419	0.714	2.72	8.38	0.571	72.89	27.11	0	3E-14	50.43	0	0.91	09/08/2025 20:22	7994	1.017	0	0	0	0	0	0	0	0	0	0	0	0	0	0	0	0	0	0	0	0	0	0	0	0
128	IAO	124	240	462	0.51	242	0	0	3.34	96.66	0.52	0	0	09/08/2025 20:23	28.18	0.436	0	0	0	0	0	0	0	0	0	0	0	0	0	0	0	0	0	0	0	0	0	0	0	0
129	IAO	222	422	731	0.66	449	0	0	0.0002	100	0.66	0	0	09/08/2025 20:23	16.15	0.368	0	0	0	0	0	0	0	0	0	0	0	0	0	0	0	0	0	0	0	0	0	0	0	0
130	IAO	292	577	1060	0.79	605	0	0	0	100	0.79	0	0	09/08/2025 20:23	11.96	0.414	0	0	0	0	0	0	0	0	0	0	0	0	0	0	0	0	0	0	0	0	0	0	0	0
131	IAO	292	563	1040	0.89	577	0	0	0	100	0.89	0	0	09/08/2025 20:23	12.1	0.405	0	0	0	0	0	0	0	0	0	0	0	0	0	0	0	0	0	0	0	0	0	0	0	0
132	IAO	272	499	884	0.93	516	0	0	0	100	0.93	0	0	09/08/2025 20:24	13.42	0.381	0	0	0	0	0	0	0	0	0	0	0	0	0	0	0	0	0	0	0	0	0	0	0	0
133	IAO	242	463	864	0.6	474	0	0	0	100	0.6	0	0	09/08/2025 20:24	14.61	0.419	0	0	0	0	0	0	0	0	0	0	0	0	0	0	0	0	0	0	0	0	0	0	0	0
134	IAO	221	408	717	0.49	426	0	0	0.0002	100	0.59	0	0	09/08/2025 20:24	16.43	0.371	0	0	0	0	0	0	0	0	0	0	0	0	0	0	0	0	0	0	0	0	0	0	0	0
135	IAO	203	375	662	0.66	391	0	0	0.0002	100	0.66	0	0	09/08/2025 20:24	17.83	0.374	0	0	0	0	0	0	0	0	0	0	0	0	0	0	0	0	0	0	0	0	0	0	0	0
136	IAO	216	387	654	0.71	408	0	0	0.0002	100	0.79	0	0	09/08/2025 20:25	17.19	0.348	0	0	0	0	0	0	0	0	0	0	0	0	0	0	0	0	0	0	0	0	0	0	0	0
137	IAO	222	395	726	0.59	393	0	0	0	100	0.59	0	0	09/08/2025 20:25	16.49	0.47	0	0	0	0	0	0	0	0	0	0	0	0	0	0	0	0	0	0	0	0	0	0	0	0
138	IAO	221	389	699	0.59	387	0	0	0	100	0.59	0	0	09/08/2025 20:25	16.74	0.429	0	0	0	0	0	0	0	0	0	0	0	0	0	0	0	0	0	0	0	0	0	0	0	0
139	IAO	219	382	646	0.82	395	0	0	0	100	0.83	0	0	09/08/2025 20:25	17.2	0.341	0	0	0	0	0	0	0	0	0	0	0	0	0	0	0	0	0	0	0	0	0	0	0	0
140	IAO	223	392	685	0.64	395	0	0	0	100	0.65	0	0	09/08/2025 20:26	16.75	0.363	0	0	0	0	0	0	0	0	0	0	0	0	0	0	0	0	0	0	0	0	0	0	0	0
141	IAO	217	382	670	0.57	384	0	0	0	100	0.67	0	0	09/08/2025 20:26	17.17	0.367	0	0	0	0	0	0	0	0	0	0	0	0	0	0	0	0	0	0	0	0	0	0	0	0
142	IAO	216	381	675	0.69	382	0	0	0	100	0.77	0	0	09/08/2025 20:26	17.22	0.372	0	0	0	0	0	0	0	0	0	0	0	0	0	0	0	0	0	0	0	0	0	0	0	0
143	IAO	216	373	625	0.68	382	0	0	0	100	0.68	0	0	09/08/2025 20:26	17.58	0.333	0	0	0	0	0	0	0	0	0	0	0	0	0	0	0	0	0	0	0	0	0	0	0	0
144	IAO	85.8	151	284	0.47	145	0	0	18.4	81.6	0.48	0	0	09/08/2025 20:29	43.02	0.404	0	0	0	0	0	0	0	0	0	0	0	0	0	0	0	0	0	0	0	0	0	0	0	0
145	IAO	95.6	163	294	0.46	157	0	0	12.3	87.7	0.47	0	0	09/08/2025 20:29	39.49	0.375	0	0	0	0	0	0	0	0	0	0	0	0	0	0	0	0	0	0	0	0	0	0	0	0
146	IAO	99.2	169	298	0.61	164	0	0	10.45	89.55	0.62	0	0	09/08/2025 20:29	38.26	0.362	0	0	0	0	0	0	0	0	0	0	0	0	0	0	0	0	0	0	0	0	0	0	0	0
147	IAO	102	172	305	0.38	166	0	0	8.96	91.04	0.39	0	0	09/08/2025 20:30	37.3	0.362	0	0	0	0	0	0	0	0	0	0	0	0	0	0	0	0	0	0	0	0	0	0	0	0
148	IAO	104	176	306	0.43	171	0	0	8.04	91.96	0.43	0	0	09/08/2025 20:30	36.66	0.354	0	0	0	0	0	0	0	0	0	0	0	0	0	0	0	0	0	0	0	0	0	0	0	0
149	IAO	107	181	315	0.55	175	0	0	7.04	92.96	0.56	0	0	09/08/2025 20:30	35.71	0.356	0	0	0	0	0	0	0	0	0	0	0	0	0	0	0	0	0	0	0	0	0	0	0	0
150	IAO	107	181	332	0.42	172	0	0	6.87	93.13	0.43	0	0	09/08/2025 20:31	35.36	0.386	0	0	0	0	0	0	0	0	0	0	0	0	0	0	0	0	0	0	0	0	0	0	0	0
151	IAO	108	182	329	0.55	174	0	0	6.58	93.42	0.55	0	0	09/08/2025 20:31	35.18	0.374	0	0	0	0	0	0	0	0	0	0	0	0	0	0	0	0	0	0	0	0	0	0	0	0
152	IAO	107	180	314	0.55	174	0	0	6.71	93.29	0.56	0	0	09/08/2025 20:31	35.68	0.356	0	0	0	0	0	0	0	0	0	0	0	0	0	0	0	0	0	0	0	0	0	0	0	0
153	IAO	109	184	323	0.56	178	0	0	6.27	93.73	0.57	0	0	09/08/2025 20:31	35.04	0.361	0	0	0	0	0	0	0	0	0	0	0	0	0	0	0	0	0	0	0	0	0	0	0	0

SD	
10PPM	12.3
15PPM	7.4

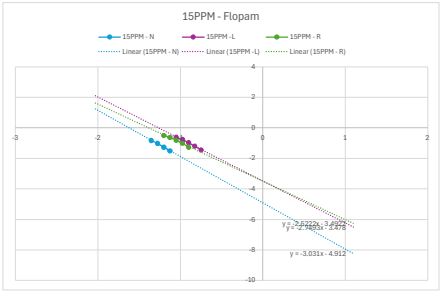




10PPM	
DF	
Normal	2.8
Shear (lowest)	1.4
Shear (regrowth)	1.8



15PPM	
DF	
Normal	3.0
Shear (lowest)	2.7
Shear (regrowth)	2.5



Appendix E : Praestol (A2) Results

E.1 Turbidity

Turbidity

The following results were captured using a turbiditimeter.

Suspension Solution and Praestol DW31

No.	IEX Solids (v/v%)	Ionic Strength (M)	Polymer Dosage (PPM)	Raw Data (NTU)																		Mean (NTU)	Standard Deviation (NTU)
1	10	0.03	0	143	198	139	196	110	93.8	136	65	74.5										128.36667	47.77248162
2	10	0.03	5	4.93	5.2	4.52	4.77	5.47	1.19	2.51	2.75	7.89	7.44									4.667	2.095620036
3	10	0.03	10	2.51	5.15	3.66	1.18	1.85	1.96	4.34												2.95	1.460182637
4	10	0.03	15	2.05	2.66	2.56	0.922	1.16	2.01	5.51												2.4102857	1.514443981
5	10	0.03	25	1.93	1.57	2.24	0.859	0.801	1.2													1.4333333	0.583132118
6	10	0.03	50	1.6	1.40	1.17	0.938	1.27	1.07													1.2413333	0.237104759
7	10	0.03	100	0.528	1.35	0.363	0.48	0.695	1.02													0.7393333	0.376083856
8	1	0.03	0	70.6	177	240	110	96.6	201	139												147.74	60.93
9	1	0.03	5	1.09	1.03	0.788	1.24	1.24	1.06													1.07	0.17
10	1	0.03	10	1.74	1.7	2.08	1.28	1.32														1.62	0.33
11	1	0.03	15	3.26	3.08	3.54	2.4	1.37														2.73	0.87
12	1	0.03	25	13.6	35.4	10.7	12.5	13.7	14.2	8.7												15.54	8.97
13	1	0.03	50	42.7	70	18.6	30.8	55.4														43.50	20.16
14	1	0.03	100	53.7	46.1	29.5	32.1	58.1														43.90	12.74
15	0.1	0.03	0	65	74.5	42.3	60.8	45.3	43.7	27.4	22.4	68.3	68.5	37.9	41.2							49.78	17.15
16	0.1	0.03	5	11.8	10.8	5.99	10.9															9.8725	2.627107091
17	0.1	0.03	10	19.2	16.9	12.4	18.7															16.8	3.095157508
18	0.1	0.03	15	19.6	31.2	17.4	19															21.8	6.335087476
19	0.1	0.03	25	46.3	47.8	39.8	19.8	31.6	26.3													35.266667	11.24662912
20	0.1	0.03	50	52.2	43.8	38.6	22.1	30.6	33.2													36.75	10.55343546
21	0.1	0.03	100	49.3	43.6	38.3	26.6	33.1	31.1													37	8.422826129

No.	IEX Solids (v/v%)	Ionic Strength (M)	Polymer Dosage (PPM)	Raw Data (NTU) - shear																		Mean (NTU)	Standard Deviation (NTU)
2	10	0.03	5	7.11	10.8	20.9																12.9	7.1
3	10	0.03	10	6.98	5.11	18.1																10.1	7.0
4	10	0.03	15	5.9	4.57	8.05																6.2	1.8
9	1	0.03	5	2.19	0.492	2.23																1.6	1.0
10	1	0.03	10	0.529	0.515	1.74																0.9	0.7
11	1	0.03	15	0.562	0.41	0.392																0.5	0.1
16	0.1	0.03	5	5.45	4.85	8.6	4.35															5.8	1.9
17	0.1	0.03	10	15.2	16.4	17.1	22.7															17.9	3.3
18	0.1	0.03	15	24.2	19.2	35.9																26.4	8.6

E.2 Zeta Potential

Zeta-Potential

The following results were captured using a zetasizer.

Suspension Solution and PRAESTOL DW31

No.	IEX Solids (v/v%)	Ionic Strength (M)	Polymer Dosage (PPM)	Raw Data (mV)																																						Mean (mV)	Standard Deviation (mV)
1	10	0.03	0	-22.4	-23.9	-22.1	-20.5	-21.7	-17.1																																			-21.3	2.32586901
2	10	0.03	5	-0.45	-0.225	-0.552	-8.1	-10.1	-3.96	-9.44	-12	-15	-10.9	-11.5	-13.6	-12.5	-12.3	-9.82	-15	-16	-11.1	-4.31	1.24	3.09																			-9.6	5.04188033
3	10	0.03	10	-2.31	4.61	14.3	-7.41	-5.64	-5.41	-11.1	-9.07	-11.7	-9.41	-8.22	-2.07	-7.39	-12.8	3.25	-11.9	-8.04	-10.3	-14.2	-14.6	-13.4	-1.95	-6.53	-10.4																	-6.8	7.12169395
4	10	0.03	15	4.86	11.1	24.7	0.757	-0.079	7.44	1.34	3	3.64	-5.28	-6.43	-13	-6.87	-9.56	-8.86	-13.8	-14.5	-8.11	-14.4	-12.1	-8.98	6.44	-3.03	-4.21																	-3.1	9.97766291
5	10	0.03	25	34.3	33.8	24.9	33.9	36.1	26.1	17.9	16.8	16.3	0.804	5.66	7.41	-3.06	-0.906	-0.0607	-11	-6.27	-9.01	-7.61	-10.4	-6.01	-13.5	-8.8	-5.78	-13.8	-13.1	-15.4	-5.26	-17.9	-10											4.8	17.2713543
6	10	0.03	50	0.628	2.98	4.74	-11	-11.5	2.05	-3.86	3.94	16	-3.79	-6.3	3.22	-5.01	-8.5	-9.56	-13.9	1.71	-6.46	-14.7	-15.1	-6.27	-11.9	-12.2	-1.96																	-3.8	7.87427025
7	10	0.03	100	1.52	11.7	13.7	4.34	8.75	11.3	4.54	6.11	6.71	-2.73	-4.06	5.01	3.18	13.4	17.9	-13.6	-15	-6.27	-7.99	0.0028	-4.27	3.94	-3.52	4.12																	2.6	8.95349812
8	1	0.03	0	-25.2	-26.1	-26.4	-32.5	-36.2	-37.6	-14.9	-14.7	-15.3																																	-25.4	8.97329371
9	1	0.03	5	25.9	28.3	21.5	39.8	45.1	44.4	36.5	42.1	39.2	35.9	40.7	42.9	-6.91	1.62	6.4	17.8	22.5	19.1	17.2	18.9	11	19.1	28.7	27.2																	26.0	14.2350425
10	1	0.03	10	41.7	46.4	45	40.2	46.6	46.2	38.4	44.5	42.2	42.7	46.6	47.1	33.3	32.4	34.6	30	33.7	33	37.2	42.1	41.6	33.2	38.5	34.6																	39.7	5.4770602
11	1	0.03	15	36.3	40	37.8	38.8	44	42.8	40.5	44.4	43.1	43.4	46.9	41.8	0.851	9.15	33.5	33.8	41	44.1	40.6	43.1	42.9	40.8	44	44	37.8	41.5	26.7													37.9	10.4430646
12	1	0.03	25	45.5	51.3	49.9	43.4	47.7	49.2	39.3	42.7	40.9	41.4	44.5	42.3	42.6	47.5	47.7	37.3	43.5	43.4	41.9	46.8	43.4	39	43.2	43.9																	44.1	3.52734401
13	1	0.03	50	45.5	49.2	47.1	43.6	48.3	48	39.7	44.6	45.3	41.5	46	48.5	29.9	33.2	31.1	36.6	37.4	43.2	38.3	43.8	42.8	38.8	41.2	39.7																	41.8	5.42550171
14	1	0.03	100	54.4	52.9	47.9	47.9	51.8	51.2	41.1	44.8	45.9	42.5	46.1	47.3	43	48	48.4	20.2	21.5	21.1	39.2	44.3	43.5	39.9	46.2	43.5	38.7	44.5	42.2													42.9	8.85278458
15	0.1	0.03	0	-28.6	-25.6	-23.6																																					-25.9	2.51661148
16	0.1	0.03	5	44	45	43.8	43	46.2	42.6	43.7	47.7	44.8	38.7	44.2	39.1	41.1	46.5	43.9	9.3	45.5	42.4	39.9	44.2	40.5																			41.7	7.80644727
17	0.1	0.03	10	43.4	47.9	46.1	42.1	47.1	44.2	42.4	46.1	44.1	40.6	47.3	42.6	37	43.9	40.3	45	40.7	41.2																					43.4	2.88509807
18	0.1	0.03	15	42.9	46.4	44.1	43.8	46.1	44.6	43.3	46.9	47.6	39.3	44.3	42.5	39.7	44.7	42	39.6	42.5	39.4																					43.3	2.60570641
19	0.1	0.03	25	42	46.8	46	42.6	47.5	47.8	42.4	47	44.1	40.7	46.1	49.6	34.8	43.3	41.1	40.5	43.6	41.7																					43.8	3.53873062
20	0.1	0.03	50	45.7	48.2	50.8	42.3	45.4	44.8	42.6	48.4	48.3	13.2	22.9	43.8	48.4	46.1	40.1																									42.1	10.3125213
21	0.1	0.03	100	43.6	47.2	50.7	42.9	46.7	47.5	44	47.3	50.3	40.7	44.7	46.7	47.5	45.8	41.7																									45.8	2.88325213

E.3 Suspended Solids

Suspended Solids

The following results were captured using filter paper, vacuum suction pump and 105'C oven

Conversion	
2ml	1
1L	500

Suspension Solution and PRAESTOL DW31

No.	IEX Solids (v/v%)	Ionic Strength (M)	Polymer Dosage (PPM)	Raw Data (g/L)									Mean (g/L)	Standard Deviation (g/L)
1	10	0.03	0	2.45	2.95								2.70	0.35
2	10	0.03	5	1.25	2.45	2.85	2.9	2.2	2.3				2.32	0.60
3	10	0.03	10	1.4	2.85	2.65	2.75	2	2.4				2.34	0.55
4	10	0.03	15	1.4	3.55	2.4	2.75	1.9	2.5				2.42	0.74
5	10	0.03	25	1.35	2.8	2.65	2.65	2.25	2.35				2.34	0.53
6	10	0.03	50	1.05	2.95	2.6	2.7	2.25	2.55				2.35	0.68
7	10	0.03	100	1.35	2.9	2.55	2.7	2.4	2.5				2.40	0.54
8	1	0.03	0	3.10	1.2	3.3	2.15						2.44	0.97
9	1	0.03	5	1.85	1.20	1.35	2.7	1.4	2.1	1.7	1.65		1.74	0.48
10	1	0.03	10	2.00	1.00	1.4	-1.25	1.6	1.9	1.85			1.21	1.14
11	1	0.03	15	2.10	1.05	1.3	0.35	1.75	1.55	1.85			1.42	0.59
12	1	0.03	25	1.25	1.00	1.4	0.55	1.55	1.7	3.2	2.15		1.60	0.80
13	1	0.03	50	2.45	1.20	3.35	1.15	1.8	1.85	3.25	1.95		2.12	0.84
14	1	0.03	100	1.40	1.20	2.15	0.7	2.05	1.7	3.3	1.9		1.80	0.77
15	0.1	0.03	0	1.9	1.6	1.9							1.80	0.17
16	0.1	0.03	5	1.75	1.8	1.65	0.9		2.15				1.65	0.46
17	0.1	0.03	10	1.85	1.7	1.7	0.95	1.9	2.1				1.70	0.40
18	0.1	0.03	15	1.85	1.85	1.6	0.85	2.15					1.66	0.49
19	0.1	0.03	25	1.9	1.9	1.85	1.25	3.4	2.25				2.09	0.72
20	0.1	0.03	50	1.9	2.1	2	0.7	3.35	2.35				2.07	0.85
21	0.1	0.03	100	1.9	2.35	2.3	0.6	3.45	2.2				2.13	0.92

No.	IEX Solids (v/v%)	Ionic Strength (M)	Polymer Dosage (PPM)	Raw Data (g/L)									Mean (g/L)	Standard Deviation (g/L)
2	10	0.03	5	2.05	1.95								2.00	0.07
3	10	0.03	10	1.85	1.8								1.82	0.04
4	10	0.03	15	1.7	1.75								1.73	0.04
9	1	0.03	5	1.55	1.8								1.67	0.18
10	1	0.03	10	1.40	1.70								1.55	0.21
11	1	0.03	15	1.45	1.90								1.68	0.32
16	0.1	0.03	5	1.75	1.4	1.55							1.57	0.18
17	0.1	0.03	10	1.65	1.7								1.68	0.04
18	0.1	0.03	15	0.85	1.75								1.30	0.64

E.4 Settled Bed Volume

Settled Bed Volume

The following results were captured using a 1000L beaker, images and a ruler. It was timed for 15min.

Suspension Solution and PRAESTOL DW31

No.	IEX Solids (v/v%)	Ionic Strength (M)	Polymer Dosage (PPM)	Raw Data (ml)														Mean (ml)	Standard Deviation (ml)
1	10	0.03	0	200	240	220	180	210	225	200	250	205	198					212.8	21.12
2	10	0.03	5	360	360	360	300	300	240	275	280	225						300.0	51.30
3	10	0.03	10	380	340	372	295	295	250	295	300	250						308.6	46.90
4	10	0.03	15	360	360	380	300	290	245	325	300	248						312.0	48.42
5	10	0.03	25	360	360	380	310	300	250									326.7	48.85
6	10	0.03	50	400	368	392	320	310	290									346.7	46.09
7	10	0.03	100	400	396	500	350	350	325									386.8	62.61
8	1	0.03	0	22.5	25	22.5	35	40										29.0	8.02
9	1	0.03	5	66	76	97.6	110	128.8	135	96	95							100.6	23.70
10	1	0.03	10	46.15	57.14	63.36	90	100	115	125	100							87.1	28.52
11	1	0.03	15	80	61	58.8	80	111.764	100	105								85.2	21.03
12	1	0.03	25	68.75	53.2	42.8	66.66	100	94.7	145.45	98	100						85.5	31.14
13	1	0.03	50	81.25	71.875	37.5	44.28	76.92	70	77.77	84.21	80	90					71.4	17.12
14	1	0.03	100	75	81.25	85	87.5	50	83.3	86.95	80	74	110.526	74	60	85		80.7	14.37
15	0.1	0.03	0	0	2	1	5	5	5									3.0	2.28
16	0.1	0.03	5	9	9	14	14	16										12.4	3.21
17	0.1	0.03	10	10	10	14	16	14										12.8	2.68
18	0.1	0.03	15	8	8	10	13	10										9.8	2.05
19	0.1	0.03	25	10	12.5	10	10	9										10.3	1.30
20	0.1	0.03	50	11.7	13	10	9	8										10.3	2.02
21	0.1	0.03	100	10	12	10	7	2										8.2	3.90

1 2 3 4 5 6 7 8 9

No.	IEX Solids (v/v%)	Ionic Strength (M)	Polymer Dosage (PPM)	Raw Data (ml)																Mean (ml)	Standard Deviation (ml)
2	10	0.03	5	260	260	265														261.7	2.89
3	10	0.03	10	275	290	295														286.7	10.41
4	10	0.03	15	300	275	305														293.3	16.07
9	1	0.03	5	96	90	75														87.0	10.82
10	1	0.03	10	125	98	90														104.3	18.34
11	1	0.03	15	100	100	95														98.3	2.89
16	0.1	0.03	5	20	15	16														17.0	2.65
17	0.1	0.03	10	30	12	13														18.3	10.12
18	0.1	0.03	15	10	20	6														12.0	7.21

E.5 Total Organic Carbon Concentration

Total Organic Carbon

The following results were captured using a TOC-analyser

Total Organic Carbon and PRAESTOL DW31

No.	IEX Solids (v/v%)	Ionic Strength (M)	Polymer Dosage (PPM)	Raw Data (ml)										Mean (ml)	Standard Deviation (ml)
1	10	0.03	0	0.6626	0.81	0								0.49	0.43
2	10	0.03	5	0.5324	0.2648	0.3402	0.3104	0.5305	0.7118					0.45	0.17
3	10	0.03	10	0.3194	0.4283	0.3022	0.2535	0.5899	0.8086					0.45	0.21
4	10	0.03	15	0.5848	0.4856	0.2724	0.2277	0.2926	0.9664					0.47	0.28
5	10	0.03	25	0.3551	0.3479	0.2406	0.4128	0.3406	0.5542					0.38	0.10
6	10	0.03	50	0.4961	0.3415	0.2777	0.3421	0.3418	0.7738					0.43	0.18
7	10	0.03	100	0.5165	0.4304	0.3576	0.4734	0.3625	0.6542					0.47	0.11
8	1	0.03	0	0.7475	1.074	0.9636								0.93	0.17
9	1	0.03	5	0.886	0.6754	0.5386	0.9249	1.736	0.386	0.05871	0.4745			0.86	0.48
10	1	0.03	10	1.872	1.028	0.9269	1.052	3.824	0.2177	0.2717	0.3367			1.49	1.26
11	1	0.03	15	1.927	1.217	1.297	0.8601	5.832	0.4221	0.4961	0.5433			1.93	1.98
12	1	0.03	25	2.681	1.735	1.88	0.9748	9.869	0.7264	1.39	0.8351			2.98	3.45
13	1	0.03	50	6.246	4.624	3.004	1.314	18.62	1.765	3.065	1.562			5.93	6.48
14	1	0.03	100	15.04	15.61	11.78	0.7918	35.68	1.758	11.325	5.253			13.44	12.66
15	0.1	0.03	0	0.9148	0.7044	0.1684	0.03694	0	0					0.30	0.40
16	0.1	0.03	5	1.369	1.151	1.422	0.8028	0.4172	0.4557					0.94	0.44
17	0.1	0.03	10	2.108	2.498	1.997	1.182	0.62	0.9448					1.56	0.75
18	0.1	0.03	15	3.891	3.644	3.108	1.848	1.189	1.401					2.51	1.18
19	0.1	0.03	25	4.88	4.049	5.519	4.086	5.47	3.617					4.60	0.80
20	0.1	0.03	50	12.45	13.91	12.71	11.21	12.555	10.48					12.22	1.21
21	0.1	0.03	100	29.63	29.78	29.46	26.98	29.805	26.3					28.66	1.58
27	0	0	5	*1.38*	1.375	**1.5**								**1.5**	0.0
27	0	0	10	*2.75*	2.75	**3**								**3.0**	0.0
27	0	0	15	*4.13*	4.125	**4.5**								**4.5**	0.0
27	0	0	25	*6.88*	6.875	**7.5**								**7.5**	0.0
27	0	0	50	*13.75*	13.75	**15**								**15.0**	0.0
27	0	0	100	*27.5*	27.5	**30**								**30.0**	0.0

Actual Measured **Theoreical Calculation**

1 2 3 4 5 6

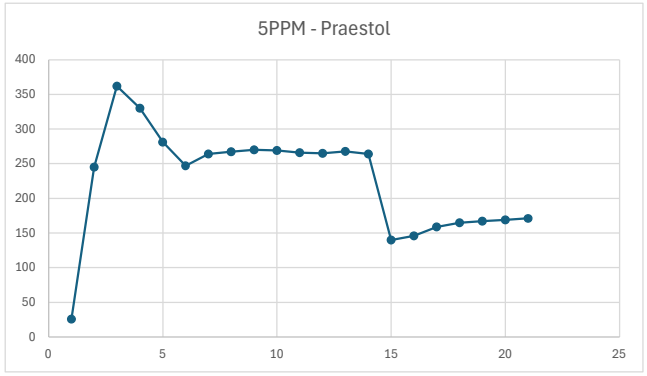
No.	IEX Solids (v/v%)	Ionic Strength (M)	Polymer Dosage (PPM)	Raw Data (mg/L)										Mean (mg/L)	Standard Deviation (mg/L)
2	10	0.03	5	0.91	0.7077									0.81	0.14
3	10	0.03	10	0.6154	0.6682									0.64	0.04
4	10	0.03	15	0.6501	0.8239									0.74	0.12
9	1	0.03	5	0.1942	-0.0116									0.09	0.15
10	1	0.03	10	1.493	-0.00938									0.74	1.06
11	1	0.03	15	0.1835	0.1365									0.16	0.03
16	0.1	0.03	5	0.4853	0.4755									0.48040	0.01
17	0.1	0.03	10	0.5891	0.3666									0.47785	0.16
18	0.1	0.03	15	1.067	0.9294									1.00	0.10

E.6 Mastersizer Data

E.6.1 5 PPM

Mastersizer Data -Praestol DW31 - 5 PPM

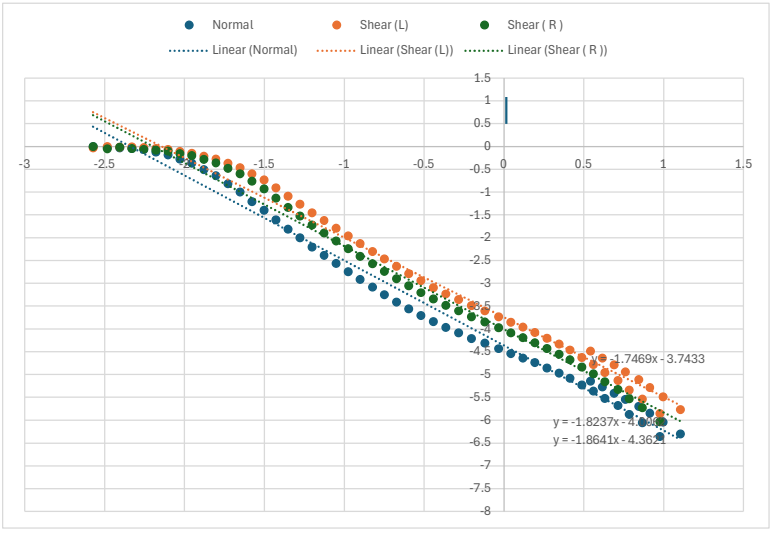
Record Nu	Sample Name	Dx (10)	Dx (50)	Dx (90)	Weighted F	Mode	Result Belc	Result In R	Result In Range	(10,1C	Result Abo	Residual	Laser Obsc	Obscuratio	Analysis Date Time	Specific Su	Uniformity	0.01	0.0114	0.0129	0.0147
1	Clinop + Praestol	3.86	25.7	78.3	0.51	33.4	4.48	18.23	72.46	4.83	0.24	38.91	25.97	09/08/2025 18:38	651.6	0.885	0	0	0	0
2	Clinop + Praestol	94.9	245	457	0.65	283	0	0.65	10.23	89.12	0.65	30.9	0	09/08/2025 18:38	43.26	0.454	0	0	0	0
3	Clinop + Praestol	164	362	646	0.59	401	0	0	3.97	96.03	0.6	25.53	13.38	09/08/2025 18:39	22.5	0.41	0	0	0	0
4	Clinop + Praestol	148	330	594	0.56	367	0	0	4.47	95.53	0.57	26.19	14.64	09/08/2025 18:39	24.55	0.414	0	0	0	0
5	Clinop + Praestol	126	281	505	0.73	314	0	0	6.21	93.79	0.74	28.41	15.62	09/08/2025 18:40	29.21	0.415	0	0	0	0
6	Clinop + Praestol	111	247	446	0.72	277	0	0.0001	8	92	0.73	30.25	0	09/08/2025 18:40	33.22	0.417	0	0	0	0
7	Clinop + Praestol	126	264	462	0.68	290	0	0	5.98	94.02	0.68	28.85	15.52	09/08/2025 18:41	29.96	0.393	0	0	0	0
8	Clinop + Praestol	128	267	462	0.78	294	0	0	5.77	94.23	0.78	28.86	15.63	09/08/2025 18:41	29.52	0.386	0	0	0	0
9	Clinop + Praestol	129	270	470	0.8	297	0	0	5.64	94.36	0.8	29.76	15.61	09/08/2025 18:41	29.24	0.39	0	0	0	0
10	Clinop + Praestol	128	269	480	0.74	293	0	0	5.68	94.32	0.74	28.58	15.47	09/08/2025 18:42	29.24	0.403	0	0	0	0
11	Clinop + Praestol	128	266	466	0.6	289	0	0	5.57	94.43	0.61	29.45	15.35	09/08/2025 18:42	29.45	0.391	0	0	0	0
12	Clinop + Praestol	130	265	459	0.76	289	0	0	5.39	94.61	0.76	28.29	15.63	09/08/2025 18:42	29.22	0.383	0	0	0	0
13	Clinop + Praestol	130	268	474	0.55	290	0	0	5.43	94.57	0.55	28.77	15.44	09/08/2025 18:42	29.01	0.396	0	0	0	0
14	Clinop + Praestol	128	264	454	0.82	289	0	0	5.77	94.23	0.82	30.52	0	09/08/2025 18:43	29.9	0.382	0	0	0	0
15	Clinop + Praestol	52.9	140	269	1.05	154	0.0004	1.26	28.09	70.64	1.04	37.64	21.81	09/08/2025 18:44	76.29	0.472	0	0	0	0
16	Clinop + Praestol	59	146	285	0.92	156	0	1.08	25.56	73.35	0.92	37.84	21.39	09/08/2025 18:44	70.07	0.475	0	0	0	0
17	Clinop + Praestol	67.9	159	303	0.95	169	0	0.83	20.98	78.2	0.94	36.97	20.61	09/08/2025 18:44	60.91	0.457	0	0	0	0
18	Clinop + Praestol	71.9	165	310	0.93	177	0	0.78	18.95	80.28	0.92	36.69	20.32	09/08/2025 18:45	58.2	0.446	0	0	0	0
19	Clinop + Praestol	74.2	167	307	0.64	180	0	0.76	17.98	81.26	0.64	36.57	20.2	09/08/2025 18:45	57.11	0.431	0	0	0	0
20	Clinop + Praestol	76.6	169	307	0.78	183	0	0.68	17.23	82.09	0.78	35.92	19.97	09/08/2025 18:45	55.12	0.422	0	0	0	0
21	Clinop + Praestol	77.2	171	308	0.77	185	0	0.69	16.77	82.54	0.77	36.09	0	09/08/2025 18:45	54.63	0.418	0	0	0	0



DF	
Normal	1.9
Shear (lowest)	1.7
Shear (regrowth)	1.8

SD

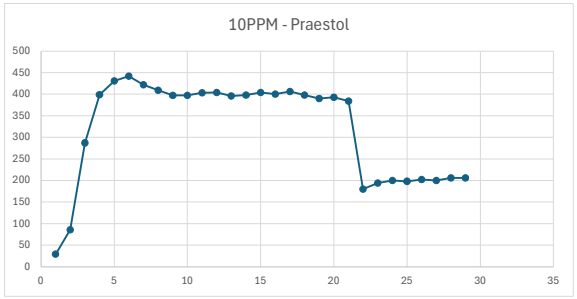
2.263846285



E.6.2 10 PPM

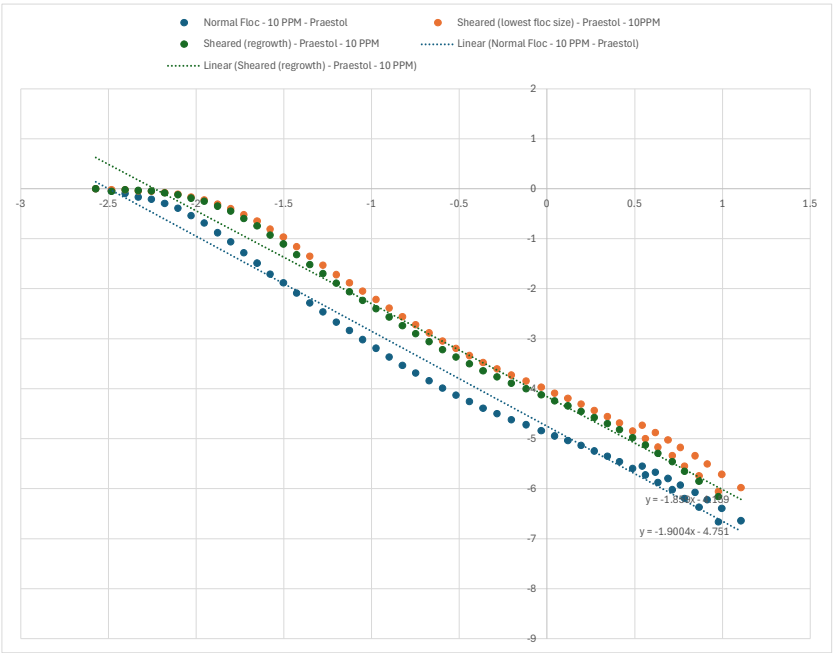
Mastersizer Data -Praestol DW31 - 10 PPM

Record Nu	Sample Na	Dx (10)	Dx (50)	Dx (90)	Weighted F	Mode	Result Belc	Result In R	Result In R	Result Abo	Residual	Laser Obsc	Obscuratic	Analysis Date Time	Specific Su	Uniformity	0.01	0.0114	0.0129	0.0147	0.0167	0.0189	0.0215	0.0244	0.0278
22	Clinop + Pr	4.06	29.3	85.2	0.67	40.1	4.66	15.93	72.99	6.42	0.47	35.37	26.48	09/08/2025 18:51	617.3	0.861	0	0	0	0	0	0	0	0	0
23	Clinop + Pr	12.4	85.7	203	1.06	123	2.04	6.45	48.65	42.86	1.03	35.85	21.73	09/08/2025 18:51	289.1	0.683	0	0	0	0	0	0	0	0	0
24	Clinop + Pr	121	287	501	0.89	326	0	0.15	7.14	92.71	0.88	28.92	15.16	09/08/2025 18:51	31.75	0.404	0	0	0	0	0	0	0	0	0
25	Clinop + Pr	184	399	700	0.9	444	0	0	3.34	96.66	0.9	24.61	12.85	09/08/2025 18:52	20.51	0.398	0	0	0	0	0	0	0	0	0
26	Clinop + Pr	201	431	764	0.51	470	0	0	2.86	97.14	0.52	23	12.42	09/08/2025 18:52	18.64	0.4	0	0	0	0	0	0	0	0	0
27	Clinop + Pr	210	442	808	0.62	472	0	0	2.53	97.47	0.64	24.05	12.61	09/08/2025 18:52	17.66	0.416	0	0	0	0	0	0	0	0	0
28	Clinop + Pr	195	422	724	1.17	474	0	0	2.97	97.03	1.17	25.06	13.91	09/08/2025 18:52	19.14	0.382	0	0	0	0	0	0	0	0	0
29	Clinop + Pr	191	409	718	0.59	450	0	0	3.07	96.93	0.6	25.19	13.49	09/08/2025 18:53	19.61	0.396	0	0	0	0	0	0	0	0	0
30	Clinop + Pr	182	397	724	0.56	434	0	0	3.18	96.82	0.57	26.22	13.7	09/08/2025 18:53	20.23	0.42	0	0	0	0	0	0	0	0	0
31	Clinop + Pr	196	397	667	0.77	433	0	0	2.91	97.09	0.78	25.29	12.36	09/08/2025 18:53	19.49	0.369	0	0	0	0	0	0	0	0	0
32	Clinop + Pr	200	403	686	0.93	440	0	0	2.67	97.33	0.94	23.82	12.25	09/08/2025 18:53	19.01	0.372	0	0	0	0	0	0	0	0	0
33	Clinop + Pr	198	404	698	0.73	441	0	0	2.54	97.46	0.74	23.92	13.02	09/08/2025 18:54	18.95	0.38	0	0	0	0	0	0	0	0	0
34	Clinop + Pr	197	396	683	0.6	428	0	0	2.59	97.41	0.61	23.71	12.08	09/08/2025 18:54	19.23	0.379	0	0	0	0	0	0	0	0	0
35	Clinop + Pr	199	398	681	0.88	432	0	0	2.44	97.56	0.88	24.19	12.8	09/08/2025 18:54	19.07	0.375	0	0	0	0	0	0	0	0	0
36	Clinop + Pr	200	404	696	0.68	437	0	0	2.48	97.52	0.7	23.66	11.83	09/08/2025 18:54	18.78	0.378	0	0	0	0	0	0	0	0	0
37	Clinop + Pr	200	400	693	0.69	432	0	0	2.54	97.46	0.7	23.38	12.28	09/08/2025 18:55	18.93	0.379	0	0	0	0	0	0	0	0	0
38	Clinop + Pr	203	406	758	0.66	419	0	0	2.48	97.52	0.68	24.9	12.43	09/08/2025 18:55	18.49	0.449	0	0	0	0	0	0	0	0	0
39	Clinop + Pr	199	398	685	0.64	431	0	0	2.61	97.39	0.65	24.59	12.78	09/08/2025 18:55	19.13	0.377	0	0	0	0	0	0	0	0	0
40	Clinop + Pr	199	390	669	0.6	418	0	0	2.62	97.38	0.62	23.31	12.33	09/08/2025 18:56	19.28	0.374	0	0	0	0	0	0	0	0	0
41	Clinop + Pr	197	393	686	0.64	421	0	0	2.5	97.5	0.66	23.13	12.09	09/08/2025 18:56	19.16	0.383	0	0	0	0	0	0	0	0	0
42	Clinop + Pr	196	384	651	0.81	415	0	0	2.61	97.39	0.82	23.17	12.22	09/08/2025 18:56	19.53	0.366	0	0	0	0	0	0	0	0	0
43	Clinop + Pr	71.2	180	339	0.7	203	0	0.77	17.39	81.85	0.69	36.8	20.09	09/08/2025 18:59	55.85	0.455	0	0	0	0	0	0	0	0	0
44	Clinop + Pr	82.6	194	358	0.8	215	0	0.56	13.91	85.54	0.79	35.58	19.32	09/08/2025 18:59	48.83	0.437	0	0	0	0	0	0	0	0	0
45	Clinop + Pr	87.4	200	364	0.62	220	0	0.54	12.56	86.91	0.62	35.32	19.99	09/08/2025 18:59	47.13	0.426	0	0	0	0	0	0	0	0	0
46	Clinop + Pr	88.1	198	363	0.86	217	0	0.53	12.41	87.06	0.85	34.72	19.09	09/08/2025 18:59	46.93	0.425	0	0	0	0	0	0	0	0	0
47	Clinop + Pr	89.8	202	362	0.73	224	0	0.52	11.89	87.59	0.73	34.97	19.25	09/08/2025 19:00	46.17	0.415	0	0	0	0	0	0	0	0	0
48	Clinop + Pr	90.3	200	355	0.85	221	0	0.53	11.76	87.72	0.85	34.9	19.58	09/08/2025 19:00	46.31	0.407	0	0	0	0	0	0	0	0	0
49	Clinop + Pr	93	206	374	0.75	225	0	0.45	11.14	88.41	0.75	34.63	19.54	09/08/2025 19:00	44.23	0.42	0	0	0	0	0	0	0	0	0
50	Clinop + Pr	92.1	206	366	0.93	228	0	0.45	11.32	88.23	0.92	34.66	0	09/08/2025 19:00	44.42	0.41	0	0	0	0	0	0	0	0	0



DF	
Normal	1.9
Shear (lowest)	1.8
Shear (regrowth)	1.9

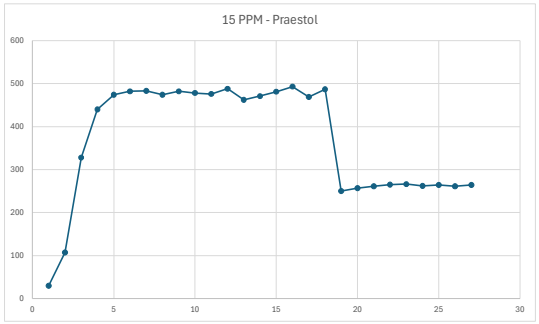
SD
6.156089



E.6.3 15 PPM

Mastersizer Data -Praestol DW31 - 15 PPM

Record Nu	Sample Name	Dx (10)	Dx (50)	Dx (90)	Weighted F	Mode	Result Belo	Result In R	Result In R	Result Abo	Residual	Laser Obscuration	Obscuratio	Analysis Date Time	Specific Su	Uniformity	0.01	0.0114	0.0129	0.0147	0.0167	0.0189	0.0215	0.0244	0.0278	0.0315	0.0358	0.0407	0.0463	0.0526	0.0597	0.0679	0.0771
51	Clinop + Praes	3.91	29.8	87.4	0.6	41.4	4.86	16.02	72.26	6.86	0.37	36.9	28.21	09/08/2025 19:05	629.3	0.867	0	0	0	0	0	0	0	0	0	0	0	0	0	0	0	0	0
52	Clinop + Praes	17.1	107	234	1.72	153	1.59	5.1	40.08	53.23	1.69	35.65	21.17	09/08/2025 19:05	232.5	0.618	0	0	0	0	0	0	0	0	0	0	0	0	0	0	0	0	0
53	Clinop + Praes	143	328	588	0.44	365	0	0.008	5.58	94.42	0.44	27.63	14.62	09/08/2025 19:06	26.88	0.415	0	0	0	0	0	0	0	0	0	0	0	0	0	0	0	0	0
54	Clinop + Praes	204	440	752	0.72	486	0	0	3.19	96.81	0.72	23.11	12.19	09/08/2025 19:06	18.82	0.384	0	0	0	0	0	0	0	0	0	0	0	0	0	0	0	0	0
55	Clinop + Praes	225	474	840	0.69	510	0	0	2.6	97.4	0.69	22.39	12.38	09/08/2025 19:06	16.99	0.398	0	0	0	0	0	0	0	0	0	0	0	0	0	0	0	0	0
56	Clinop + Praes	228	482	841	0.68	528	0	0	2.34	97.66	0.7	22.4	12.51	09/08/2025 19:06	16.37	0.39	0	0	0	0	0	0	0	0	0	0	0	0	0	0	0	0	0
57	Clinop + Praes	230	483	851	0.82	525	0	0	2.24	97.76	0.84	23.41	12.8	09/08/2025 19:07	16.16	0.394	0	0	0	0	0	0	0	0	0	0	0	0	0	0	0	0	0
58	Clinop + Praes	224	474	833	0.7	516	0	0	2.41	97.59	0.71	23.86	12.86	09/08/2025 19:07	16.62	0.394	0	0	0	0	0	0	0	0	0	0	0	0	0	0	0	0	0
59	Clinop + Praes	229	482	844	0.86	528	0	0	2.26	97.74	0.87	24.24	11.49	09/08/2025 19:07	16.21	0.391	0	0	0	0	0	0	0	0	0	0	0	0	0	0	0	0	0
60	Clinop + Praes	238	478	860	0.82	501	0	0	2.14	97.86	0.84	21.4	9.95	09/08/2025 19:07	15.92	0.403	0	0	0	0	0	0	0	0	0	0	0	0	0	0	0	0	0
61	Clinop + Praes	238	476	846	0.64	502	0	0	2.2	97.8	0.66	19.11	10.58	09/08/2025 19:08	16.03	0.394	0	0	0	0	0	0	0	0	0	0	0	0	0	0	0	0	0
62	Clinop + Praes	246	488	834	0.75	525	0	0	2.05	97.95	0.77	20.05	9.88	09/08/2025 19:08	15.57	0.37	0	0	0	0	0	0	0	0	0	0	0	0	0	0	0	0	0
63	Clinop + Praes	239	462	783	0.7	494	0	0	2.19	97.81	0.71	19.15	9.71	09/08/2025 19:08	16.33	0.364	0	0	0	0	0	0	0	0	0	0	0	0	0	0	0	0	0
64	Clinop + Praes	239	471	819	0.7	501	0	0	2.1	97.9	0.72	19.21	9.54	09/08/2025 19:09	16.09	0.38	0	0	0	0	0	0	0	0	0	0	0	0	0	0	0	0	0
65	Clinop + Praes	246	481	861	1.02	501	0	0	1.98	98.02	1.03	19.35	9.72	09/08/2025 19:09	15.52	0.414	0	0	0	0	0	0	0	0	0	0	0	0	0	0	0	0	0
66	Clinop + Praes	246	493	856	0.72	527	0	0	2	98	0.74	19.33	9.43	09/08/2025 19:09	15.48	0.382	0	0	0	0	0	0	0	0	0	0	0	0	0	0	0	0	0
67	Clinop + Praes	244	469	797	0.77	497	0	0	2.19	97.81	0.79	18.46	10.2	09/08/2025 19:09	16.03	0.364	0	0	0	0	0	0	0	0	0	0	0	0	0	0	0	0	0
68	Clinop + Praes	266	487	793	1.77	519	0	0	1.9	98.1	1.76	21.22	0	09/08/2025 19:09	15.1	0.333	0	0	0	0	0	0	0	0	0	0	0	0	0	0	0	0	0
69	Clinop + Praes	104	250	463	0.6	284	0	0.27	9.07	90.66	0.6	34.67	18.59	09/08/2025 19:12	36.84	0.442	0	0	0	0	0	0	0	0	0	0	0	0	0	0	0	0	0
70	Clinop + Praes	114	257	469	0.68	284	0	0.2	7.56	92.24	0.68	32.61	17.64	09/08/2025 19:12	34.37	0.423	0	0	0	0	0	0	0	0	0	0	0	0	0	0	0	0	0
71	Clinop + Praes	117	261	474	0.46	287	0	0.13	7.12	92.74	0.46	32.34	17.12	09/08/2025 19:12	33.19	0.42	0	0	0	0	0	0	0	0	0	0	0	0	0	0	0	0	0
72	Clinop + Praes	119	265	478	0.62	291	0	0.13	6.91	92.95	0.62	31.8	16.89	09/08/2025 19:13	32.83	0.418	0	0	0	0	0	0	0	0	0	0	0	0	0	0	0	0	0
73	Clinop + Praes	121	266	478	0.93	292	0	0.13	6.68	93.19	0.93	32.58	16.97	09/08/2025 19:13	32.51	0.413	0	0	0	0	0	0	0	0	0	0	0	0	0	0	0	0	0
74	Clinop + Praes	120	262	470	0.6	288	0	0.13	6.75	93.11	0.6	33.13	17.26	09/08/2025 19:13	32.83	0.411	0	0	0	0	0	0	0	0	0	0	0	0	0	0	0	0	0
75	Clinop + Praes	120	264	472	0.59	291	0	0.13	6.7	93.17	0.59	31.95	17.12	09/08/2025 19:13	32.62	0.411	0	0	0	0	0	0	0	0	0	0	0	0	0	0	0	0	0
76	Clinop + Praes	121	261	461	0.56	286	0	0.13	6.68	93.19	0.56	32.07	16.83	09/08/2025 19:14	32.88	0.402	0	0	0	0	0	0	0	0	0	0	0	0	0	0	0	0	0
77	Clinop + Praes	122	264	470	0.78	290	0	0.13	6.51	93.35	0.78	31.97	15.33	09/08/2025 19:14	32.48	0.405	0	0	0	0	0	0	0	0	0	0	0	0	0	0	0	0	0



DF	
Normal	1.9
Shear (lowest)	1.8
Shear (regrowth)	1.9

SD
7.970609

